Electron Structure and Charge Transport Properties of Thiols and Dithiocarbamates in Self-Assembled Monolayers

INAUGURALDISSERTATION

zur

Erlangung der Würde eines Doktors der Philosophie

vorgelegt der

Philosophisch-Naturwissenschaftlichen Fakultät

der Universität Basel

von

Florian von Wrochem

Aus Deutschland

Stuttgart, Mai 2007

Genehmigt von der Philosophisch-Naturwissenschaftlichen Fakultät auf
Antrag von:

       Prof. Dr. C. Schönenberger
       Prof. Dr. A. Baratoff
       Dr. J. M. Wessels

Basel, den 23. Februar 2007

Prof. Dr. H.-P. Hauri, Dekan

Contents

1

Introduction

The particular interest for molecular electronics developed within the last decades is motivated by the characteristic properties of organic molecules. Molecules are by definition identical building blocks, and their electronic and structural properties can be easily tuned by chemistry. Molecular structures can vary in rigidity, polarity, redox properties and conjugation. Accordingly, their response to electric fields, to the surrounding dielectrics or to mechanical load can vary significantly. The possibility of using single molecules as a functional element for electronics was first suggested by Aviram and Ratner in 1974[1]. Later, this idea was applied to a broader variety of systems, as fullerenes, carbon nanotubes and metallic or semiconducting nanowires[2]. Recently, even manipulation of single molecules became possible[3] and simple circuits built by selective deposition of atoms or molecules were realized[4]. Even though interesting from a fundamental point of view, complex circuits and devices cannot be realized by this means, and the fabrication of practical devices has to rely on self assembly.

A large number of studies have addressed the question of how to provide organic molecules with functionalities that makes them interesting as components in electronic circuits. As switches are fundamental components for memory and logic devices, several attempts have been made to implement a molecular switch. Recently, this has been realized with conjugated molecules[5], fullerenes[6] and carbon nanotubes[7]. An alternative approach relies on molecular rectification. The mechanism is either based on an asymmetry in the molecular electronic structure or on charging effects. Metzger et al. for the first time demonstrated rectification in donor-acceptor systems[8]. Finally, pronounced peaks in the current-voltage characteristics, a phenomenon called negative differential resistance, was found in resonant tunnelling diodes[9] and in substituted oligophenylenes[10].

Despite the progress that was achieved in understanding the mechanisms that govern charge transport through functional molecular wires, one of the critical issues

to be solved in molecular electronics is the contact at the molecule-metal interface, i.e. the connection of molecules to electrically conducting wires. Generally, molecules can be coupled to semiconductors or to metals. Silane based chemistry allows the functionalization of metal oxide or semiconductor surfaces[11]. A direct coupling of aryls to silicon was recently realized using diazonium compounds[12] and olefins were linked to Rutenium with a conjugated C-Ru bond[13]. However, those substrate materials are not ideal conductors. Besides amines and pyridines, weakly binding to Au, or isocyanides and selenides, there are few alternatives to the thiol anchor group to bind to Cu, Ag and Au[14]. The lack in stability of the metal-molecule contact limits the applicability of molecular devices and motivates the search for new ways to chemically link organics to metals.

A possible approach for the electrical characterization of molecules is their integration into self assembled monolayers[15]. Self assembly is the ability of small, interacting components to aggregate to a global, minimum energy structure through a statistical exploration of intermediate states[16]. Examples of structures formed by self assembly are polymers, proteins and molecular assemblies like self assembled monolayers (2D) or liquid crystals (3D). This supramolecular self assembly process is the bridge between the nanoscopic and the microscopic scale, since it allows the patterning and functionalization of extended surfaces, thus making these long range ordered structures relevant for applications. Potential implementations for organic monolayers are envisioned in chemical and biological sensing[17], biomimetics, corrosion protection[18], opto-electronics and molecular electronics[19]. In self assembled monolayers on atomically flat substrates, molecules are often organized in periodically structured overlayers and are characterized by a defined molecular orientation towards the surface[20]. This allows photoelectron spectroscopy measurements on molecules in a controlled chemical environment and STM characterisation with molecular resolution.

In the present work, the molecule-metal interface is discussed and molecules with a novel organo-metallic binding group, the dithiocarbamates, are investigated. Their electronic properties are compared to thiol derivatives, and it is shown that owing to the specific chemistry and electronic structure of the dithiocarbamate binding group, a lower contact resistance between the molecule and the metal substrate is achieved. Dithiocarbamates constitute an energetically stable interface. Furthermore, as the thiols, they form densely packed monolayers, an essential prerequisite for defect-free

junction materials. A thorough comparative study, including the investigation of electronic properties of self assembled monolayers on metals by means of photoelectron spectroscopy and conductivity measurements on three dimensional nanoparticle films is presented in chapter 3. The experimental results are compared with ab-initio calculations that clarify the mechanisms leading to this different coupling behaviour. In chapter 4, the conductance of aromatic thiols and dithiocarbamates is compared by current-distance spectroscopy in a UHV-STM, which provides a direct way to address single molecules in a monolayer. In chapter 5, conductance and monolayer growth of thiol terminated, aromatic and aliphatic bisamides is studied. These compounds have been previously characterized in three dimensional, interlinked nanoparticle films[21] and an electrical characterisation of single or of small groups of molecules by scanning tunnelling microscopy is aimed. In this chapter, the conditions for the formation of small bisamide domains in mixed dithioamide/alkanethiol monolayers are exploited and the conductance of these compounds determined via STM height profiles.

References

[1] A. Aviram, M. A. Ratner, *Chem. Phys. Lett*. **29,** 277 (1974).

[2] R. L. Carroll, C. B. Gorman *Angewandte Chemie-Int. Edition* **41**, 4378 (2002).

[3] D. M. Eigler, E. K. Schweizer *Nature* **344**, 524 (1990).

[4] A. J. Heinrich, C. P. Lutz, J. A. Gupta, D. M. Eigler *Science* **298**, 1381 (2002).

[5] F. Moresco, G. Meyer, K.-H. Rieder, H. Tang, A. Gourdon, C. Joachim, *Phys. Rev. Lett*. **86**, 672 (2001).

[6] C. Joachim, J. K. Jimzewsky, R. R. Schlittler, C. Chavy, *Phys. Rev. Lett*. **74**, 2102 (1995).

[7] S. J. Tans, A. R. M. Vershueren, C. Dekker, *Nature* **393**, 49 (1998).

[8] R. M. Metzger, B. Chen, U. Höpfner, M. V. Lakshmikantham, D. Vuillaume, T. Kawai, X. L. Wu, H. Tachibana, T. V. Hughes, H. Sakurai, J. W. Baldwin, C. Hosch, M. P. Cava, L. Brehmer, G. J. Ashwell *J. Am. Chem. Soc.* **119**, 10455 (1997).

[9] R. H. Matews, J. P. Sage, T. C. L. G. Sollner, S. D. Calava, C.-L. Chen, L. J. Mahoney, P. A. Maki, K. M. Molvar *Proc. IEEE* **87**, 596 (1999).

[10] J. Chen, M. A. Reed, A. M. Rawlett, J.M. Tour, *Science* **286**, 1550 (1999).

[11] J. Sagiv *J. Am. Chem. Soc.* **102**, 92 (1980).

[12] T. He, J. He, M. Lu, B. Chen, H. Pang, W. F. Reus, W. M. Nolte, D. P. Nackashi, P. D. Franzon, J. M. Tour *J. Am. Chem. Soc.* **128**, 14537 (2006).

[13] G. S. Tulevsky, M. B. Myers, M. S. Hybertsen, M. L. Steigerwald, C. Nuckolls *Science* **309**, 591 (2005).

[14] J. C. Love, L. A. Estroff, J. K. Kriebel, R. G. Nuzzo, G. M. Whitesides *Chem. Rev.* **105**, 1103 (2005).

[15] Cygan, M. T.; Dunbar, T. D.; Arnold, J. J.; Bumm L. A.; Shedlock, N. F.; Burgin, T. P.; Jones, L, II; Allara, D. A.; Tour, J. M.; Weiss, P. S. *J. Am. Chem. Soc.* **1998**, *120*, 2721.

[16] T. Hogg, *Nanotechnology* **10**, 300 (1999).

[17] Haussling, L.; Knoll, W.; Ringsdorf, H.; Schmitt, F.-J.; Yang, J. *Macromol. Chem, Macromol. Symp.* **1991**, *46*, 145. Zamborini, F.P.; Leopold, M.C.; Hicks, J.F.; Kulesza, P.J., Mali, M.A.; Murray, R.W. *J. Am. Chem. Soc*. **2002**, *124*, 8958. Vossmeyer, T.; Guse, B.; Besnard, I.; Bauer, R.E.; Muellen, K.; Yasuda, A. *Adv. Mater.* **2002**, *14*, 238.

[18] Wang, D. H.; Ni, Y. H.; Huo, Q.; Tallman, D. E. *Thin Solid Films* **2005**, *471*, 177.

[19] Aviram, A.; Ratner, M. A. Molecular rectifiers. *Chem. Phys. Lett.* **29**, 277 (1974).

[20] Nuzzo, R. G.; Dubois, L. H.; Allara, D. L. *J. Am. Chem. Soc.* **112**, 558 (1990).

[21] Wessels, J. M.; Nothofer H.-G.; Ford W. E.; von Wrochem, F.; Scholz, F.; Vossmeyer, T.; Schroedter, A.; Weller, H.; Yasuda, A. *J. Am. Chem. Soc.* **2004**, *126*, 3349.

2

Systems and Methods

2.1   Molecules and Self-Assembled Monolayers

Introduction

Since the early studies on amphiphile organic layers[1], originally motivated by the desire to modify the wetting properties of metal surfaces, the interest in self assembled monolayers (SAMs) has evolved into an own discipline. Depending on the binding chemistry, monolayers can be grown on different substrates, such as oxides of transition metals or noble metals such as Ag, Cu or Au[2]. The growth process of SAMs on metals is governed by a complex interplay of interaction forces, determining the structural properties of the SAM[3]. The interaction between headgroup and surface is often the dominant contribution to the overall adsorption enthalpy[4], in particular for short compounds, whose intermolecular forces are weak. The corrugation of the headgroup-substrate interaction energy affects the tendency to bind at a defined surface bonding site, eventually causing an overlayer structure that is commensurate to the metal surface lattice[5]. For monolayers whose chemisorption energy to the surface is relatively weak, as in case of thiol-based monolayers on Au(111), the detailed balance of headgroup-substrate and intermolecular interaction determine the structure and the packing properties of the monolayer. A prominent example is the $(\sqrt{3} \times \sqrt{3})R30°$ overlayer structure of alkanethiols on Au(111) (Fig. 1). Alkanethiols interact mainly through dispersion forces (van der Waals forces), which are not directional and therefore do not constrain the molecules to adopt particular relative positions within the monolayer. Furthermore, the aliphatic chains are flexible, thus enabling a versatile relaxation of the molecular medium and facilitating the self assembly process. The differences in the conformation of the molecular backbone are compensated by variation of the tilt angle of the molecular axis towards the surface, even if the molecular backbone is augmented with substituents[6]. This makes alkanethiols to ideal compounds for studies on self assembled monolayers. In contrast, the intermolecular forces can govern the formation of monolayers whose
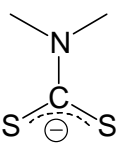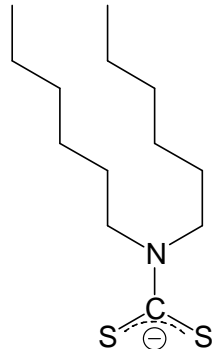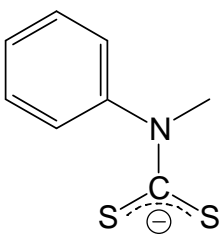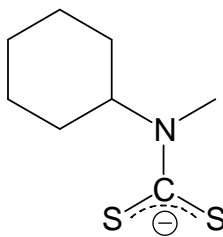
components interact via polar forces (e.g. hydrogen bonds), or strong dispersive forces (aromatic stacking), giving rise to amorphous or incommensurate structures[7].
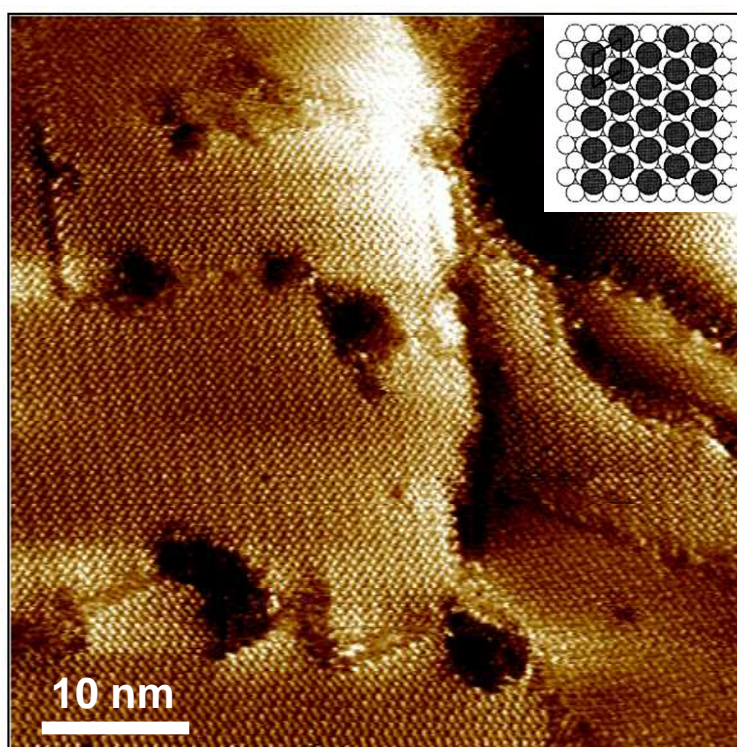
Figure 1. STM image of a hexagonally close packed octanethiol monolayer (50 nm x 50 nm). The depressions are mono-atomar vacancy islands in the Au(111) substrate. The vertically oriented intensity modulation can be attributed to the c(4 x 2) reconstruction. The scans are recorded at a bias voltage of U_{Gap} = 400 mV and a tunneling current of I_{tunn} = 2 pA. In the inset, the ($\sqrt{3}$ x $\sqrt{3}$)R30° overlayer structure on Au(111) is sketched.

Present Work

In our studies, we compare similar compounds provided with either a dithiocarbamate or a thiol binding group in order to demonstrate the effect of the binding group on the electronic properties and on molecular conductance in metal-molecule contacts (Chapters 3-4). Furthermore, the effect of conjugation along the molecular backbone is investigated both for dithiocarbamate and for thiol compounds (Chapters 3-5). In Table 1, the chemical structure of the investigated dithiocarbamate compounds is shown. Characteristic for dithiocarbamates is the presence of the nitrogen in the anchor group and the capability to bind symmetrically with both sulphur atoms to the metal surface.

N,N-dimethyl-dithiocarbamate (DMDTC)	*N,N*-dihexyl-dithiocarbamate (DHDTC)	*N*-methyl-*N*-phenyl-dithiocarbamate (MPDTC)	*N*-methyl-*N*-cyclohexyl-dithiocarbamate (MCDTC)

Table 1: Schematic representation of dithiocarbamate derivatives.

While for thiols a deprotonation during assembly directly leads to the thiolate-Au bond, dithiocarbamate monolayers are prepared following three alternative procedures. In the first procedure, an intermediate reaction, i.e. the reaction of an amine with CS_2, takes place before the assembly process[8]. This protocol offers the advantage that any compound provided with a (secondary) amine group can be converted into a dithiocarbamate compound in-situ, just by immersing the Au surfaces into solutions containing equimolar ratios of CS_2 and the corresponding amine precursor (Fig. 1). The dithiocarbamate group formed in solution is then stabilized through complexation with the Au surface.
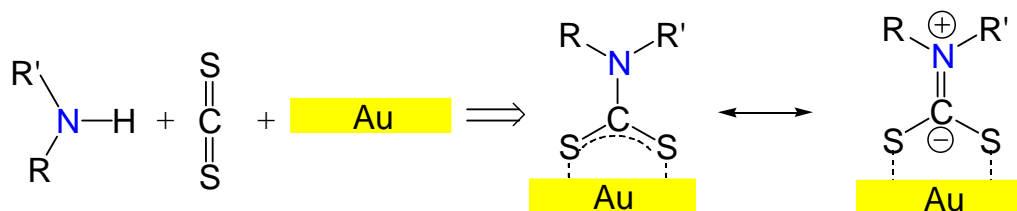
Figure 2. Dithiocarbamate SAM formation from CS_2 and secondary amines, and the resulting mesomeric forms.

According to the second procedure, the dithiocarbamate is synthesized and stabilized by the formation of a dithiocarbamate-salt (usually a dithiocarbamate-Na

complex). In this case, no further chemical reaction takes place during the assembly process, therefore the stoichiometry at surface is well defined. The dithiocarbamate-Au bond is then formed by removal of the cation in solution. Finally, also the direct reaction of thiurams with Au in the assembly solution is possible. This procedure was only used for the realization of DMDT SAMs from thiram. The resulting SAMs showed identical chemical and structural properties as those realized by the in-situ reaction of dimethyl-amine with CS_2, with the only difference that a stronger tendency to form etch pits on Au surfaces was observed for Thiram SAMs.
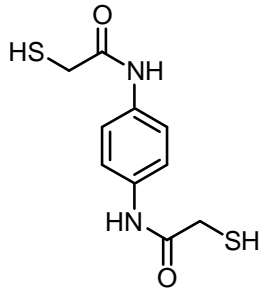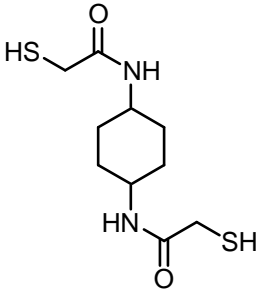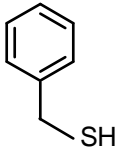
Terphenyl-bis-methyl-dithiocarbamate (TPMDTC)	Terphenyl-dithiol (TPT)	Nonanedithiol (NT)
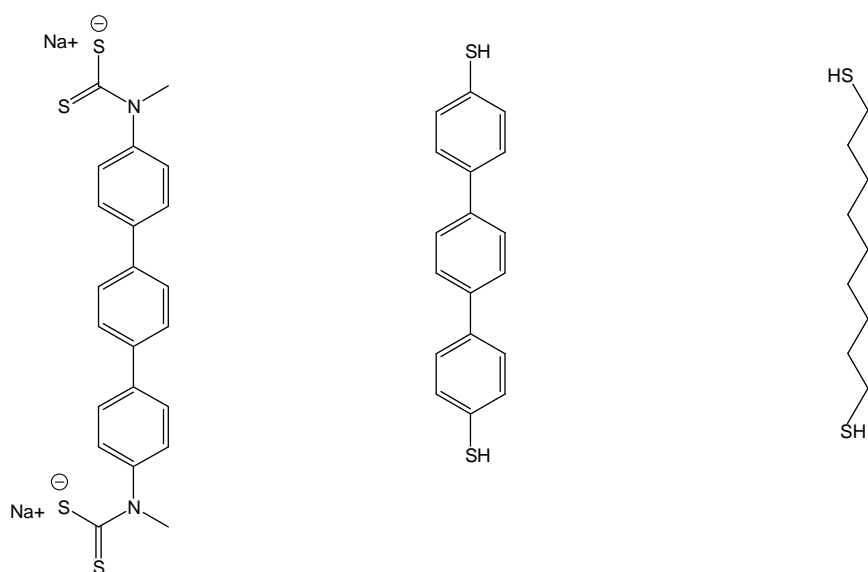
Table 3: Schematic representation of terphenyl-bis-methyl-dithiocarbamate (TPMDTC), terphenyl-dithiol (TPT) and nonane-dithiol (NT).

A direct comparison of the charge transport properties of thiols and dithiocarbamates was done using interlinked networks of Au nanoparticles. An identical terphenyl core was employed, disubstituted with a thiol group or a dithiocarbamate group (Table 3). Nonanedithiol was used as a reference compound in these studies.

In chapter 5, the monolayer formation and the electrical properties of two bisamide dithiols (Di-mercapto-acetamido-benzene (DMAAB) and Di-mercapto-acetamido-cyclohexane (DMAAcH)) are presented. Table 2 shows the molecular structure of bisamides and alkanethiols, as well as of benzylmercaptane (BM).

Di-mercapto-acetamido-benzene (DMAAB)	Di-mercapto-acetamido-cyclohexane (DMAAcH)	Benzenemercaptane (BM)	Alkanethiols

n = 1, 5, 7, 9

Table 2: Schematic representation of dithioamide derivatives, benzenemercaptane, and alkanethiols.

SAM preparation

As a substrate and bottom electrode, a crystalline Au(111) surface is employed. Atomically flat Au(111) surfaces are prepared by flame-annealing of thin Au films (100 nm) evaporated on freshly cleaved mica. SAMs are then prepared by immersing the Au surfaces into millimolar solutions of the thiols and dithiocarbamates in appropriate solvents. Self assembly from solution is a relatively easy and cost effective proceduce that avoids the need for expensive vacuum deposition equipment. Additionally, it allows the processing of a large number of samples in parallel. Finally, most of th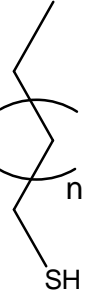e compounds utilized in this work are not suited for gas phase deposition due to their low vapor pressure. Several precaution measures are taken to guarantee a high cleanliness during each processing step and to exclude

contamination originating from the lab environment. Except for the preparation of the assembly solutions, a glove box (PlasLabs) purged with Argon is employed for all processing steps before sample characterization. Solvents are purged in Argon before usage to avoid oxidation. Glass vessels are cleaned using the RCA process (Solution of ammonia and H_2SO_2) and caps with Teflon gaskets are used. This kind of Teflon caps was appositely selected to resist to the high pressures when the samples are thermally annealed at 90°C. The thermal annealing step is introduced to accelerate the phase segregation of two component bisamide/alkanethiol SAMs by increasing the diffusion rate of molecules at Au(111) surfaces (Chapter 5). Systematic variation of the assembly time showed no significant changes in the SAM structure in STM micrographs if the samples are exposed to the solution for longer than 24h. Thus, this time was regarded as sufficient for SAM growth. To form dithiocarbamate SAMs, the corresponding amine was dissolved in ethanol, then an equimolar amount of CS_2 solution added to amine solution, before the substrate was immersed and the molecules assembled overnight. After preparation, the samples are rinsed and bathed thoroughly in the same solvent used to grow the monolayers. Finally, all samples are rinsed in ethanol and dried in argon flow.

Alkanethiol SAMs are also grown from the gas phase, since this can provide high quality, defect free monolayers with large, mono-crystalline domain sizes. For this purpose, a H_2O_2 cleaned desiccator is used and an open vial containing the pure alkanethiol substance is placed close to a neat Au(111) substrate. The desiccator is evacuated for 10 min to a pressure of 6 x 10^{-2} bar and the substrate subsequently exposed to the alkanethiol vapour for about 3h. Finally, the SAM is rinsed and bathed thoroughly in ethanol in order to remove excess alkanethiol molecules loosely bound to the SAM surface.

2.2   Interlinked Nanoparticle Films

The statistically averaged conductance of linker molecules (Table 3) can be determined by resistivity measurements on thin films of interlinked Au nanoparticles[9]. This method is applied in chapter 3, where the electronic coupling of dithiocarbamates and thiols to metals is discussed.

The Films are prepared by silanization of glass substrates decorated by lithographically defined electrode structures. The nanoparticle films are fabricated with the layer by layer technique[9b]. The silanized glass substrate is immersed for 15 min into a toluene solution of dodecylamine-stabilized Au-nanoparticles. During this time, the nanoparticles can bind to the functional amino groups of the silane monolayer. After rinsing the substrate, the sample is exposed for 15 min to a 1 mM solution of linker molecules (for dithiocarbamates a solution of amines and CS_2 is used) and subsequently washed. During this step, the nanoparticles are connected by the linker molecules by ligand exchange of the stabilizing amines with the thiol or dithiocarbamate linker molecules. Then, the films are again exposed to the nanoparticle solution and the procedure is repeated until a sufficient film growth is observed in the absorbance of UV/VIS spectra. After film preparation, the electrodes are contacted in a probe station and the resistivity measured by a source measuring unit at room temperature. Further details on the preparation of interlinked nanoparticle films are found in chapter 3.

2.3   X-ray Photoelectron Spectroscopy

Introduction

In the chemical analysis of surfaces X-ray photoelectron spectroscopy (XPS) has become one of the fundamental analytical methods[10]. Fine differences in the chemical environment and in the oxidation state of selected elements can be detected via the energy shift of its core electrons. XPS is based on the photoelectric effect[11], i.e. photons from a x-ray source (anode or synchrotron radiation with energies > 100 eV) are focused on the sample surface and electrons from the core levels or the valence band are excited and emitted from the sample, from where they are directed to an energy dispersive analyzer (Fig 2.2).
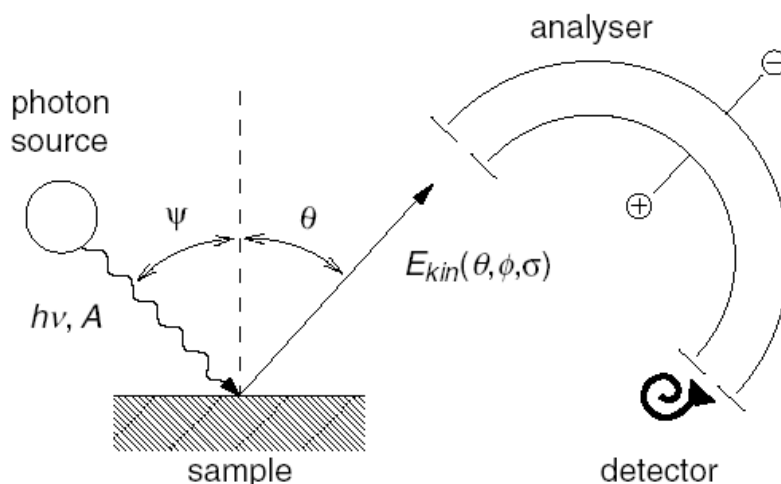
Figure 3. Schematic representation of photo-emission and electron detection in an XPS experiment (Reprint from: F. Reinert, S. Huefner *New Journal of Physics* **7**, *97* (2005)).

The significance of this method consist in the fact that the intensity distribution of the emitted electrons as a function of their kinetic energy is an image of the occupied electronic density of states of the sample. According to the approximation in Koopmans' theorem[12], it is assumed that the electronic structure of the atomic system in the final state (upon photoemission of the core electron) is the same as in the initial state prior to the photoemission process. With this assumption, the detected binding energy corresponds to the negative orbital energy of the emitted electron.
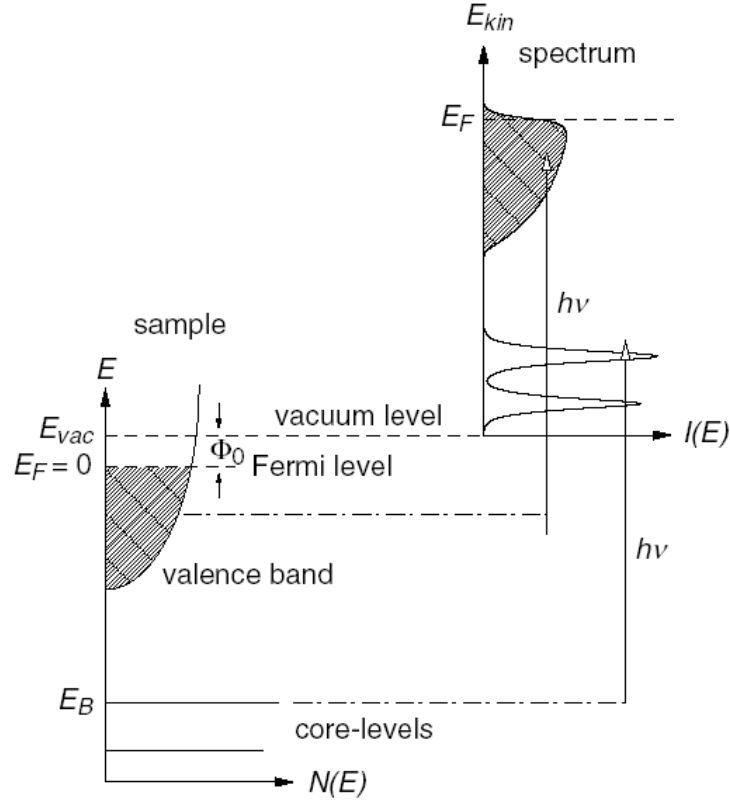
Figure 4. Core level and valence band region in a solid (left) and the corresponding photoelectron spectrum resulting from photoemission with the excitation energy $h\nu$ (right) (Reprint from: F. Reinert, S. Huefner *New Journal of Physics* **7**, *97* (2005)).

Of course, this applies only to a first approximation and there are small corrections that have to be considered to describe the exact energy of XP spectral lines[13].

$$E_B = -E_n - \Delta\varepsilon_r + \Delta\varepsilon_{rel} + \Delta\varepsilon_{corr}$$

Such corrections are due to relaxation effects $\Delta\varepsilon_r$ of the remaining core electrons surrounding the hole created by the photoemission process, relativistic effects ($\Delta\varepsilon_{rel}$) and electron correlation effects ($\Delta\varepsilon_{corr}$). Initial and final state effects can further lead to a shift or splitting of core level lines. An important example in this context is the coupling of the electron spin with the orbital angular momentum, which for $l > 0$ can give rise to states with different total angular momentum j. These states show up in the fine structure of the XP spectra with energetically separate peaks, whose area is proportional to the number of projected states m_j for each value of j. In case of sulfur *2p* for example, the separation of the S *2p$_{1/2}$* and the S *2p$_{3/2}$* components is 1.18 eV and the peak area ratio is 1:2, as expected considering the number of projections for each value of j.

An important application of XPS is the chemical analysis. For this, energy shifts of core levels are investigated. Within the charge potential model[14], the binding energy E_B of a core level state associated to a particular atom depends on the partial charge of the atom itself and on the charges of the surrounding atoms within the chemical structure:

$$E_b = E_{b_0} + \alpha \cdot q + \sum_i \frac{q_i}{r_i}$$

where E_{b0} is the binding energy of the unsubstituted atom, α is a constant, q is the partial charge on the atom, q_i the charges on the neighbouring atoms and r_i their distance from the atom of interest. Thus, the chemical shift can be deduced from electronegativity differences of neighbouring atoms within a chemical structure and can be related to Mulliken or Hirshfeld charges obtained by quantum chemistry calculations.

The width of core level lines, besides a small temperature contribution, is mainly given by the core level hole lifetime, and this depends on the intra-atomic Auger recombination process[15]. As all decay processes in quantum mechanics, this gives rise to a Lorentzian line shape. Since instrumental resolution typically shows a Gaussian line shape, XPS peaks are fitted by a convolution of a Lorentzian and a Gaussian function.

Instrumentation

In the photoelectron spectrometer (Kratos Axis Ultra), the x-rays are generated by acceleration of electrons onto a water cooled Al or Mg anode (15 kV, 12 mA). From the anode, K_α-radiation is emitted, for example at an energy of 1486,6 eV (Aluminum K_α-radiation). To reduce the width of the Al K_α-line, a crystal monochromator is utilized, leading to an instrumental resolution of about 0.45 eV. The kinetic energy of the emitted photoelectrons is measured in an energy dispersive analyzer equipped with a delay line detector. The analyzer is based on electron deflection in a homogeneous electrostatic field (hemispherical analyzer). A pass energy of 40 eV is generally sufficient to resolve the fine structure within the spectra.

The binding energy of core level electrons can be derived from the kinetic energy E_{kin} of the emitted photoelectrons and the known energy of the x-ray source according to[13]

$$E_{Kin} = h\nu - \Phi_{Sp} - E_B$$

Here, $h\nu$ is the photon energy, Φ_{Sp} the work function of the spectrometer and E_B represents the core level binding energy relative to the Fermi level.

Data Analysis

In our experiments, the product of a Gaussian and Lorentzian function with a ratio of 1:1 gave the best fit to the data. The spectra are fitted using a linear background and a slight asymmetry factor (instrumental). The linewidth of experimental spectra can vary significantly depending on the statistical variations to which the observed chemical species are subjected within the sample. For example, the sulfur *2p* doublet shows a small line width (0.7 eV) when thiolates are bound to Au in periodic structures, as in case of ($\sqrt{3}$ x $\sqrt{3}$)R30° overlayers of alkanethiols on atomically flat Au(111) surfaces. In this case, the sulfur atoms are surrounded by a very uniform chemical environment. In contrast, thiol groups that are located at the bulk-air interface of the monolayer (dithiol SAMs) show a typical line width of about 1.1 eV and more, indicating fluctuations in the dielectric environment at the monolayer-air interface as a result of e.g. presence of water and solvent molecules, chain motion, disorder.

Since self assembled monolayers are grown on gold surfaces, Au core levels can be conveniently used as a reference for calibration of the binding energy scale. According to literature, we set the Au $4f_{7/2}$ line to a binding energy of 84 eV[16]. In some cases, constraints are needed to obtain a physically meaningful fit to XPS data. This applies to the sulfur *2p* doublet, where the separation of the S *2p$_{1/2}$* and the S *2p$_{3/2}$* is kept fixed at 1.18 eV and their area ratio to 1:2.

For a correct elemental quantification, the depth of the element within the surface material has to be considered, since scattered electrons do not contribute to the signal intensity. The probability for an electron to pass the material is given by the electron attenuation length (EAL), which can be determined both experimentally and theoretically. EAL values can be computed using the NIST standard reference database 82[17]. Details on the calculation of attenuation factors using EAL values are presented in Appendix A.

Chemisorption energy studies are performed by heating the sample in a UHV chamber and simultaneously monitoring the coverage via XPS analysis. The change in the core level peak intensity is then a measure of the molecular desorption rate. Further details to this method can be found in Appendix B.

2.4   Ultraviolet Photoelectron Spectroscopy

Like XPS, UPS is based on the photoelectric effect, although in this case the electrons are excited by a low energy photon source (10 eV $< h\nu <$ 100 eV). For several reasons UPS became an important method for the determination of the electronic structure at surfaces. First, the mean free path of low energy electrons emitted from the sample is quite short, i.e. in the range of a few Angstroms. This is demonstrated in Fig. 5, which shows that using radiation from a helium UV lamp (21.2 eV and 40.8 eV) the electron attenuation length is close to the minimum in the universal mean free path curve[18]. Thus, UPS is extremely surface sensitive and appropriate for probing the electronic structure of materials within the first atomic layers of the sample surface, like organic monolayers or surface adsorbates.
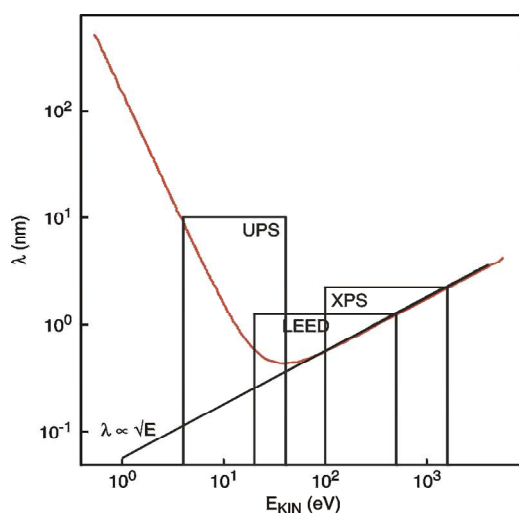
Figure 5. Universal inelastic mean free path curve for electrons in solids (Reprint from Y. Joseph, *Spektroskopische Untersuchungen zur Oberflächenchemie von einkristallinen Eisenoxidfilmen*, Dissertation (2001)).

Second, the photoelectron cross section for electrons in the valence band often increases with decreasing excitation energies, as provided by UV radiation. Finally, the small linewidth of a typical helium UV source (a few meV) allows the resolution of very fine structures in a valence band spectrum[19].

The chemical relevance of UPS relies in the fact that it allows the observation of small energy shifts caused by electronic adsorbate-substrate interactions or by surface states. Bonding shifts of adsorbates can be studied by comparison with gas phase UPS

spectra of the adsorbate particle[20]. In general, the electron binding energy E_{ad} of an adsorbate is related to the ionization energy E_g of the molecule in the gas phase via[21]

$$E_{ad} = -E_g - (\Phi + \Delta\Phi) + \Delta\varepsilon_{rel} + \Delta\varepsilon_b$$

where Φ denotes the work function of the metal and $\Delta\Phi$ the change in the surface potential induced by the adsorbate. The correction $\Delta\varepsilon_{rel}$ is due to relaxation effects within the material surrounding the hole created by the emitted photoelectron. Molecular orbitals strongly interacting with the surface (hybridization), are subjected to a chemical bonding shift $\Delta\varepsilon_b$. The strength of the bonding shift allows the distinction of physisorption and chemisorption processes involving the adsorbed species and the surface. If gas phase spectra are not available, quantum mechanical calculations (see chapter 2.6) are essential for the interpretation of UPS data. They give information on the nature of bond formation and on the energetics of the adsorption process, further allowing the calculation of the density of states, which can be directly related to the features observed in UPS spectra.

The UPS spectrum of a metal surface modified with an adsorbate layer generally shows a superposition of the band structure of the substrate material (for example the Au 5d band) with specific lines originating from the electron structure of the adsorbate[13] (Fig. 6). The intensity of the resonances associated to the adsorbate layer can be directly related to the coverage on the surface. As shown in Fig. 6a and b, the secondary electron background intensity is a characteristic feature of UPS measurements and represents all the photoelectrons that are scattered to lower kinetic energies (higher binding energy) due to interaction with the substrate material. The background rises in intensity with increasing binding energy. According to the Lambert-Beer law (Appendix A), photoelectron attenuation from the adsorbate layer results in a decrease in intensity of the Fermi edge and of the *d* band of the substrate (Fig. 6a). Typically, for low energy electrons crossing an alkanethiol monolayer, the attenuation length is about 0.5 nm[22].

The sample work function depends on the metal and on the physical and chemical properties of the employed adsorbate layer. By UPS, work function changes $\Delta\Phi$ induced by the molecular dipole layer or by charge separation at the adlayer-substrate interface can be detected. The work function is obtained from the difference of the photoelectron energy and the width $\Delta W = E_F - E_{PT}$ of the photoelectron spectrum[13].

$$\Phi = h\upsilon - \Delta W$$

where E_F is the position of the Fermi energy and E_{PT} the photoemission threshold (onset of the spectra).
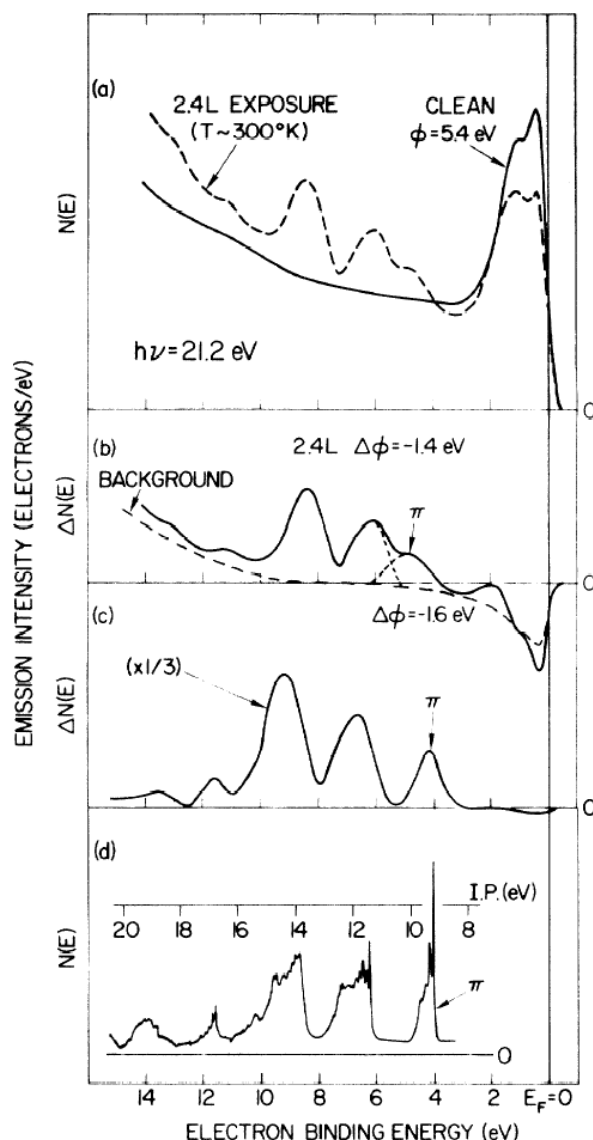
Figure 6. UPS spectra of benzene, condensed benzene and chemisorbed benzene adsorbed on a Ni(111) surface[20]. (a) Spectra of benzene on Ni(111) and of clean Ni(111) surface. (b) Difference spectrum of the spectra in (a). (c) Difference spectrum of a benzene multilayer (T = 150 K). (d) Benzene gas phase spectrum. In (a), the intensity of the d-band (0-2 eV binding energy) is attenuated by the benzene layer (Reprint from [20]).

Instrumentation

In the present work, a Kratos Axis Ultra XPS/UPS system is used. It is equipped with a helium UV-source with excitation energies at 21.2 eV (He I) and 40.8 eV (He II). A possibly high fraction of HeII photons (HeI/HeII intensity ratio of 4) is obtained by adjusting the helium lamp at the lowest possible pressure (~ 10^{-7} Torr in the

measurement UHV chamber and $\sim 3 \ 10^{-5}$ Torr in He pump gauge). The light is incident at an angle of 55° from the sample normal and the photoelectrons are collected by an energy dispersive hemispherical analyzer at a takeoff angle of 90°. Since the angular acceptance of the photoelectron spectrometer (about 11°) is much larger than the typical feature size of interference patterns from photoelectron diffraction, the angle dependence can be neglected. In order to get a high instrumental resolution, the analyzer is set to a pass-energy of 5 eV. Including the linewidth of the helium source this provides a total instrumental resolution of about 0.14 eV. Since most of the spectra are acquired on thin gold films, binding energies are usually referenced to the Fermi level of a clean, nitrogen ion-etched Au surface. The binding energies are then defined as positive for occupied states below the Fermi level.

2.5   Scanning Tunnelling Microscopy

Scanning tunnelling microscopy (STM) allows an atomically resolved characterisation of surfaces. This is exploited to investigate the topology of surfaces in real space. But also for spectroscopy studies STM offers a spatial resolution never achieved before its invention in 1981[23]. In STM, an atomically sharp probe is kept at a small distance from a metal substrate. As a result of the applied bias voltage, a current flows through the small gap (0.1-1 nm) between probe and surface. This current is a consequence of the tunnelling effect, which allows the exchange of electrons through a potential barrier at a rate which is exponentially dependent on the distance between probe and surface. The STM probe is mounted on a piezo scanner, by which the probe is scanned along the surface. In the constant current mode, the controller electronics tunes the probe-sample distance such that the measured tunnelling current is kept constant. Thus, by scanning over the surface in lines, an image of the surface topography is recorded. Due to the exponential dependence of the tunnelling current on the probe-surface distance, a high accuracy in the vertical position of the probe can be achieved (sub-angstrom regime). Figure 1 shows examples of atomically flat semiconductor and metal surfaces imaged by STM. In Fig. 1a, the 7 x 7 reconstruction of Si(111) is shown, while Fig. 1b displays the herringbone reconstruction of a Au(111) surface.
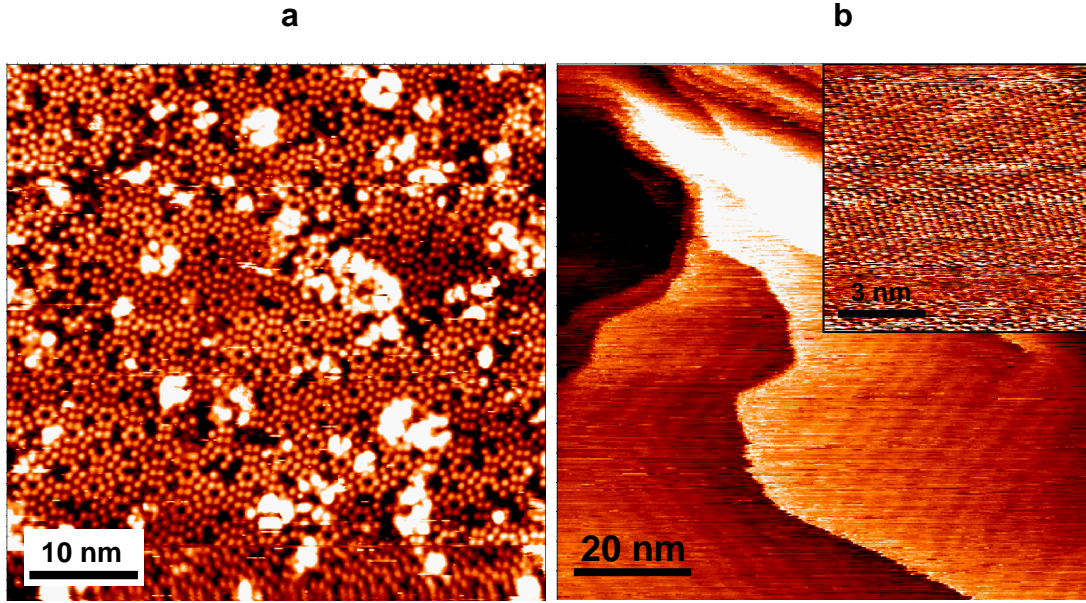
Figure 7. (a) STM scan of the 7 x 7 reconstruction of the Si(111) surface. (b) ($\sqrt{3}$ x 23) herringbone reconstruction of the Au(111) surface. In the inset the hexagonally close packed Au(111) surface is shown. The scans are recorded at a U_{Gap} = 1.8 V, I_{tunn} = 1 nA (a) and at U_{Gap} = 0.9 V, I_{tunn} = 20 pA (b).

In STM, the tunnelling current *I* depends on the distance *z*, but also on the material properties of the sample and the probe. With the approximations given by Tersoff and Hamann[24], this can be expressed as

$$I \sim V_b \cdot \rho_s(E_F) \cdot \rho_p(E_F) \cdot e^{-\frac{\sqrt{2m\phi}}{\hbar}z}$$

valid for small bias voltages. The tunnelling current depends on the bias voltage V_b applied to the probe and on the local density of states ρ_s and ρ_p at the Fermi level of the sample and the probe. The distance dependence is contained in the exponential factor, where *m* the electron mass and ϕ the tunnelling barrier height, i.e. the energy gap from the Fermi level to the lowest empty state.

Since the local density of states of the material adsorbed at surfaces varies depending on chemistry, the topography contrast in STM, besides having its origin in the surface height profile, can thus originate from the individual electronic structure of the adsorbates or adatoms on the surface. By tuning the bias voltage V_b, the energy resolved local density of states of the surface can be imaged. Depending on the alignment of electronic states with the Fermi levels, filled or empty electronic states can be imaged at different bias voltages[25]. While the dependence of the STM topographic height on V_b makes the interpretation of STM micrographs more difficult

than in AFM, it provides an additional method of probing the electronic structure of adsorbate materials at metal surfaces.

In this thesis, current-distance spectroscopy and the evaluation of height profiles from STM images are employed for the electrical characterisation of molecules in self assembled monolayers. In chapter 4 and 5, some of the relevant methodologies are described more in detail.

2.6   Density Functional Methods

Plane wave DFT calculations

According to the Kohn-Sham Theory[26,27], the electronic and spatial structure of atoms, molecules and condensed matter in the electronic ground state can be determined as functional of its electron density rather then using a complicated N-electron wave function. From this approach, the definition density functional theory (DFT) is derived.

DFT calculations based on a plane wave basis set are ideally suited to treat periodic systems, as solid state materials. A unit cell, adapted to the physical problem, has to be selected. Then, the lattice coordinates of the atoms within the unit cell can be defined. The valence electronic wavefunctions are given by a linear combination of plane waves (Fourier series) with different momentum p, and the accuracy determined by the choice of the momentum cutoff. Using "ultrasoft" pseudopotentials[28], a drastic reduction in the number of plane waves required for a calculation is acheived, therefore enabling simulations with a larger number of atoms/unit cell.

Due to their periodic character, crystalline metal surfaces can be conveniently represented as a slab model, containing only a few layers adjacent to the bulk surface. The surface can be modified with adsorbate molecules, whose packing density and arrangement is determined by experimental data gained from surface characterization methods. One of the advantages of using plane wave DFT is that to some extent the bandstructure of the metal is included in the calculation of material properties.

In our studies, a two layer Au(111) slab in a periodic $2\sqrt{3}$ x $2\sqrt{3}$ unit cell is employed to model the surface. DFT calculations are performed using a plane wave basis set with a cutoff energy of 320 eV. As DFT functional, the revised generalized gradient approximation of Perdew, Burke and Ernzerhof (RPBE) is employed, as

provided by the CASTEP code[29]. The ionic cores are described by ultrasoft pseudopotentials. The Brillouin zone is modeled including 5 Monkhorst-Pack k-points. The molecular adlayers are arranged at surface as determined from XPS investigations (packing density). From the calculations, electronic properties such as density of states $\rho(E)$ (total or projected on molecules/atoms), local electron density distribution $\rho(r)$, band structure, atomic charges and molecular multipoles are obtained. Furthermore, electron density isosurfaces (Kohn-Sham orbitals) show the local distribution of electronic charge as a function of the energy eigenvalues. Such isosurfaces can be seen as an analogue to molecular orbitals, even though they are not the same in a strict sense (only Hartree-Fock calculations yield molecular orbitals). Finally, the projection of the densitiy of states (PDOS) on the molecular adlayer allows the identification of electronic states leading to specific resonances in the photoelectron spectra.

Atomic orbital based DFT calculations.

For the evaluation of partial charges and wavefunctions on small molecule-Au complexes, DFT calculations at the B3LYP theory level with a LanL2DZ basis set are carried out using the Gaussian 98 program suite[30]. The simulations are done on molecules coupled to a single Au atom through their anchor groups. Energy levels and molecular orbital isosurfaces are obtained upon relaxation of the structures. Hirshfeld charges are computed at the BLYP theory level using Dmol3[31].

References

[1] Emmons, H. *Trans. Am. Inst. Chem. Eng.* **1939**, *35*, 109.

[2] A. Ulman, *Ultrathin Organic Films* Academic Press (San Diego, CA).

[3] F. Schreiber, *Progress in Surface Science* **65**, *151* (2000).

[4] D. J. Lavrich, S. M. Wetterer, S. L. Bernaseck, G. Scoles, *J. Phys. Chem. B* **102**, 3456 (1998).

[5] C. E. D. Chidsey, G.-Y. Liu, P. Rowntree, G. Scoles, *J. Chem.Phys.* **91**, 4421 (1989).

[6] For wetting studies and for biological sensing applications, the alkyl chains are terminated with different functional groups, exceeding the volume of a methyl endgroup.

[7] Jaschke, M.; Schönherr, H.; Wolf, H.; Butt, H. -J.; Bamberg, E.; Besocke, M. K.; Ringsdorf, H. *J. Phys. Chem.* **1996**, *100*, 2290.

[8] Zhao, Y., Perez-Segarra, W., Shi, Q., Wei, A. *J. Am. Chem. Soc.* **127**, 7328 (2005).

[9] (a) Liao, J., Bernard, L., Langer, M., Schönenberger, C., Calame, C. *Adv. Mat.* **18**, 2444 (2006). (b) Wessels, J. M.; Nothofer H.-G.; Ford W. E.; von Wrochem, F.; Scholz, F.; Vossmeyer, T.; Schroedter, A.; Weller, H.; Yasuda, A. *J. Am. Chem. Soc.* **2004**, *126*, 3349.

[10] C. Nordling, E. Sokolowsky, K. Siegbahn, *Phys. Rev.* **105**, 1676-1677 (1957).

[11] A. Einstein, *Ann. Physik* **17**, 132 (1995).

[12] Koopmans Theorem (1934). Ueber die Zuordnung von Wellenfunktionen und Eigenwerten zu einzelnen Elektronen eines Atoms. *Physica 1*: 104-113.

[13] G. Ertl, J. Küppers, *Low Energy Electrons and Surface Chemistry*, VCH (Weinheim, 1985).

[14] K. Siegbahn, C. Nordling, A. Fahlman, R. Nordberg, K. Hamrin, J. Hedman, G. Johansson, T. Bergmark, S. E. Karlsson, I. Lindgren, B. Lindberg, *ESCA-Atomic, Molecular and Solid State Structure Studied by Means of Electron Spectroscopy*. Almquist and Wicksell (Uppsala, 1967).

[15] J. C. Fuggle, S. F. Alvarado, *Phys. Rev. A* **22**, 1650 (1980).

[16] W. McLean, C. A. Colmenares, R. L. Smith, G. A. Somorjai, *J. Phys. Chem.* **87**, 788 (1983).

[17] *NIST Electron Effective-Attenuation-Length Database*, Version 1.1 (2003).

[18] M. P. Seah, W. A. Dench, Quantitative Electron Spectroscopy of Surfaces: A Standard Data Base for Electron Inelastic Mean Free Paths in Solids. *Surf. Interf. Anal.* **1**, 1-11 (1979).

[19] D. W. Turner, C. Baker, A. D. Baker, C. R. Brundle, *Molecular Photoelectron Spectroscopy*. Wiley Interscience (London, 1970).

[20] J. E. Demuth, D. E. Eastman, *Phys. Rev. Lett.* **32**, 1123 (1974).

[21] K. Christmann, *Introduction to Surface Physical Chemistry*, Steinkopff Verlag & Springer Verlag (Darmstadt, 1991).

[22] A.-S. Duwez, G. Pfister-Guillouzo, J. Delhalle, J. Riga, *J. Phys. Chem. B* **104**, 9029 (2000).

[23] G. Binnig, H. Rohrer, C. Gerber, E. Weibel, *Phys. Rev. Lett.* **50**, 120 (1983).

[24] J. Tersoff, D. Hamann, *Phys. Rev. B.* **31**, 805 (1985).

[25] D. K. Biegelsen, L. J. Swartz, R. D. Bringans, *J. Vac. Sci. Technol. A* **8**, 280 (1990).

[26] P. Hohenberg, W. Kohn, *Phys. Rev.* **136**, B864 (1964).

[27] W. Kohn, L. J. Sham, *Phys. Rev.* **140**, A1133 (1965).

[28] Vanderbilt, D. *Phys. Rev. B*, **41**, 7892-7895 (1990).

[29] Segall, M. D., Lindan, P. J. D., Probert, M. J., Pickard, C. J., Hasnip, P. J., Clark, S. J., Payne, M. C. *J. Phys.: Cond. Matt.* **14**, 2717-2743 (2002).

[30] M. Frisch et al., *Gaussian 98*, Revision A.11, Gaussian Inc., Pittsburgh, PA, 1998.

[31] Delley, B. *J. Chem. Phys.* **92**, 508 (1990).

3

A Stable 'Low Ohmic' Metal-Molecule Interface: Dithiocarbamates versus Thiols

Abstract

A stable, 'low impedance' metal – molecule interface is crucial for the realization of molecular electronic devices. Dithiocarbamate derivatives offer an alternative to the commonly used thiol anchor group, and we show that they improve the coupling to the metal due to the presence of delocalized electronic states at 0.5±0.1 eV below the Fermi level of Au. Photoelectron spectroscopy reveals a significantly increased density of states at the interface and density functional theory calculations prove that they are attributed to the hybridization of metal *d* states with resonant molecular orbitals on the dithiocarbamate anchor group. As a consequence, a low charge injection barrier between molecule and metal is formed, improving the contact at the metal-molecule interface. The improved coupling is reflected in the conductivity of thin films of interlinked nanoparticle networks. Moreover, thermal desorption experiments show an increased stability of dithiocarbamates on gold. These results suggest that organic molecules strongly coupled to metals via the dithiocarbamate anchor group could overcome some of the fundamental limitations currently encountered in molecular electronics.

1. Introduction

The development of information technology beyond the limits of CMOS requires new ways of physically processing and storing information.[1] Since the seminal publication of Aviram and Ratner[2] that marked the beginning of molecular electronics, substantial work on exploring nanoscale molecular devices has been carried out.[3] A nonlinearity/asymmetry in the electrical response of metal/molecule/metal junctions could be achieved by mechanisms such as resonant tunneling,[4] coulomb blockade or conformational switching.[5] Furthermore, in recent years a great number of studies have elucidated the structure and surface chemistry of

organic monolayers,[6,7,8] which are often considered as the basis for the fabrication of molecular devices via self-assembly techniques.

Despite the progress in the realization of molecular devices, several difficulties are still encountered, some of them related to stability issues at the metal-molecule interface.[1] The metal-molecule contact is most commonly realized using the thiol anchor group, which does not provide an efficient pathway for charge transport due to the local character of the sulfur $3p$ orbitals that are involved in the metal-molecule bond formation.[9] Thiols are known to form highly ordered monolayers on gold and to stabilize the metal surface. However, XPS results[10] and theoretical studies[11] suggest the presence of different hybridization states of the sulfur headgroup (sp and sp^3). Related changes in the metal-molecule contact geometry have been reported to have a significant impact on contact resistance.[12] Indeed, STM investigations showed evidence of conductance instabilities that are attributed to changes in the molecular orientation[13] or to thermally activated stochastic bond fluctuations.[14] Finally, it is conceivable that the low energy barriers for molecular desorption[15] and diffusion of thiols on metals, even though very beneficial for the self-assembly process, can be critical in the realization of thiol based devices.
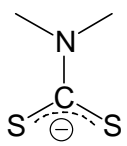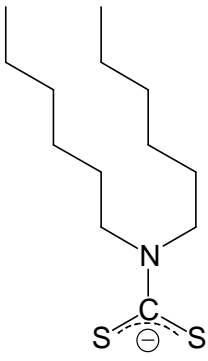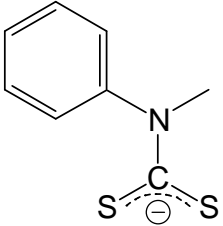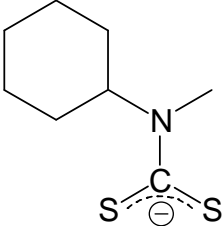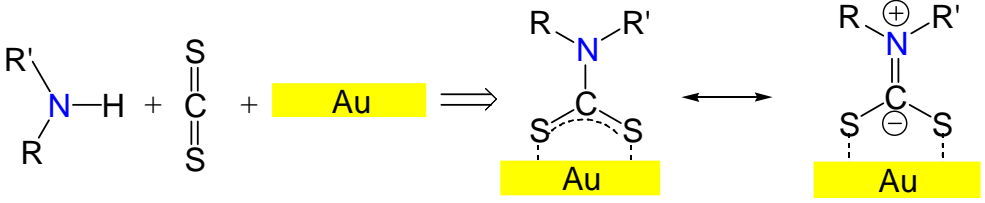
Dithiocarbamate derivatives are well known to form chelate complexes with metals.[16,17] They can either be isolated as salts and assembled onto metals from solution[18] or simply grown in a one pot procedure by immersing metal substrates into solutions of carbon disulfide and organic amines.[19] Recent studies have indicated that dithiocarbamates provide a low resistance in thin films of interlinked nanoparticles[18] and that they bind as a bidentate to Au surfaces.[20] In this report, we show evidence that a low charge injection barrier is created at the dithiocarbamate-Au interface. Photoelectron spectroscopy and density functional theory (DFT) calculations of self-assembled monolayers on Au demonstrate that this is related to the specific electronic structure of the dithiocarbamate anchor group. The charge transport through the metal-organic interface is compared based on conductivity measurements in films of Au nanoparticles interlinked by rigid aromatic linkers, showing the improved coupling provided by the dithiocarbamate group. Furthermore, thermal desorption experiments reveal a significantly higher stability of dithiocarbamates compared to thiols on Au, an aspect of fundamental importance in view of device processing.

2. Results and Discussion

2.1. Ultraviolet photoelectron spectroscopy and DFT calculations

Self-assembled monolayers (SAMs) of N,N-dimethyl-dithiocarbamate (DMDTC), N-methyl,N-cyclohexyl-dithiocarbamate (MCDTC), N-methyl,N-phenyl-dithiocarbamate (MPDTC) and N,N-dihexyl-dithiocarbamate (DHDTC) molecules were prepared by immersing atomically flat Au(111) surfaces into ethanolic solutions containing equimolar ratios of CS_2 and the corresponding amine precursor **(Table 1)**. This direct assembly of dithiocarbamate derivatives provides a versatile synthesis pathway for the formation of dithiocarbamate derivatives with a broad variety of substituents.[19]

N,N-dimethyl-dithiocarbamate	*N,N*-dihexyl-dithiocarbamate	*N*-methyl-*N*-phenyl-Dithiocarbamate	*N*-methyl-*N*-cyclohexyl-dithiocarbamate
DMDTC	**DHDTC**	**MPDTC**	**MCDTC**

Table 1. Schematic representation of dithiocarbamate derivatives, the SAM formation from CS_2 and secondary amines, and the resulting mesomeric forms.

Surface chemistry, elemental quantification and monolayer coverage of dithiocarbamate and thiol SAMs were investigated by X-ray photoelectron spectroscopy (XPS). The XPS data shows that DMDTC, MCDTC, MPDTC and DHDTC chemisorb to Au and form densely packed monolayers (*vide infra*). The valence band structure of dithiocarbamate and thiol monolayers on Au was studied by ultraviolet photoelectron spectroscopy (UPS).[21] Butanethiol and DMDTC have been selected for comparison of the electronic structure of thiols and dithiocarbamates

since both compounds have a short molecular backbone with roughly the same length, thus allowing to neglect differences in the attenuation of the photoelectron intensity.
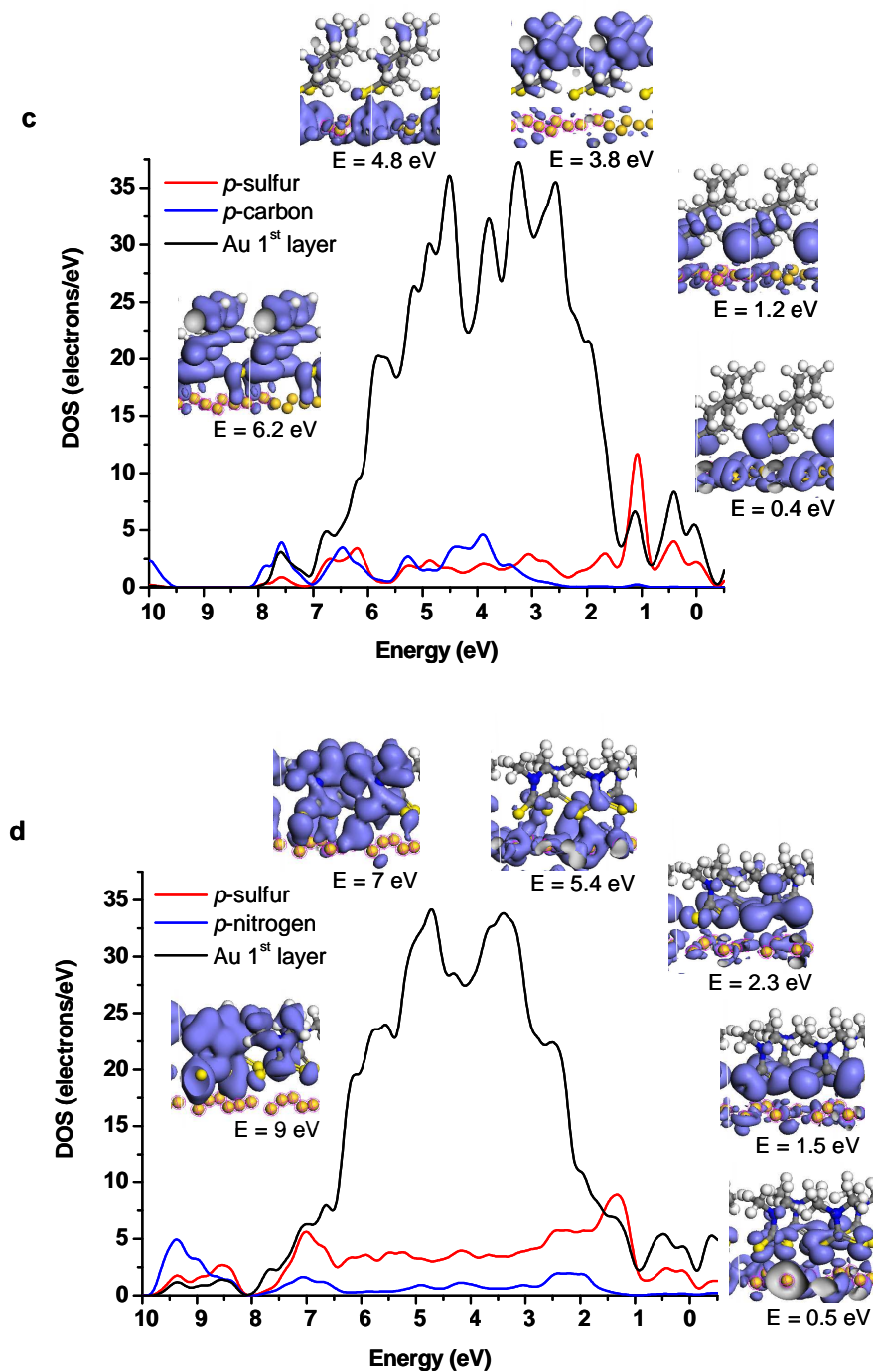
Figure 1 shows UPS spectra of butanethiol (a) and DMDTC (b) monolayers on Au(111), as well as the projected density of states (DOS) obtained from electronic structure calculations based on plane wave DFT (a-d). At binding energies between 1.5 and 8 eV the UPS spectra of thiol and dithiocarbamate monolayers are dominated by a superposition of the Au $5d$ band from the substrate and of specific lines originating from the electron structure of each of the molecular adlayers. While the spectral features of butanethiol SAMs resemble those reported in the work of Duwez et al,[22] we observe a pronounced difference in the spectra of butanethiol and DMDTC in the low energy band at 1-2 eV binding energy (BE). For thiols it is reported[23] that in this BE region sulfur p states mix with metal states, forming antibonding molecule-Au hybrids. Whereas these hybrids are only barely visible in the butanethiol spectrum, showing a weak signal[24] related to the antibonding HOMO (Figure 1a), they are dominant in the DMDTC spectrum, showing a distinct resonance that is centered at ~1.5 eV (low energy onset at ~0.9 eV) (Figure 1b). To localize the electronic states contributing to this resonance, dialkyl-dithiocarbamates with different alkyl chainlenghts were compared (Supporting information, Figure S1). The resonance intensity decreases with increasing chainlength as a consequence of the inelastic scattering of photoelectrons by the chains, thus leading to the conclusion that the resonance is related to states belonging to the molecule-Au interface. A further characteristic of the DMDTC spectrum are the bands at 7 and 9.5 eV. According to previous UPS studies on trimethylamine,[25] a closely related compound, these states can be attributed to DMDTC orbitals with contributions from nitrogen and carbon $2p$ states. Finally, the resonance at 3.7 eV is not reproduced by DFT calculations and its origin is not clarified so far.

a
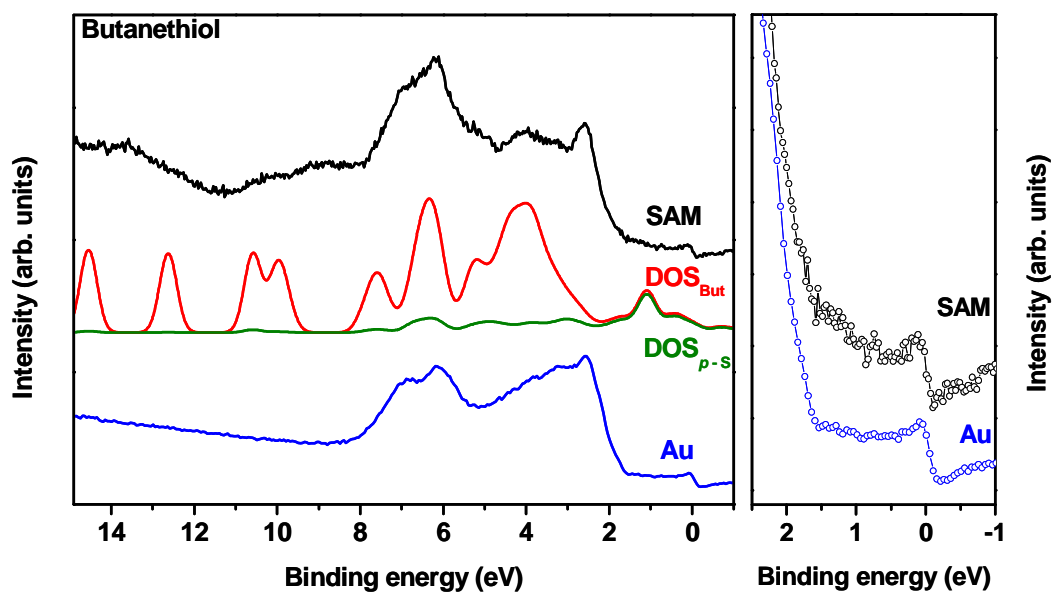
b
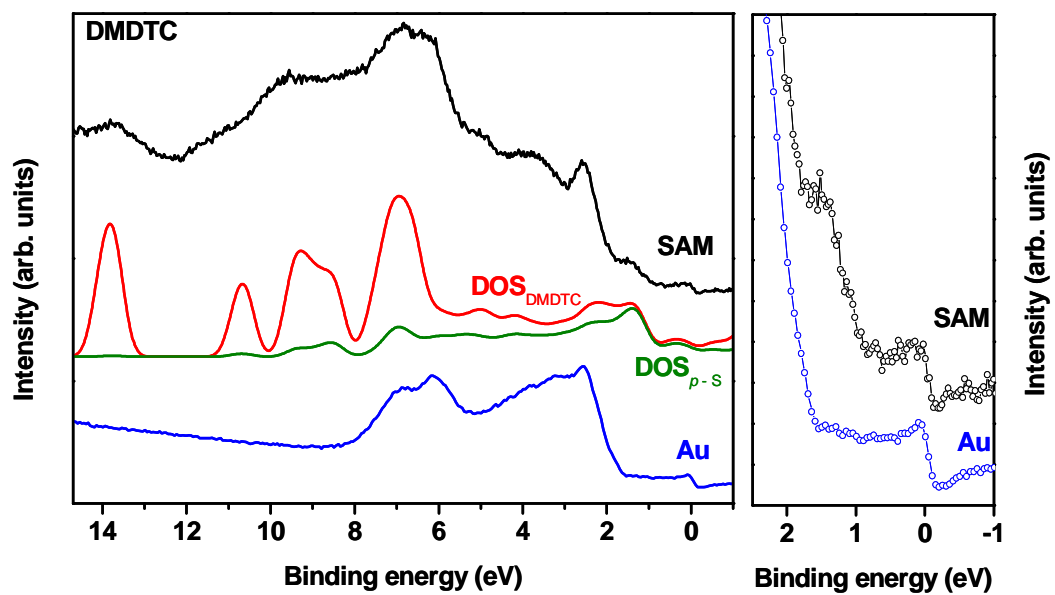
Figure 1. UPS spectra of butanethiol **(a)** and DMDTC **(b)** monolayers (black) on Au(111). The spectrum of a clean Au surface is shown for comparison (blue). The intensity of the spectra is normalized at the Fermi level and an arbitrary offset between the plots is introduced for clarity. The DOS projected on the adlayer (red) and on sulfur p states (green) is obtained from plane wave DFT calculations with an Au surface slab model. In the right panel, the UPS spectrum in the Fermi edge region is shown. A pronounced difference in the photoemission intensity is observed in the low energy band centered at 1.5 eV, where $(DOS)_{DMDTC}$ shows a resonance in the range from 0.9 eV to 2 eV. **(c)** Calculated DOS projected on p-sulfur, p-carbon (2nd carbon on alkyl chain) and on the first Au layer for butanethiol on Au. **(d)** Calculated

DOS projected on *p*-sulfur, *p*-nitrogen and on the first Au layer for DMDTC on Au. Electron density isosurfaces corresponding to relevant bands in the DOS are shown with their respective energies. The band at 1.2 eV is related to antibonding-type sulfur-Au orbitals. While in butanethiol they are restricted to Au *d* and sulfur *p* states, in DMDTC they consist of sulfur *p*, nitrogen *p* and Au *d* states. Above 1.5 eV, the nitrogen *p* contribution becomes significant.

DFT calculations were performed to understand the origin of the features observed in the UPS spectra. DOS and orbitals of the adlayer-Au(111) system are obtained from plane wave DFT calculations (CASTEP) in a periodic slab model, (Figure 1c and 1d). Technical details concerning those calculations are found in the experimental section. Upon relaxation of the molecular adlayer, the projection of the density of states on the DMDTC adlayer $(DOS)_{DMDTC}$ and on the butanethiol adlayer $(DOS)_{But}$ is obtained. The molecular coverage used for these calculations is derived from XPS intensities using hexagonally close packed dodecanethiol SAMs as a reference. $(DOS)_{But}$ shows two pronounced bands centered at 6.2 eV and 4 eV (Figure 1a). To a large extent, they originate from orbitals on the hydrocarbon chain. However, at 6.2 eV, a structure in the *p*-sulfur projection $(DOS)_{p\text{-}S}$ is observed (Figure 1c). This structure, together with the feature at 4.8 eV, is assigned to sulfur-Au bonding orbitals resulting from hybridization of butanethiol frontier orbitals with Au *d* and *s* states. In turn, the band at 1.1 eV represents the corresponding antibonding states. These consist of sulfur 3*p* and Au 5*d* orbitals and do not mix with wavefunctions on the hydrocarbon chain (see the low $(DOS)_{p\text{-}carbon}$ in the region up to 3 eV). The formation of bonding and antibonding states below and above the metal *d* band is a characteristic of molecular chemisorption on metal surfaces[26] and was already reported for cysteine on Au.[23]

In contrast to $(DOS)_{But}$, $(DOS)_{DMDTC}$ shows pronounced resonances around 7 eV and 9 eV (Figure 1b). They originate from non-hybridized orbitals on DMDTC (9 eV) and from bonding type sulfur-Au orbitals (7 eV). Characteristic for $(DOS)_{DMDTC}$ is the high intensity in the range from 1 eV to 7 eV, mainly resulting from sulfur 3*p* and nitrogen 2*p* contributions. In this range, hybridization of DMDTC with metal states occurs and the $(DOS)_{DMDTC}$ deviates significantly from the DOS of a DMDTC layer which is not coupled to Au (Supporting information, Figure S3). Examples for hybrids are the two σ-type sulfur-Au bonding orbitals at 5.4 eV and at 7 eV (Figure 1d). The orbitals show an enhanced overlap of sulfur *p* with Au *d* and *s* states, favored

by the particular geometry of the dithiocarbamate anchor group (Supporting information, Figure S6). In the part of the spectrum which is most relevant for charge transport, i.e. in the region close to E_F, the $(DOS)_{DMDTC}$ exhibits an extended double peaked resonance (~1.5 eV). A closer look at the corresponding molecular orbitals reveals that π-type and σ-type sulfur-Au antibonding states characterize this feature, causing the high photoemission intensity observed in the UPS spectra. However, in contrast to the thiolate case, the DOS and the orbital isosurfaces of DMDTC on Au show that the states from 1.5 eV to 2.8 eV are delocalized from the Au to the nitrogen (Figure 1d), reflecting the resonant structure that dithiocarbamates form in the Lewis picture (Table 1) and showing the nonlocal character of the frontier orbitals on the dithiocarbamate anchor group. The resonant character is attributed both to the planarity of DMDTC (π-system) and to the presence of the nonbonding lone pair on nitrogen, which is energetically close to sulfur *2p* and hence mix with this, forming wavefunctions distributed on the entire dithiocarbamate group (Figure 1d). We stress here that the pseudo-conjugation of the dithiocarbamate-Au antibonding states is considered as one of the main reasons for the efficient coupling of dithiocarbamates to metals, as will be outlined more in detail later. Upon adlayer formation, significant changes are observed in the *d*-band structure of the upper Au layer as a result of molecule-metal interaction. For DMDTC, a depletion in the DOS of the top Au layer is observed between 1.6 eV and 3 eV, whereas the DOS increases in the range from 4.5 eV to 7.5 eV and in a small region around 1 eV (Figure 1d, S3c and S8). Where the $(DOS)_{Au-layer}$ increases, hybrids are formed with the molecular adlayer,[27] as shown by the concomitant features found in $(DOS)_{p-sulfur}$ at 1.3 eV and at 7 eV. A comparison with butanethiol reveals that hybridization-induced changes in $(DOS)_{Au-layer}$ are much more pronounced for dithiocarbamates than for thiols. This is also apparent in charge density difference plots, which show that hybridization of DMDTC states with Au *d* states leads to pronounced charge reorganization (Figure 2).
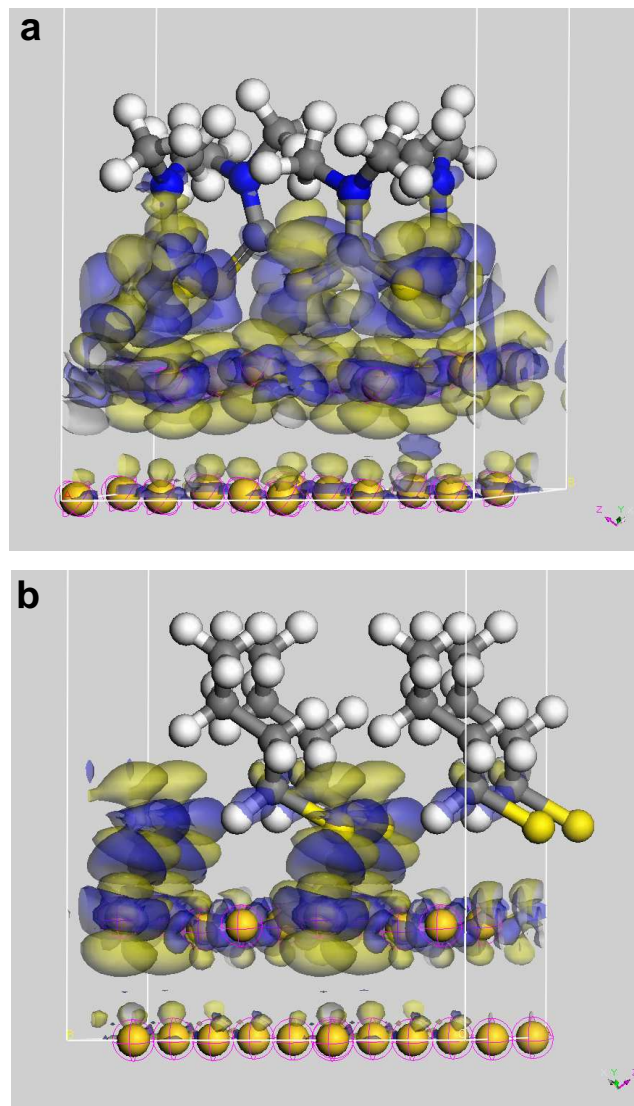
Figure 2. Isosurface plots of the electron density difference between the organic adlayer on Au(111) and the two separate subsystems adlayer and Au(111). The isosurfaces reveal the charge redistribution upon bond formation at the metal-molecule interface. The blue areas indicate an increase of the electron density while the yellow areas indicate electron depletion. The isosurface value was set to 0.01 electrons/Å^3**. a**, DMDTC on Au shows a spatially quite extended charge rearrangement upon hybridization with Au. This involves the whole dithiocarbamate anchor group including the nitrogen atom and the entire first Au layer. **b**, In butanethiol, the isosurfaces are more localized, indicating that hybridization is limited to the sulfur-Au bond. The isosurfaces are displayed in the unit cell volume, while the molecules are represented across the cell boundary. Therefore in **b** the isosurface on the left cell side belongs to the thiolates protruding from the right cell boundary.

As a result of their conductive character, π-conjugated oligomers are of particular interest in molecular electronics and were widely discussed as potential molecular wires.[28,29] We compared the coupling of the aromatic molecular backbone to the metal through dithiocarbamate/thiol anchor groups using two compounds, MPDTC and benzylmercaptane (BM) (Figure 3).
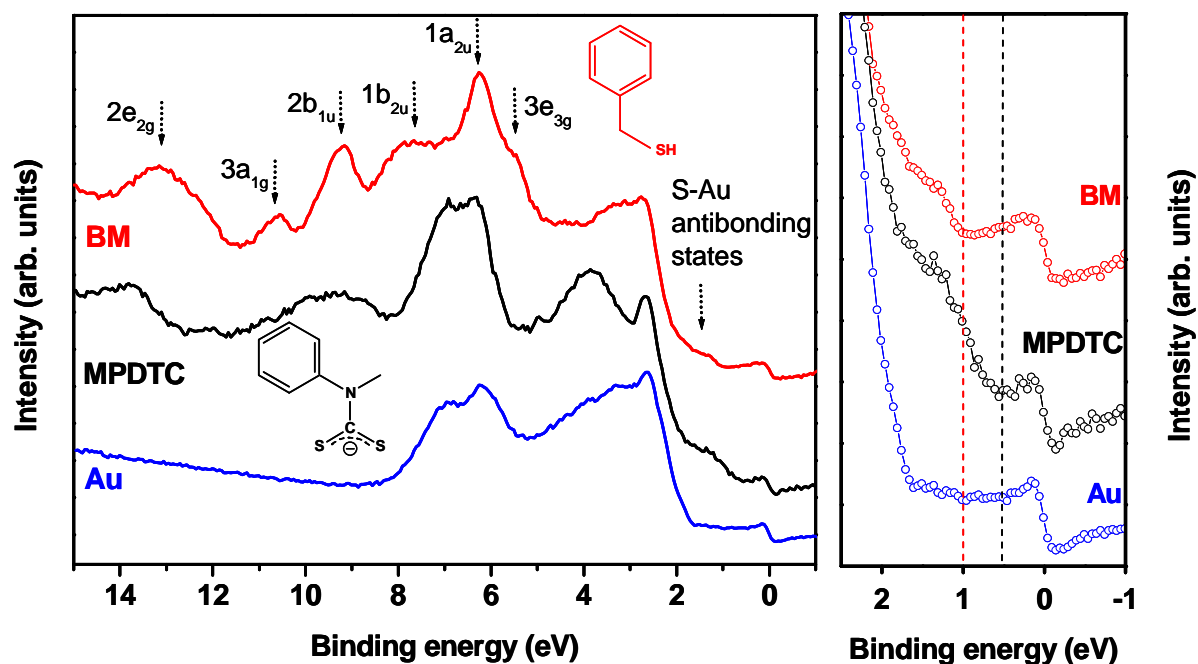
Figure 3. UPS spectra of MPDTC (black) and benzylmercaptane (BM) (red) monolayers on Au(111). The spectrum of a clean Au surface is shown for comparison (blue). The UPS intensity is normalized at the Fermi edge and an arbitrary offset between the plots is introduced for clarity. The resonances in the BM monolayer are energetically close to the lines observed in gas phase spectra of benzene[30] and spectra of benzene multilayers[31]. The position of these lines is indicated by arrows in the figure. They are assigned to molecular orbitals based on DFT calculations by Gokhale et al. on benzene[31]. In MPDTC monolayers, these states are broadened. A line-shift of 0.6 eV results from the higher dipole moment of MPDTC compared to BM. The right panel shows the difference in location and intensity of the bands related to the S-Au antibonding orbitals (HOMOs) close to the Fermi edge. The photoemission threshold of the corresponding resonances is located at 1.0 eV for BM and at 0.5 eV for MPDTC.

The UPS spectra of densely packed BM monolayers (Figure 3) show similar bands as those observed in benzene multilayers,[31] suggesting a weak electronic coupling of the phenyl to the metal substrate. The bands can be attributed to benzene states as reported by Gokhale et al.[31] (Supporting information, Figure S4). Significant changes in the valence band spectrum are observed if the aromatic ring is linked to Au via the dithiocarbamate anchor group. In analogy to DMDTC, the UPS spectrum of MPDTC features a clear resonance centered at 1.5 eV (Figure 3). The photoemission threshold is found at 0.5 eV, i.e. much closer to the Fermi level (E_F) than the threshold for BM monolayers (1.0 eV), indicating that the HOMO of the MPDTC adsorbate is 0.5 eV closer to E_F as well. Such a difference in the position of the adsorbate HOMO is crucial, since it results in a lower energy barrier and thus in a higher conductance across the molecule-Au interface.[32] At higher BE, the bands of MPDTC are shifted and broadened if compared to BM. In particular, the three separate bands in the BM spectrum found at 8 eV, 9.2 eV and 10.7 eV are merged in MPDTC to form a broad band centered at 9.3 eV. DFT calculations show that the structures found in the UPS spectra are well described by the projected density of states of BM and MPDTC on Au (Figure 4). In the whole energy range from the Fermi energy up to 1.6 eV, $(DOS)_{MPDTC}$ is significantly enhanced compared to $(DOS)_{BM}$. The DOS in this range can be related to electronic bands resulting from antibonding sulfur-Au hybrids (both BM and MPDTC), but also from highly delocalized molecular orbitals on MPDTC (right orbital in Figure 4). Indeed, in the planar structure assumed by MPDTC on Au, the *p* orbitals on the nitrogen and on the sulfur atoms hybridize with the π states on benzene forming a pseudo-conjugated system that extends from the phenyl ring to the dithiocarbamate anchor group (right orbital in Figure 4).
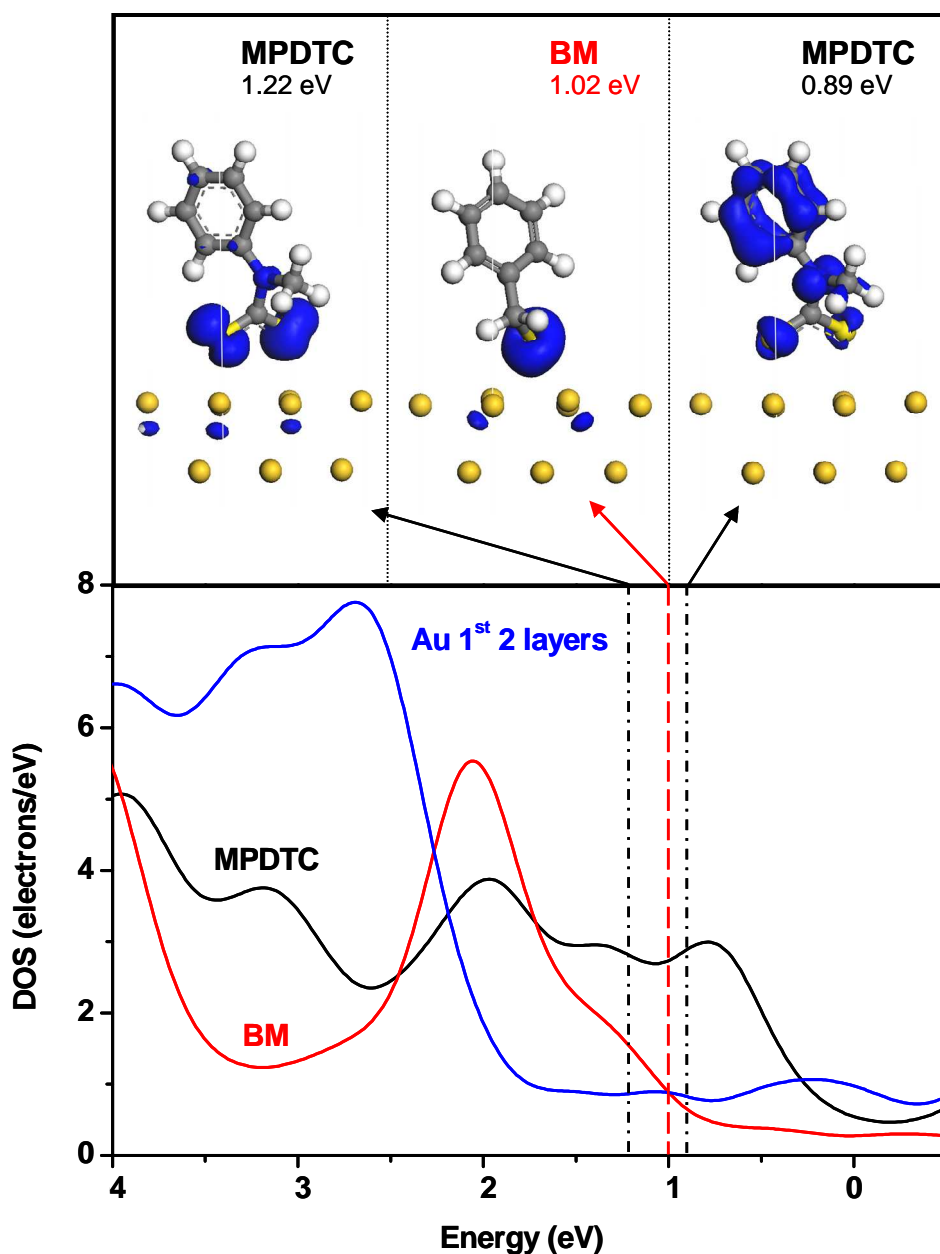
Figure 4. Calculated density of states projected on MPDTC (black) and benzylmercaptane (BM) (red) in an adsorbate-slab model representing the monolayer on Au. In blue, the $(DOS)_{Au}$ of the first 2 layers of a clean Au(111) slab is shown for comparison (divided by 2 for clarity). The isosurfaces in the upper part of the figure show the electron density distribution for those bands that are centered between 0 eV and 1.5 eV. The band centers are marked by red and blue dashed lines for BM and MPDTC, respectively. Due to the pronounced energy dispersion in k-space at the Fermi energy, the bands contribute to the DOS over a broad range from 0 eV to 2 eV. The enhanced DOS of MPDTC compared to BM in the low energy regime is consistent with results from UPS (Figure 3). The bands centered at 1.22 eV (MPDTC) and 1.02 eV (BM) are related to σ^*-type sulfur-Au orbitals. The electron density distribution of the band centered at 0.89 eV reflects the conjugation of MPDTC. The *p* orbitals on the nitrogen and sulfur atoms overlap with the π states on benzene forming a highly delocalized molecular orbital.
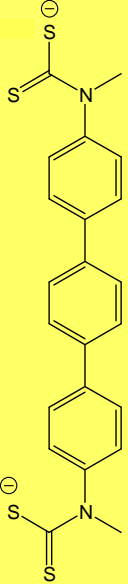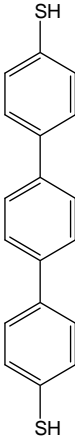
37

A direct consequence is a more efficient electronic coupling between the aromatic molecular backbone and the dithiocarbamate anchor group. Interestingly, in the UPS spectra, a shift of all features to higher BE (ΔE ~0.7 eV) is found for MPDTC. An analog shift (ΔE ~0.6 eV) is observed for the carbon 1s core level (XPS). We believe that this effect, observed for all dithiocarbamates studied in this work (Table 1), results from a surface potential shift[33] induced by the strong molecular dipole moment of the dithiocarbamate anchor group (vide infra).

The body of UPS and DFT data presented so far allows us to point out the main differences that distinguish thiols and dithiocarbamates with regard to their electronic structure. Dithiocarbamates show a significantly higher DOS close to the Fermi level of Au. The DOS is attributed to sulfur-Au antibonding states derived from the molecular HOMO. They show a significant nitrogen contribution and are delocalized both on the entire anchor group and on the metal. The energy gap between the HOMO and the Fermi level, E_F-E_{HOMO}, is 0.5 eV lower than in the thiolate-Au case. Finally, dithiocarbamates show an enhanced overlap of sulfur p states with Au d and s states, which has been reported to improve the electronic coupling between adsorbate and metal[34,12] (Supporting information, Figure S6). All of these factors should result in a lower charge injection barrier across the interface, thus affecting the conductance in metal-molecule-metal junctions.

2.2. Conductivity of three dimensional networks of interlinked nanoparticles

The impact of the dithiocarbamate anchor group on charge transport has been investigated experimentally by comparison of the conductivity of 3-dimensional networks of Au nanoparticles[35,18,36] interlinked with terphenyl-dithiols (TPT) and terphenyl-bis-dithiocarbamates (TPMDTC) (Table 2 and supporting information). These two molecules consist of an identical aromatic backbone substituted with either a thiol or a dithiocarbamate end-group, allowing a direct comparison of the electrical coupling of thiolates and dithiocarbamates to Au. Since the nanoparticle networks consist of a very large number of metal-molecule-metal junctions, the measured conductivity values represent a statistical average. The conductivity of nanoparticle films interlinked with terphenyl-bis-dithiocarbamates ($\sigma = 22.7 \pm 6~\Omega^{-1}m^{-1}$) is found to be about one order of magnitude higher than that of nanoparticle films interlinked

with terphenyl-dithiols ($\sigma = 2.8 \pm 3 \ \Omega^{-1}m^{-1}$). This difference in conductivity is in agreement with the conclusions we derived from the UPS and DFT results presented above.

TPMDTC	TPT
$\sigma = 22.7 \ \Omega^{-1}m^{-1}$	$\sigma = 2.8 \ \Omega^{-1}m^{-1}$

Table 2. Molecular structure of terphenyl-dithiol (TPT), terphenyl-bis-dithiocarbamate (TPMDTC) and conductivity values of TPT- and TPMDTC-interlinked nanoparticle networks.

2.3. XPS characterization of dithiocarbamate and thiol monolayers

For the chemical analysis of the monolayers, XPS measurements are done on DMDTC, MCDTC, MPDTC and DHDTC monolayers (Table 1). In the sulfur $2p$ region, a characteristic $2p_{1/2}/2p_{3/2}$ doublet structure with the $2p_{3/2}$ component centered at a binding energy of 161.9 eV is observed (Figure 5). This value is ~0.2 eV lower compared to the typical binding energy measured for thiolates chemisorbed on Au,[37] indicating that in dithiocarbamates the sulfur atoms are more negatively charged than in thiolates.[20]
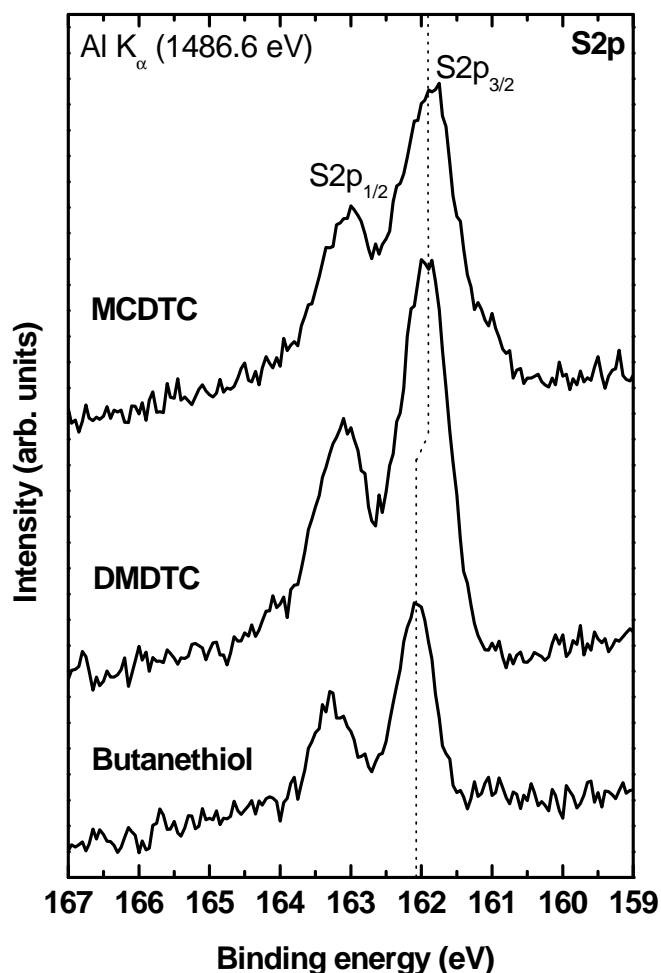
Figure 5. XPS spectra of butanethiol, DMDTC and MCDTC monolayers on Au(111) in the sulfur $2p$ region. The sulfur $2p_{3/2}$ and $2p_{1/2}$ components are separated by 1.18 eV and the relative $2p_{3/2}/2p_{1/2}$ area ratio is 2/1. An arbitrary offset between the plots has been introduced for clarity. The characteristic energy of ~162 eV for the right peak ($2p_{3/2}$) of the sulfur $2p$ doublet is indicative of chemisorption to Au. A relative chemical shift by 0.2 eV to lower binding energy and an increase in the FWHM by 0.3 eV distinguish dithiocarbamates from butanethiol. A small component at 161 eV is detected in MCDTC monolayers, possibly caused by dithiocarbamates bound to Au as a monodentate.

As a further distinction, the full width at half maximum of the sulfur $2p_{3/2}$ and $2p_{1/2}$ components in the XPS spectra of dithiocarbamate monolayers is roughly 0.3 eV larger than in thiol SAMs. We attribute this effect to a partial reconstruction of the Au(111) surface upon monolayer formation. This is supported by observations of strongly corrugated Au step edges in STM images, suggesting a perturbation of the Au(111) surface lattice due to the dithiocarbamate adlayer. A comparison of the

nitrogen $1s$ and sulfur $2p_{1/2}/2p_{3/2}$ peak areas shows a reasonable agreement with the expected stoichiometric value of 1:2 for all compounds, ruling out any decomposition of dithiocarbamates at the surface. The coverage of MCDTC, MPDTC, and DHDTC monolayers on Au, as determined from the sulfur $2p$/Au $4f$ intensity ratio, is approximately 25% lower than that of DMDTC, butanethiol and BM monolayers. At the given coverage, plane wave DFT calculations with a Au slab model provide evidence that all compounds assume a "standing-up" orientation on Au, forming close packed monolayers (Supporting information, Figure S2). The shift to lower binding energy in the sulfur $2p_{3/2}$ component of dithiocarbamates is consistent with DFT calculations, that show a nitrogen-mediated transfer of negative electronic charge from the two methyl groups to the two sulfur atoms of DMDTC, causing a higher negative charge on DMDTC sulfur (-0.1 e) compared to butanethiol sulfur (-0.04 e). The charge transfer from the methyl groups to the sulfur atoms further results in a dipole moment of 4.4 Debye for DMDTC (1.8 Debye for butanethiol), which is expected to create a dipole layer at the surface[33] and thus to modify the work function of the metal. Consistently, UPS measurements reveal a 0.2 eV lower work function (4.0 eV) of the DMDTC-modified surface compared to the thiol-modified Au(111) surface (Supporting information, Figure S7).

2.4. Chemisorption energy of dithiocarbamates and thiols to Au

The thermal stability of the metal-molecule interface is a key factor for the fabrication of molecular-based devices. In consideration of the particular binding geometry of dithiocarbamates to metals, one would expect a higher binding energy of these compounds compared to thiolates. To verify this hypothesis, we determined the chemisorption energy of thiols and dithiocarbamates to Au(111) by thermal desorption of the SAMs, i.e. by monitoring the changes of the sulfur $2p$ and nitrogen $1s$ XPS signals while the sample temperature is ramped from 300 K to 500 K in an UHV chamber (see Appendix B for experimental details). The desorption peaks of butanethiol and DMDTC are found at a temperature of 380 ± 10 K and 450 ± 10 K, respectively. Using the Redhead equation[38] we obtain approximate desorption energies of 119 ± 2.7 kJ/mol for butanethiol and of 138 ± 2.8 kJ/mol for DMDTC. In case of butanethiol, just before the onset of desorption (T ~370-380 K) we observe a shift in the sulfur $2p$ binding energy from 162 eV to 161 eV, which could indicate the

beginning of lateral diffusion of thiols on the Au surface. This is in agreement with the solid-liquid phase transition at 370 K reported for a full coverage dodecanethiol SAM.[15] In contrast, the sulfur $2p$ signal of the DMDTC SAM remains stable up to a temperature of ~450 K. The higher chemisorption energy of dithiocarbamates to Au is regarded as a consequence of their bidentate binding to the Au surface. It is consistent with experiments showing that dithiocarbamate SAMs are stable towards displacement by thiols from solution.

3. Conclusions

In conclusion, electron spectroscopy and simulation methods have shown the presence of delocalized electronic states on the dithiocarbamate anchor group linked to Au. The proximity of these states to the Fermi level of Au and the enhanced DOS that they provide in this energy range let us conclude that the dithiocarbamate anchor group reduces the charge injection barrier, thus promoting the formation of a more conductive metal-molecule interface compared to the well known thiol-Au contact. The electronic structure, the bond stability and the ability to functionalize metal surfaces with a broad range of substituents are features that make the dithiocarbamate anchor group promising for molecular electronic devices and interesting as a metal-organic interface in organic light emitting diodes and light sensitive devices. Since the described binding behavior is of general nature, dithiocarbamates are expected to show similar properties upon binding to other metals.

4. Experimental Section

Self-assembled monolayers. Atomically flat Au(111) surfaces are prepared by flame-annealing of thin Au films (100 nm) evaporated on freshly cleaved mica. Dithiocarbamate SAMs are prepared in a glove box by immersing the Au(111) surfaces into a 10 mM ethanolic mixture of CS_2 and the corresponding amine precursor. Butanethiol, dodecanethiol and benzylmercaptane SAMs are obtained by immersing the Au surfaces in 0.5 mM ethanolic solutions of the respective thiols. After preparation, the samples are rinsed thoroughly in ethanol. Both for dithiocarbamates and for thiols the assembly time is ~24 hours. All solvents are saturated with argon before usage. All chemicals, except for N,N-dimethylamine

(Fluka), are obtained from Sigma-Aldrich and used without further purification. The monolayer structure could be determined by STM only for dodecanethiol and benzylmercaptane SAMs, revealing a hexagonally close packed ($\sqrt{3}$ x $\sqrt{3}$)R30° phase on Au(111). The adlayer coverage is extracted from XPS data as referenced to a hexagonally close packed dodecanethiol monolayer.

UPS spectroscopy. UPS spectra are obtained using a helium UV lamp as a source. The gas pressure in the lamp is adjusted in such a way that He I (hυ= 21.2 eV) and He II (hυ = 40.8 eV) light is emitted at a ratio of approximately 4:1. The light is incident at an angle of 55° from the sample normal and the photoelectrons are collected by an energy dispersive hemispherical analyzer at a takeoff angle of 90°. The analyzer is set to a pass energy of 5 eV, providing an instrumental resolution of about 0.14 eV. Binding energies are referenced to the Fermi level of a clean, argon ion-etched Au surface and defined as positive for occupied states below the Fermi level.

XPS spectroscopy. XPS spectra are recorded using an Al K_α (1486.6 eV) line as a source. With an X-ray monochromator and a pass energy of 20 eV for the analyzer an instrumental resolution of 0.45 eV is achieved (Kratos Axis Ultra). Elemental ratios are determined by comparison of the normalized peak areas from the respective core level spectra. Sensitivity factors are obtained from the Kratos database and calibrated using reference samples. Monolayer coverages are determined from sulfur 2p/Au 4f intensity ratios and are referenced to dodecanethiol SAMs. Desorption experiments are performed ramping the sample temperature and acquiring XPS spectra at temperature intervals of 10 K. During XPS acquisition, the temperature is kept constant. The heating rate, averaged over the entire measurement, is ~1 K/min. A first order desorption kinetics is assumed and a value of 10^{13}/s for the frequency factor is employed. Since the heating rate is not constant and the coverage determined at discrete temperatures, the chemisorption energies determined using the Redhead equation are approximate values.

Plane wave DFT calculations. For butanethiol, DMDTC, BM and MPDTC, a two layer Au(111) slab in a periodic (2$\sqrt{3}$ x 2$\sqrt{3}$)R30° unit cell is employed to model the surface. In agreement with experimental packing densities, 4 molecules/cell for butanethiol and DMDTC are chosen. For BM and MPDTC, the calculations were also done using a Au slab having 4 atomic layers and a periodic ($\sqrt{3}$ x $\sqrt{3}$)R30° unit cell. The vacuum gap thickness between adlayer and the Au layer of the adjacent cell is

about 20 Å. DFT calculations are performed using a plane wave basis set with a cutoff energy of 320 eV. For the DFT functional, the revised generalized gradient approximation of Perdew, Burke and Ernzerhof (RPBE) is employed, as provided by the CASTEP code.[39] The ionic cores are described by ultrasoft pseudopotentials. The Brillouin zone is modeled including 5 Monkhorst-Pack k-points in the (2√3 x 2√3)R30° unit cell and 18 Monkhorst-Pack k-points in the (√3 x √3)R30° unit cell. Comparison of the calculations using 2 and 4 Au layers show that two Au layers are sufficient to reproduce the density of states of the molecular adlayers. The adlayers are first relaxed and the DOS subsequently obtained from the energy minimized structures. For comparison with UPS data, the projection of the density of states on the molecular adlayer or on single atoms (including specific angular momentum components) is computed. In all plots, the DOS is shifted in energy by 0.35 eV to match the UPS spectrum. The energy scale in the plots is referenced to the Fermi level. Details about the structure of the adlayers on Au are provided in Figure S2 (supporting information).

Atomic orbital based DFT calculations. DFT calculations at the B3LYP theory level with a LanL2DZ basis set are performed using the Gaussian 98 program suite.[40] The simulations are done on molecules coupled to a single Au atom through their anchor groups. Energy levels and molecular orbital isosurfaces are obtained upon relaxation of the structures. Hirshfeld charges are computed at the BLYP theory level using Dmol3.[41] The molecule-Au_1 complex is a simplified model system to understand the electronic structure of dithiocarbamates on Au.

Supporting Information

Figure S1: UPS spectra of Dialkyl-dithiocarbamate SAMs on Au(111) with different chainlengths: Dimethyl-dithiocarbamate (DMDTC) (black), N,N-dihexyl-dithiocarbamate (DHDTC) (blue) and N,N-didecyl-dithiocarbamate (DDDTC) (red). An arbitrary offset between the plots and scaling factors for DHDTC (x 2) and DDDTC (x 4) were introduced for clarity. The resonance at 1.5 eV binding energy decreases in intensity with increasing thickness of the hydrocarbon layer. This is a consequence of inelastic scattering of photoelectrons emitted from the dithiocarbamate anchor group, yielding an electron attenuation length of ~0.5 nm for alkanethiol SAMs.
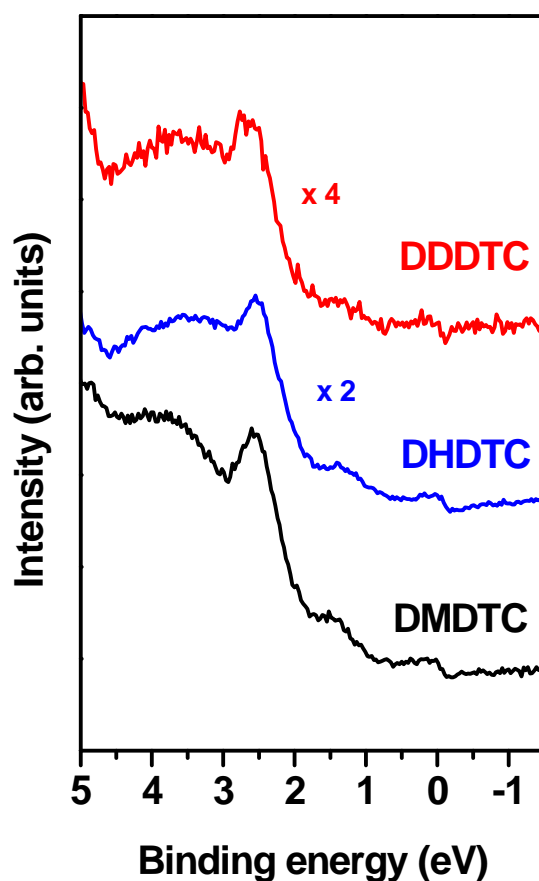
Figure S2: Relaxed structure of butanethiol (a) and DMDTC (b) monolayers on a periodic Au(111) slab. (a) The number of butanethiol molecules/unit cell corresponds to the packing density of a hexagonally close packed dodecanethiol monolayer on Au(111)(($\sqrt{3}$ x $\sqrt{3}$)R30° overlayer structure), since XPS results show comparable coverages for butanethiol and close packed dodecanethiol monolayers. In the relaxed structure (equilibration of butanethiol and of the top Au layer), butanethiol is chemisorbed to Au(111) with the sulfur atom located in between a "bridge site" and an "on top site". The next-neighbor S-Au bond distance is 2.32 Å and the tilt angle of the butane backbone towards the surface normal is 30°. (b) The same number of molecules/unit cell is employed for DMDTC and for butanethiol monolayers, based on experimental packing densities (see XPS analysis in text). In the equilibrium structure, DMDTC is mostly chemisorbed to Au(111) with one sulfur atom at the "bridge site" the other one close to the "on top site", resulting in an orientation of the S-S axis along the [11-2] direction. The S-S distance is 3.03 Å and the next-neighbor S-Au distance varies between 2.42 Å and 2.6 Å. The DMDTC backbone is oriented perpendicularly to the surface. Due to the larger number of possible local energy minima in the potential energy surface of DMDTC on Au, other equilibrium structures cannot be ruled out. Note that the intermolecular dispersion forces are not fully accounted for within the DFT model.

Figure S2:

a
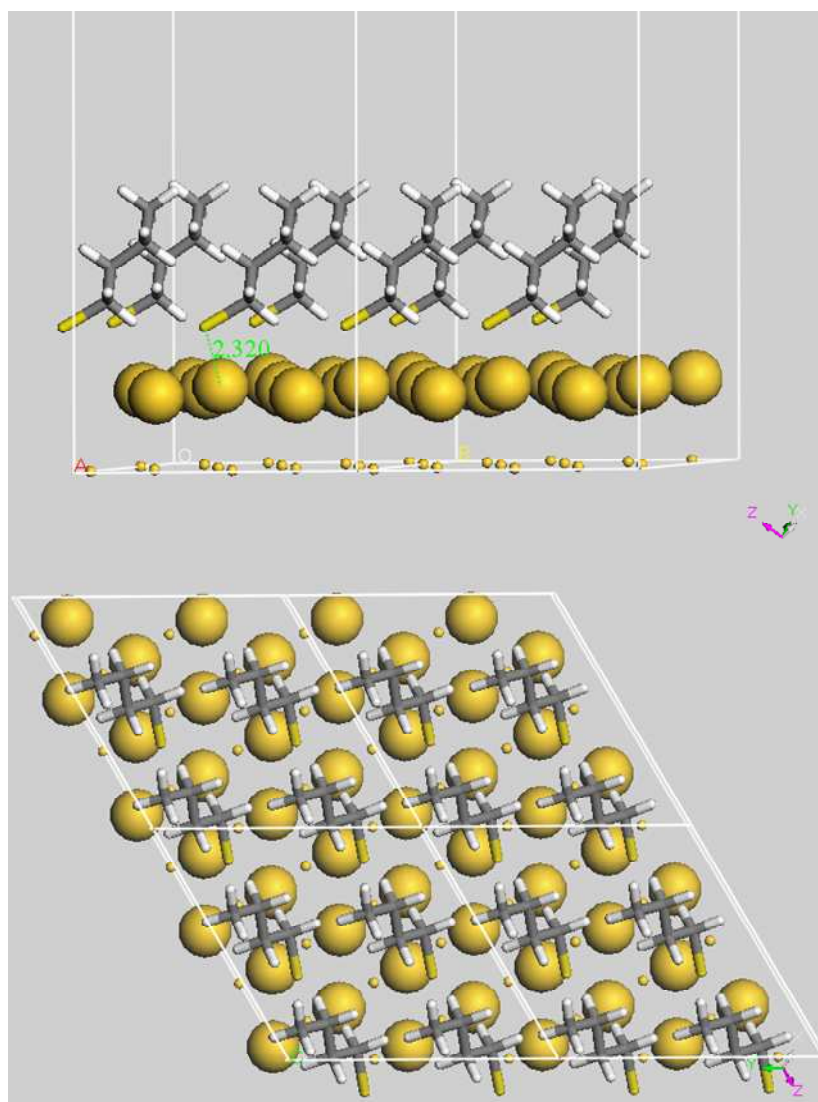
b
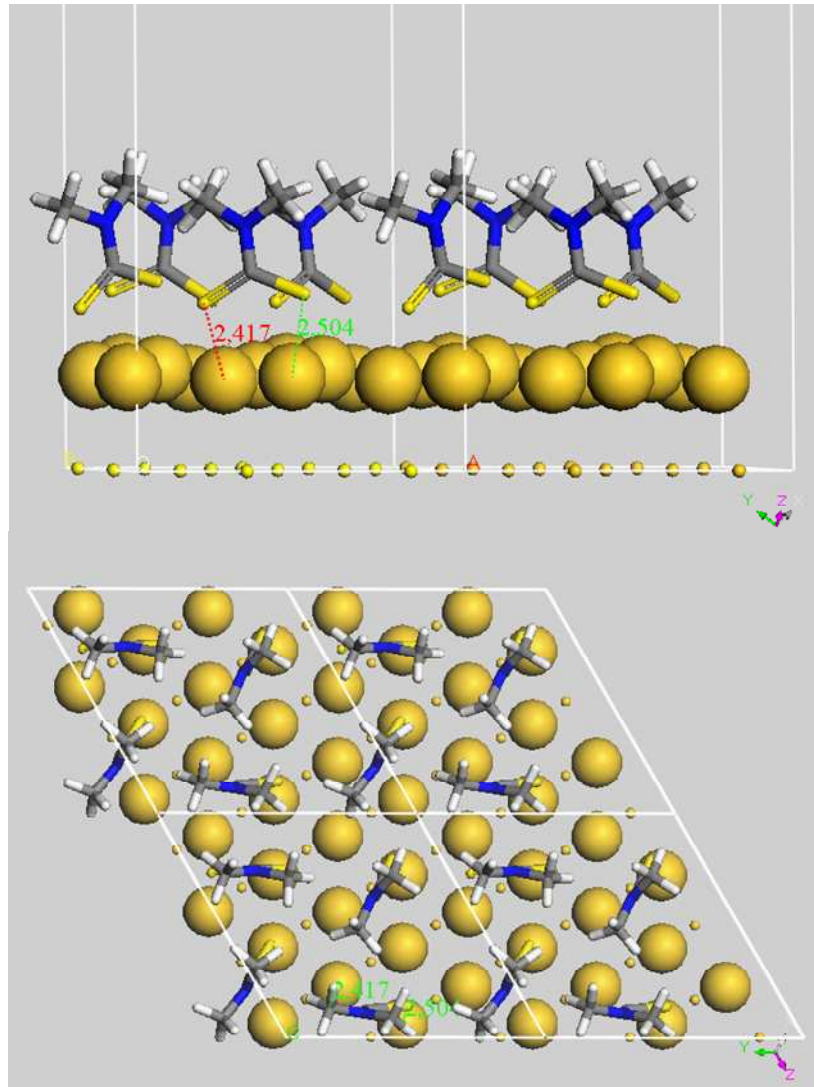
Figure S3: **(a and b)** Comparison of the DOS obtained from an uncoupled molecular adlayer with the projection of the DOS on the adlayer $(DOS)_{adlayer}$ in a coupled adlayer-Au system. Energies are negative for occupied states in the valence band. **(a)** $(DOS)_{DMDTC}$ on Au shows a pronounced valence band reconstruction between 0 eV and -6 eV. **(b)** $(DOS)_{But}$ on Au shows a less pronounced reconstruction, mainly in the region between 0 eV and -2.5 eV. **(c)** DOS projected on the first Au layer in the slab model of DMDTC on Au (blue), butanethiol on Au (red) and without the presence of an adlayer (black). The pronounced difference in the $(DOS)_{1st\ Au\ layer}$ observed between the DMDTC-Au system and the slab without adlayer is a result of the hybridization of DMDTC states with the Au *d*-band, also expressed in a shift of the whole d band to lower energies and in the formation of a shoulder at ~1 eV. For comparison with Fig. 1a-d the DOS has to be shifted in energy by - 0.35 eV.
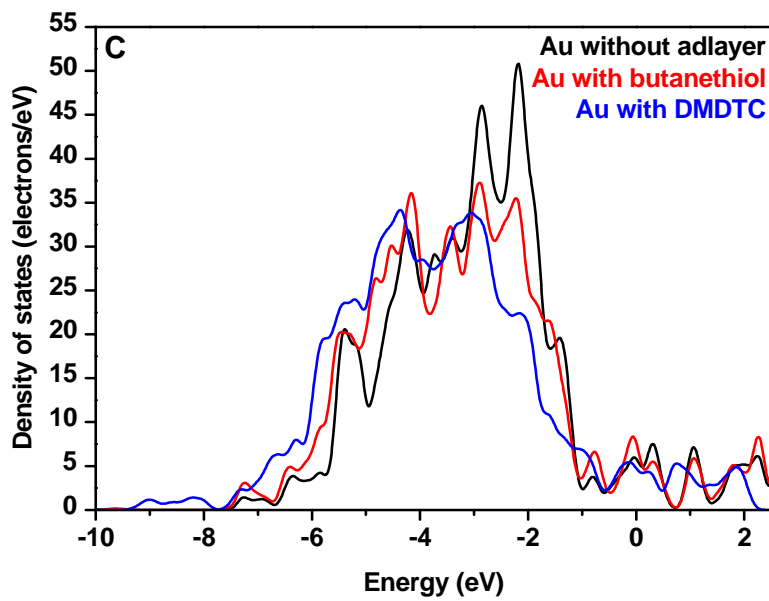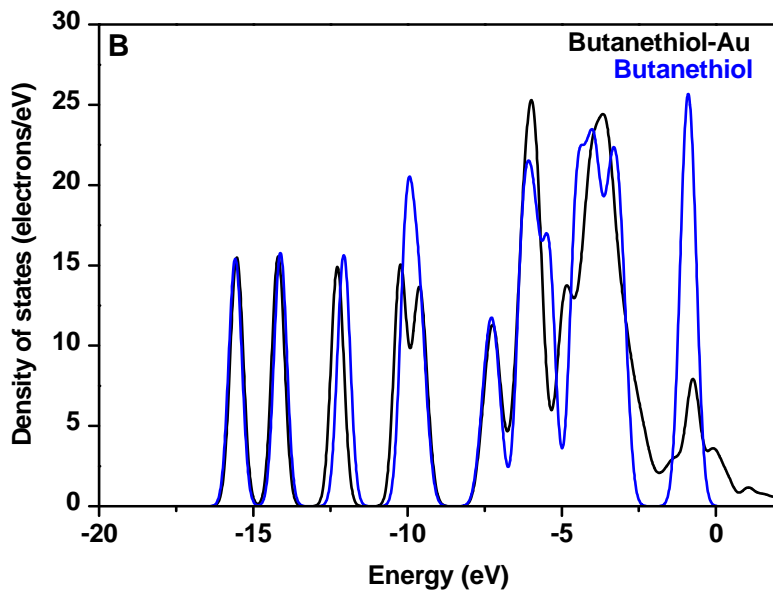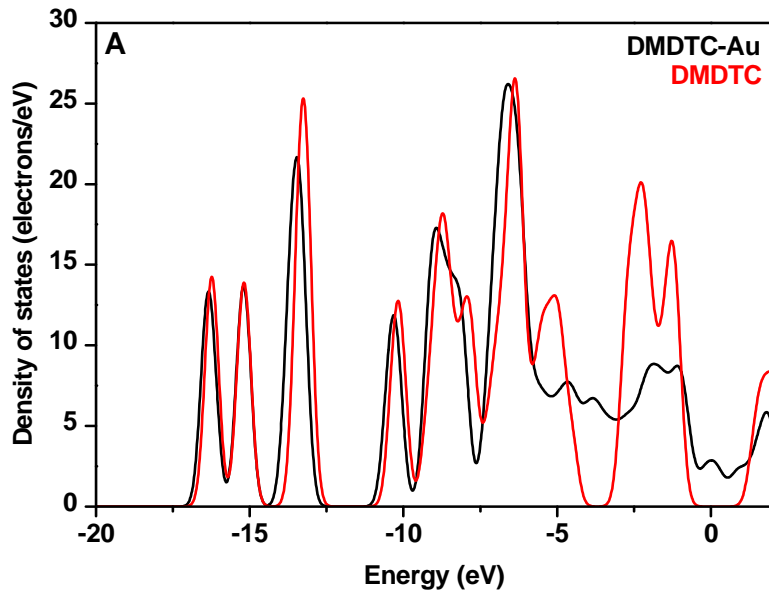
Figure S4: UPS difference spectra (the spectrum of a clean Au surface is subtracted) of BM and MPDTC monolayers on Au(111). The typical benzene bands observed in BM monolayers are related to electronic states obtained from benzene calculations (at the LCGTO-DF level) from Gokhale et al. (Ref. 30 in article). For MPDTC, these bands are shifted and broadened. The line at 13.1 eV, corresponding to the $2e_{2g}$ orbital of benzene, is shifted to 13.8 eV, while the three separate bands at 8 eV, 9.2 eV and 10.7 eV($1b_{2u}$, $2b_{1u}$ and $3a_{1g}$) are merged and form a broad band centered at 9.3 eV. The two lines at 5.6 eV and 6.3 eV ($3e_{2g}$ and $1a_{2u}$) are shifted by 0.7 eV to higher BE as well, showing a decrease in peak resolution. Finally, the spectrum shows a broad resonance centered at 4 eV, which is not found in BM. Overall, a rigid shift of benzene lines by ~0.7 eV towards higher binding energies is found, consistently with a shift by ~0.6 eV observed for the carbon 1s XPS signal. It is interpreted as a result of the strong dipole moment of MPDTC and is also observed in SAMs of other dithiocarbamate monolayers.
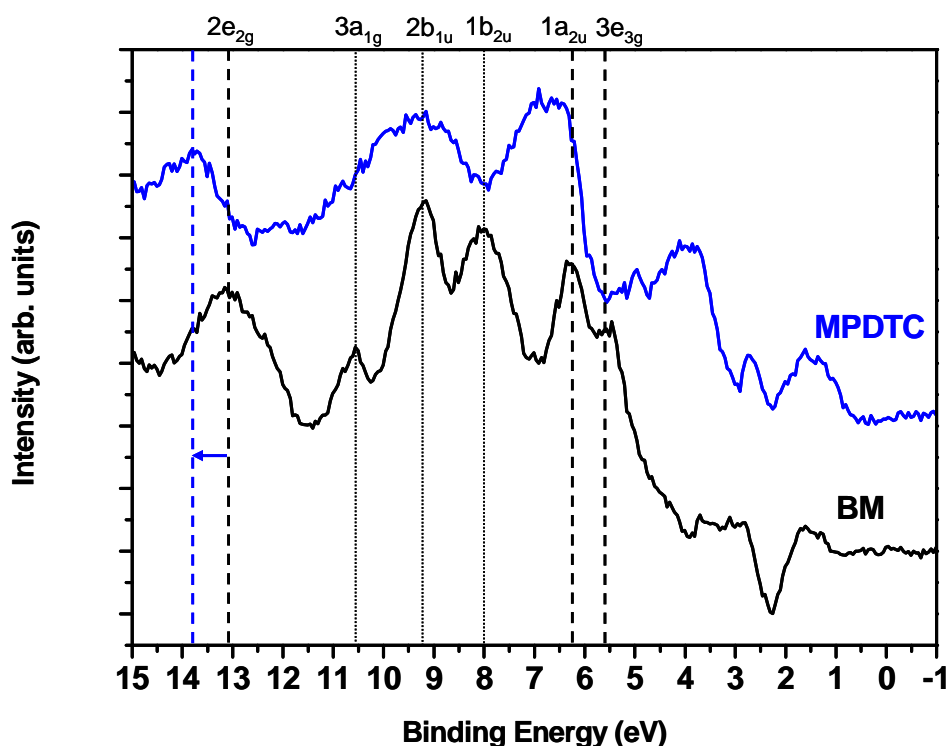
Figure S5. Molecular orbital surfaces illustrating the dependence of conjugation on the tilt angle between the CS_2 plane and the plane of the benzene ring in MPDTC. Upon relaxation in the gas phase, the two planes are orthogonal and the electronic states on the dithiocarbamate anchor group are well separated from π states on benzene. In the planar geometry, the p_z orbitals of the nitrogen atom overlap with the π states of the benzene forming a partially conjugated system delocalized over the whole molecular structure, including Au d states. The MPDTC-Au_1 complex is modeled by an atomic orbital based DFT calculation (Gaussian B3LYP/LanL2DZ).

MPDTC

Orientation in gas phase (orthogonal geometry)	Orientation in SAM (planar geometry)
E_{HOMO} - 2.1 eV	E_{HOMO} - 2.3 eV
E_{HOMO} - 0.8 eV	E_{HOMO} - 0.5 eV
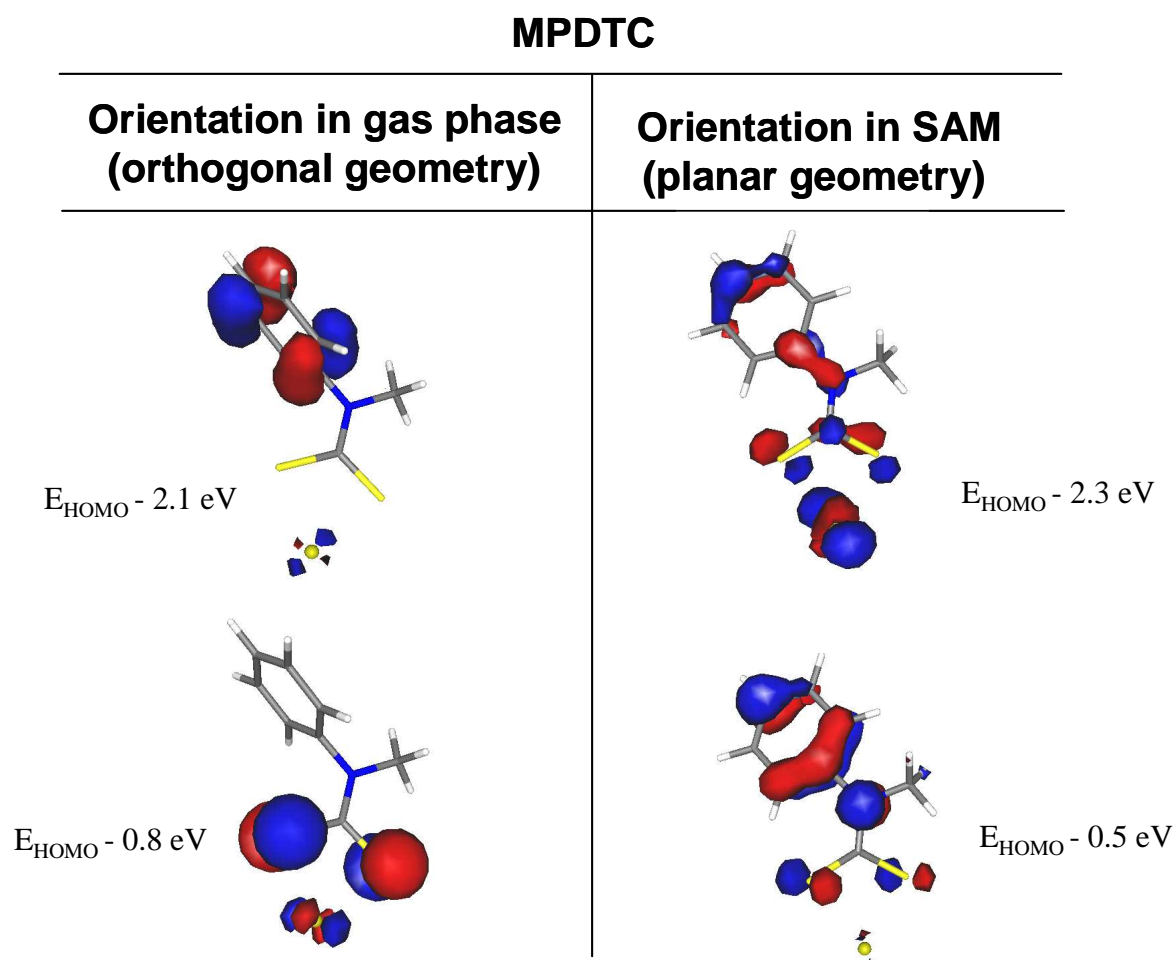
Figure S6: Selected bonding sulfur-Au molecular orbitals of a DMDTC-Au$_1$ and a butanethiol-Au$_1$ complex derived from DFT calculations using the B3LYP/LanL2DZ theory level. The molecule-Au$_1$ complex is utilized to exemplify the molecular orbital structure in a simplified model system. The calculations show that, as a result of the geometry of the dithiocarbamate anchor group, both sulfur $3p$ lobes of DMDTC are oriented towards the Au atom, increasing the overlap between metal and molecular states (Ref. 13 and 33 in article).

DMDTC	Butanethiol
E_{HOMO} - 4 eV	E_{HOMO} - 5.5 eV
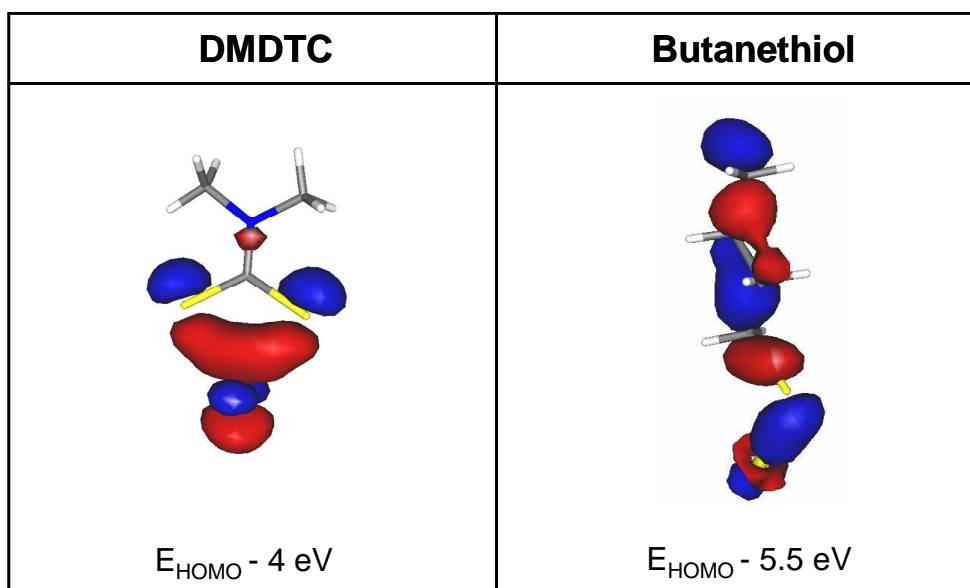
Figure S7: Photoemission threshold in the UPS spectra of DMDTC and butanethiol monolayers on Au(111). The work function, as determined from the position of the photoemission threshold and the Fermi edge, is 4.2 eV for butanethiol and 4.0 eV for DMDTC. This difference is related to the larger molecular dipole moment of DMDTC (4.4 Debye) compared to butanethiol (1.8 Debye).
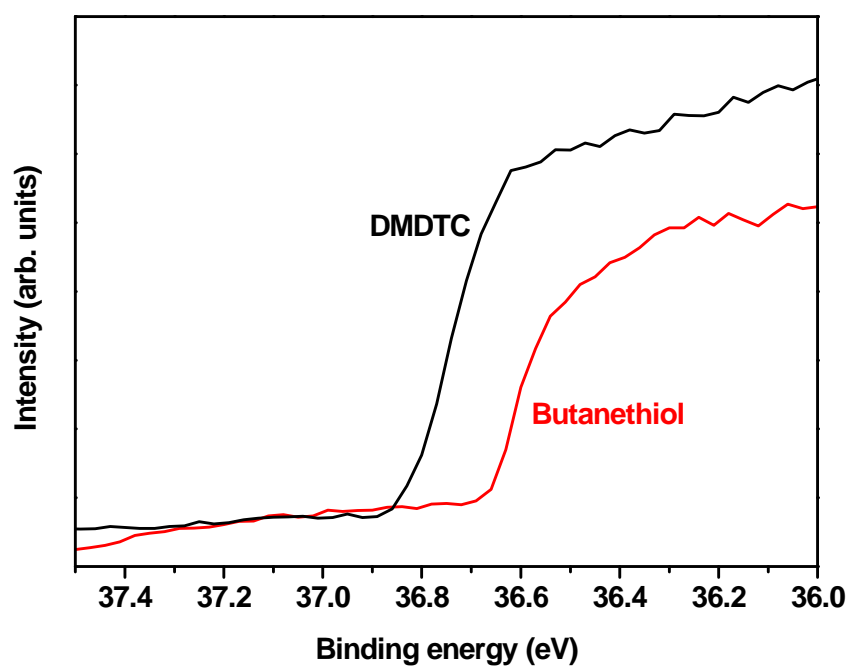
Figure S8: *s*, *p* and *d* components of (DOS)$_{1st\ Au\ layer}$ for the adlayer-Au(111) system in a slab model. (a) Butanethiol adlayer. (b) DMDTC adlayer. Note the high contribution of Au *s* states in the range where sulfur-Au bonding states are formed, e.g. from -5.5 eV to -8 eV. Au *s* and *p* states also contribute in the Fermi energy region. In the graph, energies are negative below E$_{Fermi}$.
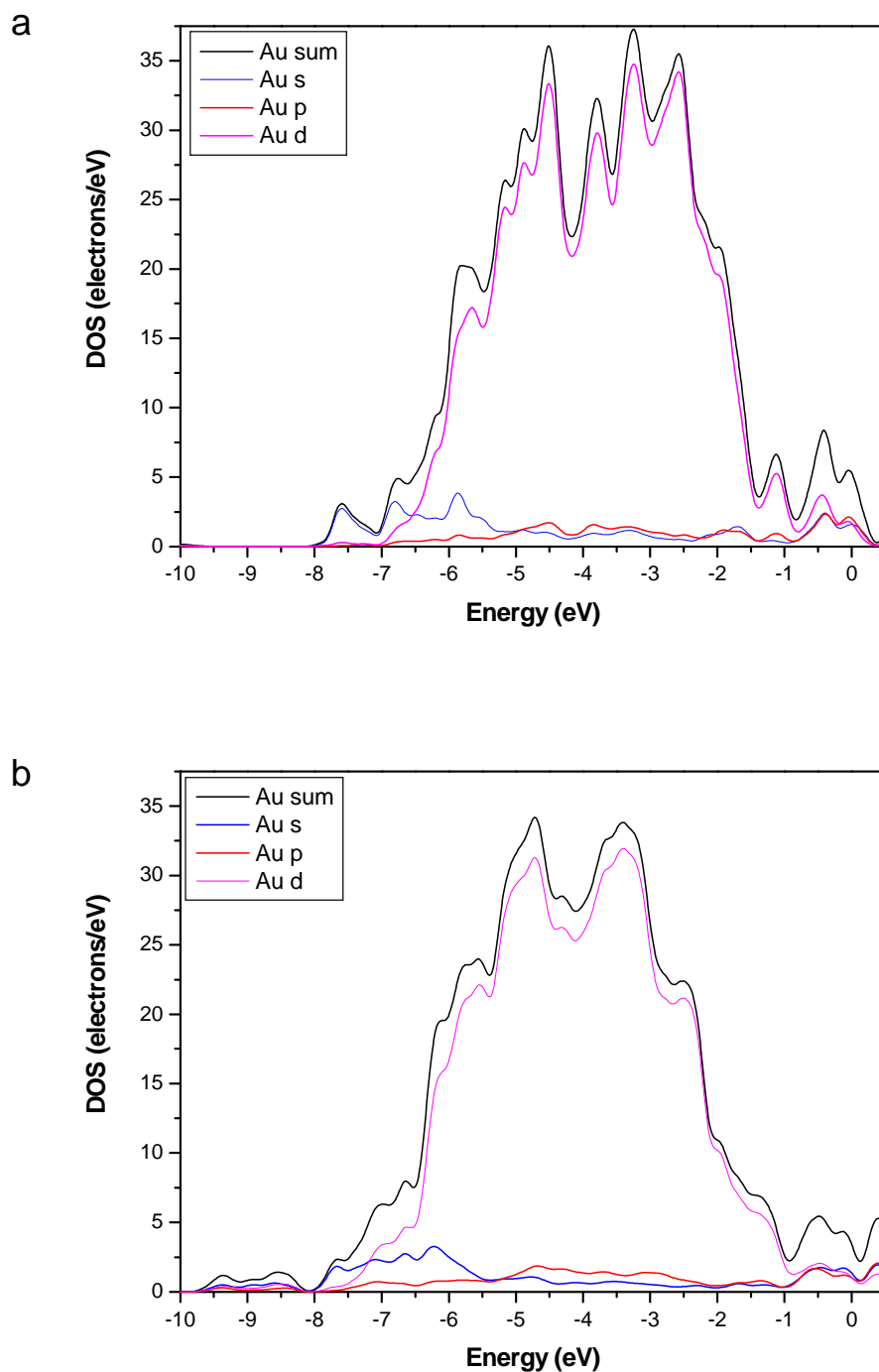
Synthesis:

^{1}H/^{13}C-NMR spectra are recorded on a Bruker AV400 instrument. Chemical shifts are given in ppm relative to TMS. Abbreviations: *s*, singlet; *d*, doublet; *t*, triplet; *q*, quartet; *m*, multiplet. All chemicals are used as provided without any further purification. Solvents used are of HPLC grade. EL analysis is done by Mikroanalytisches Labor Pascher (An der Pulvermühle 1, D-53424 Remagen-Bandorf, Germany). MS analysis is performed with a Shimadzu LC-MS 2010.

1,1´:4,1´´-terphenyl-4, 4´´-dithiol (TPT) is prepared according to literature procedures.[1]

The preparation of N,N'-dimethyl-1,1':4',1"-terphenyl-4,4"-diamine (MATP) is done in close analogy to the synthesis of the corresponding N,N'-diethyl-1,1':4',1"-terphenyl-4,4"-diamine.[2]

N,N'-dimethyl-1,1':4',1''-terphenyl-4,4''-diamine (MATP):

A 250 ml 2-neck flask equipped with a condenser and a rubber stopper is charged with 4´-bromo-*N*-methylaniline (4,38 g, 186,05 gmol^{-1}, 24 mmol, 2.6 eq.), 1,4-phenylenebisboronic acid (1.5 g, 165.75 gmol^{-1}, 9 mmol, 1 eq.), K_3PO_4 (13.45 g, 212.27 gmol^{-1}, 63 mmol, 7 eq.). 40 ml DMF and 40 ml H_2O are added and the mixture is flushed with a stream of argon for about 10 min to remove remaining oxygen. $PdCl_2(PPh_3)_2$ (640 mg, 701.89 gmol^{-1}, 1 mmol, 0.1 eq.) is added and the solution is heated under reflux and argon atmosphere for 2 hrs at 110°C (oil bath temperature) while vigorously stirred. After cooling down to room temperature the reaction mixture is diluted with chloroform (~ 100 ml) and excess solid particles are filtered off. Water is added to the organic phase until a phase separation occurrs. The organic phase is further diluted with chloroform (~ 100 ml) and washed several times with

---

[1] de Boer, B.Meng,H., Perepichka, D. F., Zheng, J., Frank, M. M., Chabal, Y. L., Bao Z. *Langmuir* **2003,** *19,* 4272-4284.

[2] Tominaga, M., Masu, H., Katagiri, K., Kato, T., Azumaya, I. *Organic Letters* **2005**, 7 (17), 3785-3787.

water, finally dried over $MgSO_4$ and the solvent is evaporated *in vacuo*. The crude product is purified via column chromatography (silica gel, dichloromethane as eluent, $R_f = 0.9$). Yield 1.27 g (49%).

^{1}H-NMR (400.13 MHz, CD_2Cl_2) δ: 2.85 (s, 6H, -CH_3), 3.86 (s, 2H, -NH-), 6.67 (d, $^2J = 8.8$ Hz, 4H, -Ar-H), 7.46 (d, $^2J = 8.8$ Hz, 4H, Ar-H), 7.55 (s, 4H, Ar-H).

^{13}C-NMR(100.62 MHz, $CDCl_3$) δ:148.60 (C_q), 138.95 (C_q), 129.86 (C_q), 127.68 (*C*H), 126.45 (*C*H), 112.65 (*C*H), 30.76 (CH_3). MS (APCI, *m/z*) calcd. for $C_{22}H_{24}N_3$ (M+H$^+$+CH_3CN) 330.20, found 330.0, calcd. for $C_{24}H_{27}N_4$ (M+H$^+$+2*CH_3CN) 371.22, found 371.0. Elemental analysis calcd. $C_{20}H_{20}N_2$ (%): C 83.30, H 6.99, N 9.71; found: C 83.28, H 6.87, N 9.58.

UV/Vis ($CHCl_3$): $\lambda_{max} = 323$ nm ($\varepsilon = 39500$ cm^{-1}M^{-1})

References

[1] 2005 Semiconductor Industry Association, International Technology Roadmap for Semiconductors 2005 Edition, Emerging Research Devices; www.itrs.net/Common/2005ITRS/Home2005.htm.

[2] A. Aviram, M. A. Ratner, *Chem. Phys. Lett.* **1974**, *29*, 277.

[3] C. Joachim, J. K. Gimzewski, A. Aviram, *Nature* **2000**, *408*, 541.

[4] R. Landauer, *IBM J. Res.* **1957**, *1*, 223-231.

[5] A. Nitzan, M. A. Ratner, *Science* **2003**, *300*, 1384.

[6] R. G. Nuzzo, D. L. Allara, *J. Am. Chem. Soc.* **1983**, *105*, 4481.

[7] A. Ulman, *An Introduction to Ultrathin Organic Films*, Academic Press, **1991**.

[8] F. Schreiber, *Prog. Surf. Sci.* **2000**, *65*, 151.

[9] Y. Xue, S. Datta, M. A. Ratner, *J. Chem. Phys.* **2001**, *115*, 4292.

[10] T. Ishida, M. Hara, I. Kojima, S. Tsuneda, N. Nishida, H. Sasabe, W. Knoll, *Langmuir* **1998**, *14*, 2092.

[11] H. Sellers, A. Ulman, Y. Shnidman, J. E. Eilers, *J. Am. Chem. Soc.* **1993**, *115*, 9389.

[12] P. E. Kornilovitch, A. M. Bratkovsky, *Phys. Rev. B* **2001**, *64*, 195413.

[13] Z. J. Donhauser, B. A. Mantooth, K. F. Kelly, L. A. Bumm, J. D. Monnell, J. J. Stapleton, D. W. Price, Jr., A. M. Rawlett, D. L. Allara, J. M. Tour, P. S. Weiss, *Science* **2001**, *292*, 2303.

[14] G. K. Ramachandran, T. J. Hopson, A. M. Rawlett, L. A. Nagahara, A. Primak, S. M. Lindsay, *Science* **2003**, *300*, 1413.

[15] F. Schreiber, A. Eberhardt, T. Y. B. Leung, P. Schwartz, S. M. Wetterer, D. J. Lavrich, L. Berman, P. Fenter, P. Eisenberger, G. Scoles, *Phys. Rev. B.* **1998**, *57*, 12476.

[16] D. Coucouvanis, *Progress in Inorganic Chemistry* **1970**, *11*, 233.

[17] G. D. Thorn, R. A. Ludwig, *The Dithiocarbamates and Related Compounds*, Elsevier, Amsterdam-New York, **1962**.

[18] J. M. Wessels, H.-G. Nothofer, W. E. Ford, F. von Wrochem, F. Scholz, T. Vossmeyer, A. Schroedter, H. Weller, A. Yasuda, *J. Am. Chem. Soc.* **2004**, *126*, 3349.

[19] Zhao, Y., Perez-Segarra, W., Shi, Q., Wei, A. J. Am. Chem. Soc. **2005**, 127, 7328.

[20] P. Morf, F. Raimondi, H.-G. Nothofer, B. Schnyder, A. Yasuda, J. M. Wessels, T. A. Jung, *Langmuir* **2006**, *22*, 658.

[21] A.-S. Duwez, S. Di Paolo, J. Ghijsen, J. Riga, M. Deleuze, J. Delhalle, *J. Phys. Chem. B* **1997**, *101*, 884.

[22] A.-S. Duwez, G. Pfister-Guillouzo, J. Delhalle, J. Riga, *J. Phys. Chem. B* **2000**, *104*, 9029.

[23] R. Di Felice, A. Selloni, E. Molinari, *J. Phys. Chem. B* **2003**, *107*, 1151.

[24] D. M. Alloway, M. Hofmann, D. L. Smith, N. E. Gruhn, A. L. Graham, R. Colorado, Jr., V. H. Wysocki, T. R. Lee, P. A. Lee, N. R. Armstrong, *J. Phys. Chem. B* **2003**, *107*, 11690.

[25] K. Kimura, *Handbook of HeI Photoelectron Spectra of Fundamental Organic Molecules*, Japan Scientific Societies Press, Tokyo, **1981**.

[26] J. K. Norskov, B. Hammer in *Chemisorption and Reactivity of Supported Clusters and Thin Films* (Eds.: R. M. Lambert, G. Pacchioni), Kluwer Academic, The Netherlands, **1997**.

[27] P. Monachesi, L. Chiodo, R. Del Sole, *Phys. Rev. B* **2004**, *69*, 165404.

[28] L. Jones, J. S. Schumm, J. M. Tour, *J. Org. Chem.* **1997**, *62*, 1388.

[29] L. A. Bumm, J. J. Arnold, M. T. Cygan, T. D. Dunbar, T. P. Burgin, L. Jones II, D. L. Allara, J. M. Tour, P. S. Weiss, *Science* **1996**, *271(5256)*, 1705-07.

[30] P. A. Agron, T. A. Carlson, *J. Vac. Sci. Technol.* **1982**, *20*, 815.

[31] S. Gokhale, P. Trischberger, D. Menzel, W. Widdra, H. Droge, H.-P. Steinbrück, U. Birkenheuer, U. Gutdeutsch, N. J. Rösch, *Chem. Phys.* **1998**, *108*, 5554.

[32] L. Patrone, S. Palacin, J. Charlier, F. Armand, J. P. Bourgoin, H. Tang, S. Gauthier, *Phys. Rev. Lett.* **2003**, *91*, 96802.

[33] I. H. Campbell, S. Rubin, T. A. Zawodzinski, J. D. Kress, R. L. Martin, D. L. Smith, N. N. Barashkov, J. P. Ferraris, *Phys. Rev. B* **1996**, *54*, 14321.

[34] M. Di Ventra, S. T. Pantelides, N. D. Lang, *Phys. Rev. Lett.* **2000**, *5*, 979.

[35] Wuelfing, W. P.; Murray, R. W. J. Phys. Chem. B **2002**, 106, 3139.

[36] Zabet-Khosousi, A.; Trudeau, P.-E.; Suganuma, Y.; Dhirani, A.-A.; Statt, B. Phys. Rev. Lett. **2006**, 96, 156403.

[37] P. E. Laibinis, G. M. Whitesides, D. L. Allara, Y.-T. Tao, A. N. Parikh, R. G. Nuzzo, *J. Am. Chem. Soc.* **1991**, *113*, 7152.

[38] P. A. Redhead, *Vacuum* **1962**, *12*, 203.

[39] M. D. Segall, P. J. D. Lindan, M. J. Probert, C. J. Pickard, P. J. Hasnip, S. J. Clark, M. C. Payne, *J. Phys.: Cond. Matt.* 2002, *14*, 2717-2743.

[40] M. Frisch et al., Gaussian 98, Revision A.11, Gaussian Inc., Pittsburgh, PA, 1998.

[41] B. J. Delley, *Chem. Phys.* 1990, *92*, 508.

4

Molecular Conductance of Aromatic Thiol and Dithiocarbamate Derivatives Investigated by Current Distance Spectroscopy in UHV-STM

Abstract

The overlayer structure of alkanethiol, benzenemercaptane and highly conjugated methyl-phenyl-dithiocarbamate self-assembled monolayers on Au(111) was studied by STM and the conductance of those monolayers determined by current-distance spectroscopy. Whereas alkanethiol monolayers exhibit the known c(4 x 2) overlayer structure, BM monolayers show a novel reconstruction, resulting from thermal annealing at 368 K. Extended, striped phase domains having a commensurate, p(4½√3 x 2) overlayer structure with an oblique unit cell are observed. In contrast, methyl-phenyl-dithiocarbamate monolayers are found to be disordered. The tunnelling decay constants β_v for the vacuum gap and β_M for the molecular medium, as well as the molecular conductance G at the STM tip-monolayer contact point, are determined by I-Z spectroscopy. Measurements on alkanethiols with different chain-lengths (C8 and C10) yield values in agreement with previous studies. The tunnelling decay constant of $\beta = 1/\text{Å}$ for alkanethiols and $\beta = 0.5/\text{Å}$ for the phenyl ring is in line with reported values. Methyl-phenyl-dithiocarbamate is roughly 1 order of magnitude more conductive than benzenemercaptane. This difference in conductance can be attributed to the difference in the electronic coupling of the two anchor groups.

Introduction

For the development of molecular electronics, a thorough understanding of the correlation between electrical properties and molecular structure is of fundamental importance. Charge transport properties are strongly dependent on the particular local environment within the metal-molecule junction and on unknown parameters such as molecular conformation, binding properties and interaction with solvents. All these

factors can complicate the interpretation of experimental results. A number of studies have addressed the issue of electron transport through single molecules, mainly by two terminal measurements on thiol-terminated oligo-phenylene and oligo-phenylene-ethynilene derivatives[1,9a]. The two contacts are established with the break junction approach[2] or by bridging the molecule between tip and surface in an STM/AFM setup[3]. Recently, transport in the coherent tunnelling regime has been reported by Vankataraman[4] and Tao[5] by STM spectroscopy in a liquid environment. For the determination of tunnelling barrier heights, current-voltage spectroscopy was employed[5], while the tunnelling decay constant was obtained from current-distance (I-Z) spectroscopy[15] and from STM height profiles[6] (chapter 5). I-Z spectroscopy offers the possibility of investigating mono-functionalized compounds, i.e. compounds that are linked to the substrate with only a single anchor group. However, it has to be recalled that the physical tip-molecule contact provides a different electrical coupling than a covalent metal-molecule bond. Thus, significant differences in conductance are expected when comparing transport data from molecules chemically connected to one or to both electrodes (vide infra). In order to provide a possibly stable and defined tip-molecule contact, I-Z characterisation requires the presence of a densely packed, oriented monolayer.

In previous studies, the tunnelling attenuation factor β has been determined with different approaches, and values for β were found within a range from 0.7/Å to 1.2/Å for alkanethiols[7], from 0.4/Å to 0.6/Å for oligo-phenylenes[8] and from 0.4/Å to 1.2/Å for oligo-phenylenevynilenes[9].

In this report, we compare the aromatic compounds benzylmercaptane (BM) and methyl-phenyl-dithiocarbamate (MPDTC), whose electronic structure was studied in chapter 3, with two well known alkanethiol compounds. Alkanethiols and BM both form crystalline and commensurate monolayers on Au(111),[10,11] however, upon annealing, BM monolayers show a novel reconstruction related to the π-interactions between neighbouring aromatic rings. The monolayer structure differs from the (√3 x √3)R30° lattice previously reported by Tao and Chen[11,12] and from the c(5√3 x 3) structure found for thio-oligophenyls by Wöll et al.[13] Rather, we observe a lattice with a reduced packing density having an oblique p(4½√3 x 2) unit cell. The two compounds BM and MPDTC both possess an aromatic ring, but differ in their anchor groups. The decay constant β and the conductance of the molecular layers at the

probe-molecule contact point are determined by current-distance (I-Z) characteristics. They provide us with a direct method to determine the molecular conductance of the monolayers and the results can be related to the experimental and theoretical findings presented in chapter 3.

Current-distance and current-voltage spectroscopy

In I-Z spectroscopy, the current is recorded as a function of the vertical position of the tip over the sample. In the exponential electron tunnelling model, a coherent electron tunnelling process is assumed and the dependence of the current on the distance h is expressed by the equation

$$G = G_0 \cdot \exp(-\beta h)$$

where G_0 is the contact conductance, β the tunneling decay constant, and h the tunneling distance. The conductance G can be separated into two contributions, one from tunneling through the molecular medium (G_M) and one from the tunneling gap between the molecular layer and the tip (G_G)

$$G_M = A_M \cdot \exp(-\beta_M h_M)$$

$$G_G = B \cdot \exp(-\beta_v h_G)$$

where A_M is the contact conductance between the metal substrate and the molecule, B is the contact conductance between the molecular layer and the vacuum gap, β_M and β_v are the tunnelling decay constants of the molecule and of the vacuum respectively, h_M the thickness of the molecular layer and h_G the distance between the tip and the SAM. The total conductance is proportional to the product of the two exponentials describing the transparency of the vacuum and the molecular medium. When the tip-sample separation is modulated, the tunnelling decay constant β is obtained by

$$\beta = \frac{d(\ln I)}{dz} .$$

Depending on whether the tip is located in the vacuum region or within the SAM, this expression allows the extraction of β_M and β_v. In the low bias regime, i.e. if V_{bias} is smaller than the apparent barrier height ϕ, the tunnelling decay constant can be related to ϕ via

$$\beta = \sqrt{\frac{8m\phi}{\hbar}} ,$$

thus

$$\phi[eV] = 0.952 \left(\frac{d(\ln I)}{dz[\mathring{A}]} \right)^2$$

ϕ depends on the work function of the tip and the metal surface, but also on the electronic structure of the molecular medium filling the tunnelling gap.

When the tip is stopped at a selected location above the sample and the current is recorded as a function of V_G, a current-voltage (I-V) spectrum is acquired. I-V spectroscopy enables the determination of the energy-resolved local density of states, which can be extracted from the data as was suggested by Feenstra et al.[14]

$$\frac{dI/dV}{I/V} \propto \rho_s(eV) \cdot \rho_t$$

where ρ_s and ρ_t is the density of states of the surface and the tip, respectively. In this way, I-V spectroscopy helped in understanding the electronic structure of semiconductor surfaces and of adsorbates on metals with atomic scale resolution.

Experimental

Sample preparation and chemicals are fully described in chapter 2.1 and chapter 3. Upon preparation, the samples are introduced into an UHV-STM (Omicron VT-STM) chamber at a base pressure of 9 x 10^{-10} mbar. The instrument is equipped with a low current IV-converter that allows scanning tunnelling spectroscopy in the femto-ampere range. Before imaging, the samples are thermally annealed at ~ 368 K for 10 min. to remove chemisorbed molecules and to allow further equilibration of the monolayer. For alkanethiols, the tunnelling parameters are $V_G = 0.8 - 1$ V (both positive and negative values) and $I_t = 5\text{-}10$ pA, corresponding to a tunnel impedance of about 100-200 GΩ. BM and MPDTC, having a higher molecular conductance, are scanned with $V_G = -0.2$ V and $I_t = 20\text{-}30$ pA, corresponding to an impedance of ~ 10 GΩ. A low bias voltage is selected in consideration of the higher polarizability of these aromatic compounds. As a probe a Pt-Ir (80:20) tip is used. To record an I-Z curve, the feedback loop is interrupted and the tip drawn back by 0.5 nm. After a short delay (1ms), the acquisition starts while the tip approaches the surface at a rate of 107 $\mathring{A}$/s. During the approach, the current is measured at 60 points with an acquisition time of 0.65 ms/point.

Results

Monolayer structure. Figure 1 shows STM scans of octanethiol and decanethiol monolayers, which are used as reference compounds for transport studies. As already mentioned, the monolayers are annealed in UHV to improve the cleanliness of the tip-SAM contact, which generally resulted in superior film quality. In both SAMs, the ($\sqrt{3}$ x $\sqrt{3}$)R30° overlayer structure of alkanethiols on Au(111) is visible. Octanethiol SAMs form extended, crystalline domains, separated by large domain boundaries (Fig. 1a).
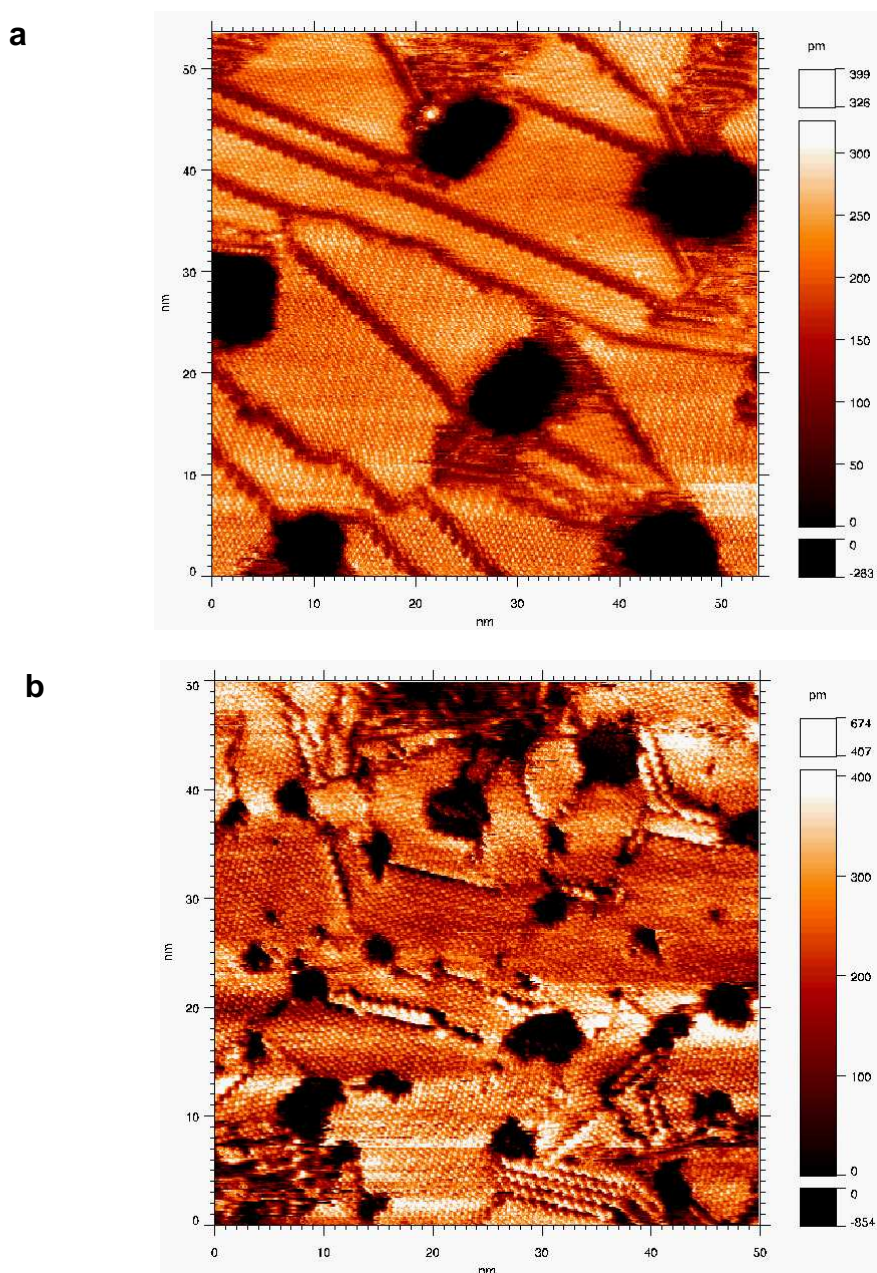

Figure 1. STM scans of an octanethiol (a) and a decanethiol (b) monolayer. Domain boundaries of the polycrystalline films are polygonal due to the equilibration by thermal annealing.

The clear separation between domains is a result of thermal annealing in UHV, which initiates molecular diffusion and partial desorption of alkanethiols at the domain boundaries. Also, an alignment of domain boundaries and vacancy island step edges along preferential directions at surface is observed, which is related to the minimization of the monolayer free energy. In decanethiol SAMs, changes in the monolayer structure, induced by thermal annealing, are less pronounced as a consequence of the stronger van der Waals interactions between longer alkyl chains, which energetically stabilize the monolayer.

Fig. 2a and 2b show high resolution STM images of BM monolayers on Au(111). Upon thermal annealing at 368 K in UHV, extended, crystalline BM domains evolve (30-50 nm in diameter), showing a striped phase pattern that is periodically repeated in the [121] direction of the substrate. A careful analysis of the present STM topographs shows a commensurate Au(111) p(4½√3 x 2)BM structure with a primitive oblique unit cell (Fig. 2b). The p(4½√3 x 2) lattice is in good agreement with the experimentally determined lengths of the unit cell vectors ($a = 5.8 \pm 0.1$ Å, $b = 22.8 \pm 0.2$ Å), since they coincide with the theoretical values ($a = 5.77$ Å, $b = 22.82$ Å) of this structure. The cell parameters yield a molecular area of 32.6 Å^2, which is 50% higher than the area found in the (√3 x √3)R30° phase (21.6 Å^2). In previous STM studies of thio-oligophenylene monolayers, molecular resolution of the overlayer lattice has been achieved[15]. For BM monolayers, Tao et al. determined a (√3 x √3)R30° lattice structure[11]. The transition from the (√3 x √3)R30° to the p(4½√3 x 2) lattice that we observe here is attributed in the first place to the thermal annealing procedure that progressively reduces the density of the BM monolayer by thermal desorption of molecules from the surface[16], subsequently to a reorganization of the whole monolayer, resulting in an energetically more favourable bond angle arrangement and phenyl ring stacking. The crystallographic orientation of the unit cell relative to the surface is determined by reference to the Au(111) step edge direction (Fig. 2b). The slightly oblique character of the unit cell (angle $\alpha \sim 80°$, Fig. 2b) is consistent with an offset of 1½ a_{Au} along the [10$\bar{1}$] direction ($a_{Au} = 2.884$ Å), which is a consequence of the fact that the repeat unit in the [121] direction is not a multiple integer of √3.
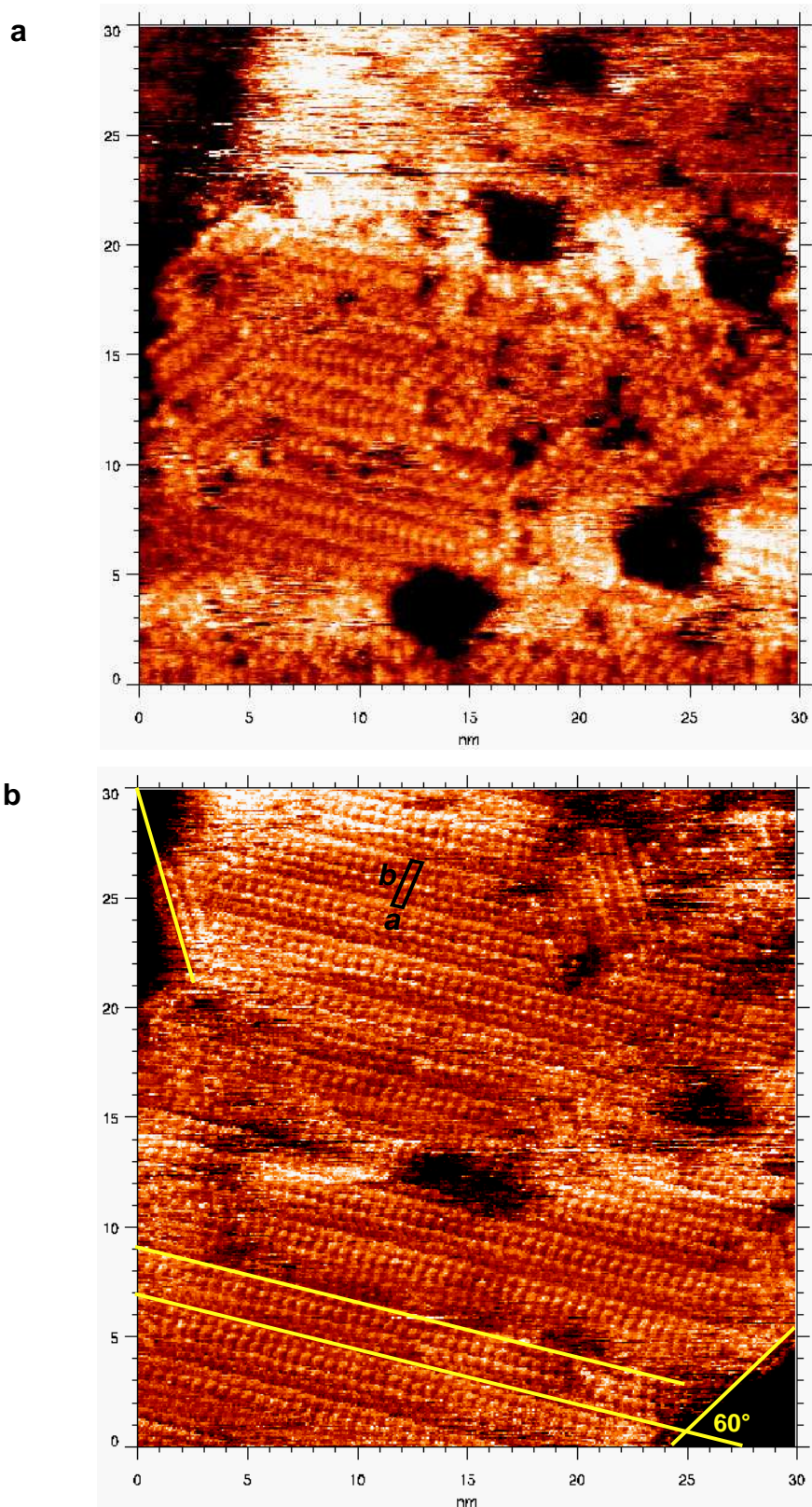
Figure 2. STM scans of a BM monolayer, forming the Au(111) p(4½√3 x 2)BM structure. (a) Herringbone pattern in a polycrystalline area, showing BM-rows with different orientations relative to the substrate. (b) High resolution STM image of an ordered BM domain showing a striped phase with a periodicity of 22.4 Å (parallel yellow lines), corresponding to 4 BM rows in parallel (scan range: 30 x 30 nm^2). In black, the primitive oblique unit cell of the p(4½√3 x 2) structure and the unit cell vectors a and b is drawn. The direction of the unit cell vector a relative to the Au(111) step edge is 60°.

67

As we observed in earlier experiments with dialkyl dithiocarbamate monolayers, MPDTC monolayers do not show any structure and ordering (Fig. 3a,b). Recent work[17] revealed that dithiocarbamates on Au(111) show strong etching properties, probably due to the chelating nature of the dithiocarbamate anchor group. In STM micrographs, an increase in the number of vacancy islands and a roughening of Au step edges is observed. Furthermore, DFT calculations using a Au(111) slab model demonstrated a tendency to reconstruct the upper Au layer (chapter 3). Thus, dithiocarbamates are likely to lift the periodicity of the Au(111) surface, creating dense, but disordered monolayers. Rarely, MPDTC molecules could be resolved in STM images, as shown in Fig. 3b. Elemental areas obtained from XPS spectra (sulfur 2p signal) prove that the packing density of MPDTC molecules on Au is close to that of alkanethiols (see Chapter 3) and slab model calculations show evidence that under these conditions MPDTC molecules assume an upright orientation on the Au surface.

a **b**
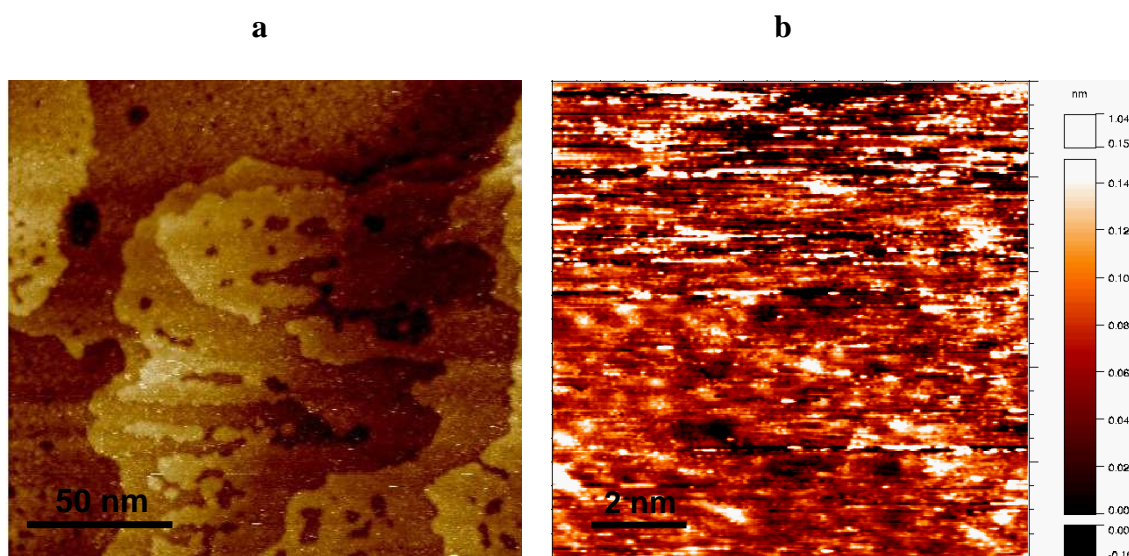
Figure 3. STM scans of dithiocarbamate monolayers on Au(111). (a) STM image of a densely packed dioctyl-dithiocarbamate SAM, recorded at ambient conditions. The adsorption of the monolayer induces an etching of the surface (deformed Au(111) step edges). (b) Small area scan on a MPDTC SAM, imaged under UHV conditions. Despite thermal annealing of the monolayers in UHV, tip instabilities are visible in the upper part of the image. In the bottom, the bright dots identify single MPDTC molecules.

I-Z spectroscopy. Fig. 4 shows current-distance scans on molecularly resolved octanethiol and decanethiol domains, as they are presented in Figure 1. The tunnelling current shows a steep exponential decay in the vacuum region above the sample.

a   **b**
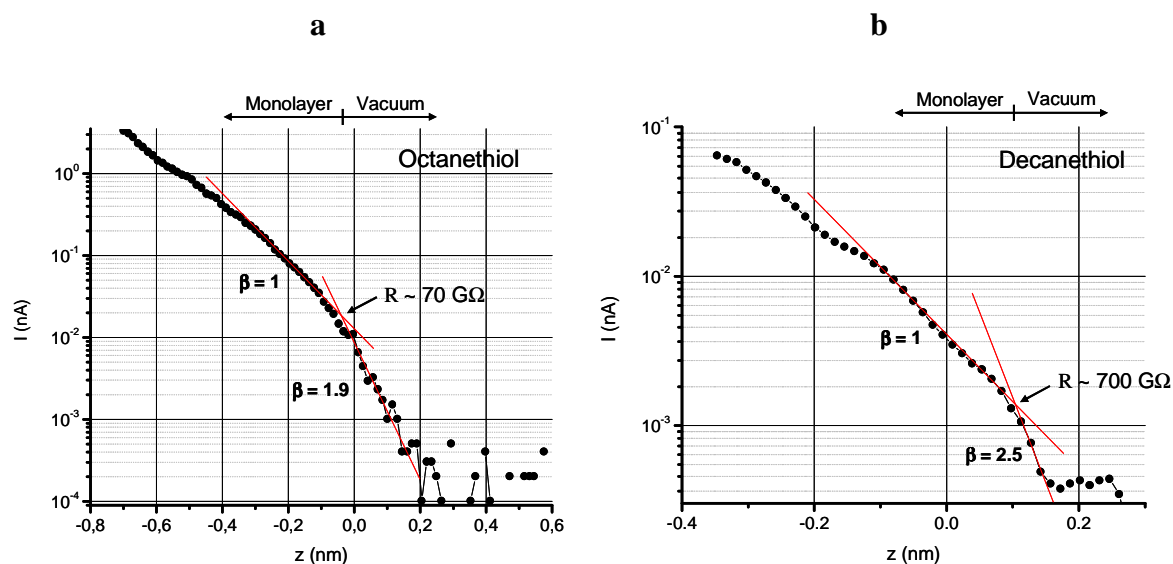
Figure 4. Semilogarithmic plot of representative I-Z characteristics on octanethiol (a) and decanethiol (b) monolayers on Au(111). The intercepts of the two linear fits for the monolayer and the vacuum region represent the point contact of the tip with the monolayer. The tunnelling resistance at the contact is obtained from the intercept currents and the bias voltage $V_G = -0.8$ V (a) and $V_G = -1$ V (b).

For octanethiol monolayers, a tunnelling decay constant of $\beta_v = (2 \pm 0.1)/\text{Å}$ is found in the vacuum region. This is in good agreement with previous STM data both from ambient[6] and UHV[18] measurements. For decanethiol, β_v ranges between 2.2/Å and 2.5/Å but is more difficult to determine, since the contact with the monolayer is established at a tunnelling current of 1-2 pA, which is close to the noise level of the amplifier (Fig. 4b). Upon contact, the tip moves through the bulk monolayer, and at least for the first Angstroms of displacement across the SAM the recorded current reflects the decay constant of the molecular medium. In the monolayer region, we find an average of $\beta = (0.95 \pm 0.05)/\text{Å}$ for both alkanethiols, which is consistent with previous reports[6,18]. The average tunnelling resistance at the point contact of the tip with the monolayer can be determined from the intersection of the two linear fits in Fig. 4. From the data we obtain a tunnelling resistance of $R \sim 100$ GΩ for octanethiol and $R \sim 700$ GΩ for decanethiol, where the difference in conductance is attributed to the difference in chainlength. The resistance values are in good agreement with those

69

estimated by Frisbie and Wold using conductive AFM[19], but roughly one order of magnitude higher then those found by Yasutake et al. in analogous I-Z experiments[18]. Moreover, our values deviate significantly from those obtained with the break junction technique, where octanedithiols[20] and octanediamines[4] show a resistance in the $G\Omega$ range, i.e. about two orders of magnitude lower than the results presented here. This is not surprising since in a break junction, unlike in our STM I-Z scans, a chemical bond to both electrodes is established, significantly improving the electrical coupling of the molecule to the contacts. A previous comparison between physical and covalent contacts reported conductance differences of approx. one to two orders of magnitude[21], consistent to our observations.

It is interesting to note that at the given loop conditions ($I_T = 5$ pA, $V_G = -1$ V), the STM tip does not scan above the monolayer surface when imaging a decanethiol SAM. The origin of the distance axis in Fig. 4 denotes the constant current condition and the intersection of the two linear fits for β_M and β_v is found at about 1 Å above this position (Fig. 4b). Thus, the tip travels through the monolayer during imaging, which could account for the limited resolution commonly achieved for long-chains alkanethiols (Fig 1b) and for the low apparent tunnelling barrier height previously observed for alkanethiols in I-Z modulation spectroscopy[1b].

For the aromatic derivatives BM and MPDTC, the point contact is established at much lower tunnelling impedances. Fig. 5 shows the current-distance spectra for BM (a) and MPDTC (b). For BM, the I-Z spectra show two intersections. One is given by the vacuum-phenyl interface, and the second one could result from the methylene unit next to the benzene ring. We find an average of $\beta = (1.9 \pm 0.15)/$Å for the vacuum gap, and $\beta = (0.5 \pm 0.1)/$Å for the phenyl. The measured decay constants are in agreement with values measured in oligophenyl and OPE compounds[22].

Figure 5. Semilogarithmic plot of representative I-Z characteristics on benzylmercaptane (a) and MPDTC (b) monolayers on Au(111). The intercepts of the two linear fits for the monolayer and the vacuum region represent the point contact of the tip with the monolayer. The tunnelling resistance at the contact is obtained 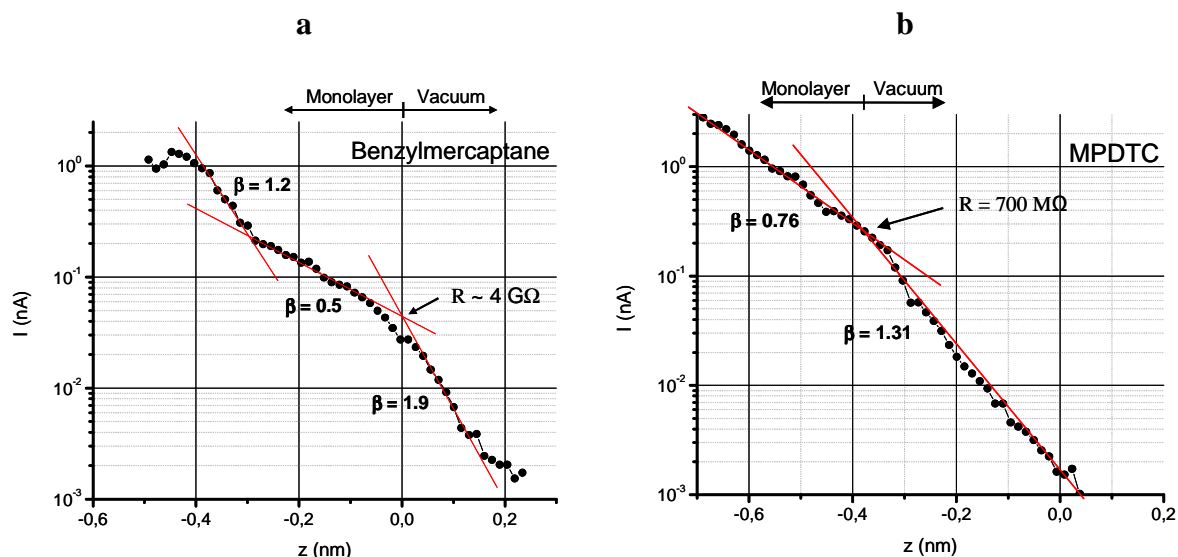from the intercept and the bias voltage $V_G = -0.2V$ (a,b). The vacuum tunnelling decay constant for MPDTC SAMs (b) deviates from values measured on BM and alkanethiols (see text).

For BM, the average tunnelling resistance ($\sim$ 5 GΩ) is lower by a factor of 20 compared to the resistance of octanethiol monolayers. In case of the dithiocarbamate derivative MPDTC, the tip-monolayer contact occurs at even higher tunnelling currents (200-1000 pA), corresponding to an average tunnelling resistance of $\sim$ 700 MΩ. In contrast to BM, the value for β varies between 0.5/Å and 0.75/Å in the monolayer region and between 1.2/Å and 1.6/Å in the vacuum region. Both in β and in contact resistance, the MPDTC data shows a significant statistical variation, which is attributed to the disorder in dithiocarbamate SAMs and to the stronger electrostatic forces acting between molecules and tip. Furthermore, despite thermal annealing of the samples, tip instabilities during imaging indicate the presence of adsorbates on the monolayer. These adsorbates could bridge the gap between tip and monolayer before the point contact is established, reducing the tunnelling decay constant in the vacuum region, as observed in Fig. 5b.

Conclusions

High resolution STM scans have shown a novel p(4½√3 x 2) reconstruction in BM monolayers on Au(111), which is attributed to the thermal annealing process with dense BM monolayers in UHV. STM current-distance spectroscopy revealed

tunnelling decay constants and conductance values for a series of four aromatic and aliphatic compounds linked to the substrate by thiolate and dithiocarbamate anchor groups. While the values obtained for the tunnelling decay constant β_M in alkyls and phenyls are in good agreement with previous reports, we find that the conductance across the junction in UHV-STM is low compared to other methods providing an all covalent contact between the molecule and the electrodes (e.g. break junction and conductive AFM). This observation is related to the higher resistance at the physical contact between STM probe and the monolayer. However, relative consistency in the conductance of alkanethiols with different chainlengths is achieved, allowing us to compare compounds with different molecular conjugation and binding chemistry. We find roughly a one order of magnitude difference in the conductance of the aromatic derivatives BM and MPDTC, indicating that the dithiocarbamate anchor group in MPDTC provides an improved electronic coupling to Au. The present results support the data obtained from networks of nanoparticles interlinked by aromatic dithiols and bis-dithiocarbamates (chapter 3), that revealed a lower metal-organic injection barrier and thus a lower resistance at the dithiocarbamate-Au interface.

References

[1] (a) Bumm, L. A.; Arnold, J. J.; Cygan, M. T.; Dunbar, T. D.; Burgin, T. P.; Jones, L. II; Allara, D. L.; Tour, J. M.; Weiss, P. S. *Science.* **1996**, *271*, 5256. (b) Cygan, M. T.; Dunbar, T. D.; Arnold, J. J.; Bumm L. A.; Shedlock, N. F.; Burgin, T. P.; Jones, L, II; Allara, D. A.; Tour, J. M.; Weiss, P. S. *J. Am. Chem. Soc.* **1998**, *120*, 2721. (c) F. R. F. Fan, J. P. Yang, L. T. Cai, D. W. Price, S. M. Dirk, D. W. Konsynkin, Y. X. Yao, A. M. Rawlett, J. M. Tour, A. J. Bard *J. Am. Chem. Soc.* **124**, 5550 (2002). (d) Xiao, X.; Nagahara, A. L.; Rawlett, A. M.; Tao, N. J. *J. Am. Chem. Soc.* **127**, 9235 (2005).

[2] Rechert, J., Ochs, R., Beckmann, D., Weber, H. B., Mayor, M., v. Löhneysen, H. *Phys. Rev. Lett.* 88, 176804 (2002).

[3] Cui, X. D.; Primak, A.; Zarate, X.; Tomfohr, J.; Sankey, O. F.; Moore, A. L.; Moore, T. A.; Gust, D.; Harris, G.; Lindsay, S. M. *Science.* **2001**, *294*, 571.

[4] Venkataraman, L., Klare, J., Tam, I. W., Nuckolls, C., Hybertsen, M. S., Steigerwald, M. L. *Nano Letters* **6**, 458 (2006).

[5] Xu, B., Tao, J. *Science* **2003**, *301*, 1221.

[6] Bumm, L. A.; Arnold, J. J.; Charles, L. F.; Dunbar, T. D.; Allara, D. L.; Weiss, P. S. *J. Am. Chem. Soc.* **1999**, *121*, 8017.

[7] T. Lee, W. Wang, J. Klemic, J. J. Zhang, J. Su, M. Reed, *J. Phys. Chem. B* **108**, 8742 (2004).

[8] A. Helms, D. Heller, G. McLendon, *J. Am. Chem. Soc.* **114**, 6227 (1992).

[9] (a) K. Moth-Poulsen, L. Patrone, N. Stuhr-Hansen, J. B. Christensen, J.-P. Bourgoin, T. Bjoernholm, *Nano Letters* **5**, 783 (2005). (b) Seferos, D. S.; Blum, A. S.; Kushmerick, J. G.; Bazan, G. C. *J. Am. Chem. Soc.* **128**, 11260 (2006).

[10] Schreiber, F. *Prog. Surf. Sci.* **2000**, *65*, 151.

[11] Tao, Y.-T.; Wu, C. C.; Eu, J.-Y.; Lin, W.-L.; Wu, K.-C.; Chen, C. *Langmuir* **1997**, *13*, 4018.

[12] Hallmann, L.; Bashir, A.; Strunskus, T.; Adelung, R.; Staemmler, V.; Wöll, C.; Tuczek, F. *Langmuir* **2008**, *24*, 5726.

[13] Cyganik, P.; Buck, M.; Azzam, W.; Wöll, C. *J. Phys. Chem. B* **2004**, *108*, 4989.

[14] R. Feenstra, J. Stroscio, A. Fein, *Surf. Sci.* **181**, 295 (1987).

[15] (a) H. Wolf, H. Ringsdorf, E. Delamarche, T. Takami, H. Kang, B. Michel, C. Gerber, M. Jaschke, H.-J. Butt, E. Bamberg *J. Phys. Chem.* **99**, 7102 (1995). (b) A. Dhirani, R. W. Zehner, R. P. Hsung, P. Guyot-Sionnest, L. R. Sita *J. Am. Chem. Soc.* **118**, 3319 (1996).

[16] Schreiber, F.; Eberhardt, A.; Leung, T. Y. B.; Schwartz, P.; Wetterer, S. M.; Lavrich, D. J.; Berman, L.; Fenter, P.; Eisenberger, P.; Scoles, G. *Phys. Rev. B.* **1998**, *57*, 12476.

[17] Morf, P. *et al. Langmuir* 22, 658 (2006).

[18] Yasutake, Y.; Shi, Z.; Okazaki, T.; Shinohara, H.; Majima, Y. *Nano Letters* **2005**, *5*, 1057.

[19] Wold, D. J.; Frisbie, C. D. *J. Am. Chem. Soc.* **123**, 5549 (2001).

[20] Gonzalez, M. T.; Wu, S.; Huber, R.; van der Molen, S. J.; Schönenberger, C.; Calame, M. *Nano Letters* **2006**, *6*, 2238.

[21] Engelkes, V. B.; Beebe, J. M.; Frisbie, C. D. *J. Am. Chem. Soc.* **126**, 14287 (2004).

[22] Wakamatsu, S., Fujii, S., Akiba, U., Fujihira, M. *Ultramicroscopy* **2002**, *97*, 19.

5

Structure and Conductance of Aromatic and Aliphatic Dithioacetamide Monolayers on Au(111)

Abstract

The structure and electrical properties of self-assembled monolayers of cyclic aromatic and aliphatic dithioacetamides (1,4-bis(mercaptoacetamido)benzene and 1,4-bis(mercaptoacetamido)cyclohexane) and of mixed dithioacetamide/alkanethiol monolayers are characterized by X-ray photoelectron spectroscopy (XPS), scanning tunneling microscopy (STM) and contact angle goniometry. Both dithiolacetamides are found to pack densely on Au(111), however the monolayers are poorly ordered as a result of hydrogen bond formation between the amide groups. The co-assembly and the insertion method are compared for the formation of mixed dithioacetamide/alkanethiol monolayers. By co-assembly, islands of dithio-acetamides in a dodecanethiol matrix can only be obtained at a low dithio-acetamide/dodecanethiol concentration ratio in solution (1/10) and by thermal annealing of the resulting monolayers. Small and well defined dithioacetamide domains are realized by insertion of dithioacetamides into defect sites of closely packed octanethiol monolayers. These domains are used to determine the molecular conductance by means of STM height profiles and molecular lengths resulting from density functional theory (DFT) calculations. The difference in the tunneling decay constant β measured for aromatic dithioacetamides ($\beta = 0.74\text{-}0.76/\text{Å}$) and for aliphatic dithioacetamides ($\beta = 0.84\text{-}0.91/\text{Å}$) highlights the influence of the conjugation within the cyclic core on molecular conductance.

Introduction

Since the early studies on amphiphile organic layers, driven by the desire to modify the wetting properties of metal surfaces,[1] self-assembled monolayers (SAMs) have

attracted a significant interest and are considered promising systems for potential applications in areas such as chemical and biological sensing,[2] biomimetics, corrosion protection,[3] opto-electronics and molecular electronics.[4] By intentionally combining compounds with different chemical properties to form mixed SAMs, the wetting properties of surfaces could be systematically tuned.[5] Recently, mixed monolayers became also an interesting system for the electrical characterization of functional molecules.[6] With scanning probe methods such as STM or AFM,[7] which allow the resolution of single or of small groups of molecules, the investigation of active compounds inserted into a structurally well-defined, insulating matrix became possible.[8]

The growth process of thiol based self-assembled monolayers on noble metals like Au is governed by a complex interplay of interaction forces, determining the structural properties of such monolayers.[9] This particularly applies to mixed monolayers, where structural properties such as crystalline order or phase segregation are determined by the chemical nature of the respective molecular backbones. For alkanethiol self-assembled monolayers on Au, the corrugation energy of the headgroup-substrate interaction is the dominant driving force for the formation of the $(\sqrt{3} \times \sqrt{3})R30°$ phase.[34] Even if part of the molecular backbone is modified by substituents, the related difference in bulkiness within the backbone is often compensated by variation in the tilt angle of the molecule towards the surface normal.[10] In contrast, molecules interacting through polar forces, hydrogen bonds, or π-stacking can form monolayers whose structure is dominated by the molecular interaction energy, eventually forming overlayer structures with different periodicity or even giving rise to monolayers incommensurate to the substrate lattice.[11] In mixed monolayers, the different strength of these intermolecular forces can be exploited to drive phase segregation of chemically distinct components. The order within the alkanethiol matrix should not be substantially altered by the presence of aromatic or polar guest molecules if phase separation can be achieved. In this case, despite the presence of guest molecules, alkanethiols will form crystalline domains having a well-defined molecular orientation with respect to the substrate, as has been demonstrated in previous studies.[12]

The dithioacetamides 1,4-bis(mercaptoacetamido)benzene (DMAAB) and 1,4-bis(mercaptoacetamido)cyclohexane (DMAAcH) (Fig. 1) allow the investigation of self-assembled monolayers of aromatic and aliphatic derivatives interacting through

hydrogen bonds.[13] In contrast to oligo-phenylenes,[14] the amide groups in dithioacetamides lead to strong polar intermolecular interactions, facilitating phase segregation in mixed monolayers.[13] Furthermore, the two dithioacetamides allow a direct comparison of the influence of the aromatic or aliphatic cyclic core on charge transport. In this paper, we present XPS and STM results from dithioacetamide monolayers adsorbed to Au(111) from the liquid phase by two different methods, co-assembly[15] and insertion. The monolayer growth as well as the detailed adsorption chemistry is investigated by XPS, while monolayer structure and phase segregation are determined by STM. Well-defined and oriented dithioacetamide domains in hexagonally close packed octanethiol monolayers are obtained by the insertion method.[16] They are utilized to determine the molecular conductance of the aromatic and the aliphatic dithioacetamide by evaluation of STM height profiles.[17] By combination of XPS, molecular modeling and scanning tunneling microscopy, a detailed understanding of the monolayer structure is gained, supporting the interpretation of electrical data obtained from STM height profiles.
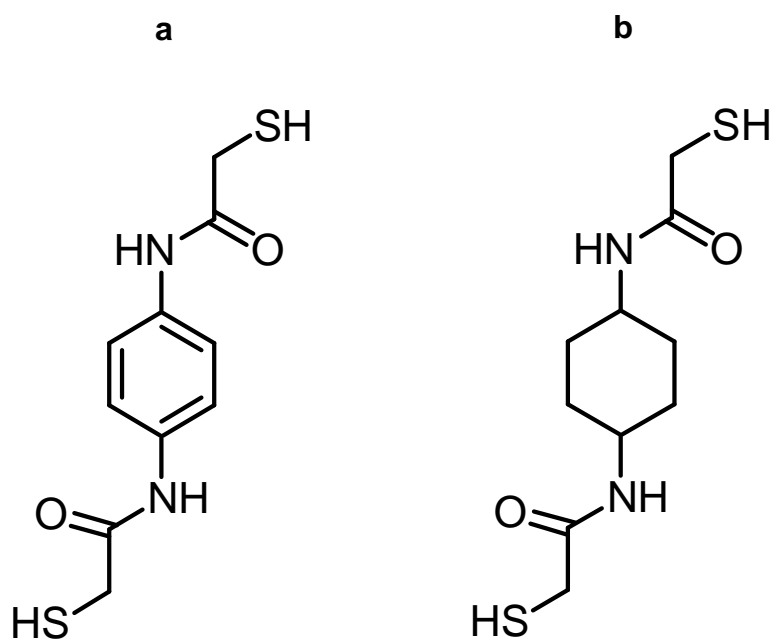
Figure 1: Chemical structures of the dithioacetamides: (a) 1,4-bis(mercaptoacetamido)benzene (DMAAB) and (b) 1,4-bis(mercaptoacetamido)cyclohexane (DMAAcH).

Experimental Methods

All chemicals and solvents are of spectrophotometric grade and used as received without any further purification. To avoid oxidation processes, methanol, ethanol, and dimethylformamide (DMF) are saturated with argon before usage. The synthesis of DMAAB and DMAAcH is described elsewhere.[18] Octanethiol and dodecanethiol are obtained from Sigma-Aldrich and used as received. Polycrystalline Au substrates are obtained by thermal evaporation (at a pressure of 5×10^{-6} mbar) of 100 nm Au (purity 99.99%, Umicore) on freshly cleaved mica substrates (Ted Pella, Inc., 1 x 1 cm pieces). Atomically flat Au(111) surfaces are obtained by flame annealing of the substrates in a butane flame and consecutive quenching in methanol. Subsequently, the samples are transferred into the glove box in methanol. The SAMs are prepared in argon environment by immersing the Au(111) surfaces into dithioacetamide/alkanethiol solutions according to the following procedures:

One component SAMs: DMAAB or DMAAcH monolayers are prepared by immersion of the Au substrates in a 0.2 mM solution of the dithioacetamides in DMF at room temperature for 24h. To exclude the formation of disulfide bonds, some of the samples are prepared by addition of an equimolar amount of n-butylphosphine to the assembly solution. Octanethiol or dodecanethiol monolayers are assembled from a 0.2 mM solution in ethanol for the same time. After preparation, the samples are rinsed thoroughly with DMF and ethanol (dithioacetamide SAMs) or with ethanol (alkanethiol SAMs).

Mixed SAMs by co-assembly: 0.2 mM solutions of DMAAB and dodecanethiol in DMF are mixed in the desired ratios, before immersion of the Au substrates. Upon exposure to the mixed solutions for 24h, the samples are rinsed in DMF and subsequently annealed at 80°C for 1 h in the gas phase of the assembly solution in pressure proof vessels. Subsequently, the samples are immersed in a fresh 0.1 mM dodecanethiol solution for 3 days to fill the gaps and defects created during the annealing step. After preparation, the samples are rinsed thoroughly with DMF and ethanol. Single DMAAB molecules in a low density dodecanethiol SAM are obtained by exposing the Au-surface to the mixed solutions as described and by subsequently annealing the samples in solution at 95-100°C for 2h. Finally, the sample is cooled down to RT in the assembly solution and rinsed thoroughly.

Mixed SAMs by insertion: Au substrates are immersed into a 0.2 mM solution of octanethiol for 24 h. Subsequently, the substrates are rinsed in DMF and immersed

into 0.2 mM solutions of DMAAB or DMAAcH for 3 days. After preparation, the samples are rinsed thoroughly with DMF and ethanol.

Instrumentation: XPS spectra are recorded with a Kratos Axis Ultra instrument using an Al K_α (1486.6 eV) source operated at 15 kV and 180 W. The photoelectrons are collected by the spectrometer in normal emission geometry. With an X-ray monochromator and a pass energy of 20 eV for the analyzer, an instrumental energy resolution of 0.45 eV is achieved. The energy scale is referenced to the Au *$4f_{7/2}$* line at a binding energy (BE) of 84 eV. For all samples, a survey spectrum and high resolution spectra of the S *2p*, C *1s*, N *1s*, O *1s* and Au *4f* regions are acquired. The spectra are fitted using a linear background and Voigt functions with a 50:50 Lorentz-Gaussian ratio, including a slight asymmetry factor (instrumental). The line shape parameters are determined by least square fitting to carbon or sulfur core level lines of known reference samples. The S *2p* spectrum consisting of two components $S_{2p3/2}$ and $S_{2p1/2}$ is fitted with a relative $S_{2p3/2}/S_{2p1/2}$ area ratio of 2/1 and a peak separation of 1.18 eV. Elemental ratios are determined by comparison of the normalized peak areas from the respective core level spectra. Sensitivity factors are obtained from the Kratos database and calibrated using reference samples.[19]

The structural properties of the films are characterized using an ambient condition STM (Multimode, Digital Instruments) equipped with a low current amplifier. The STM micrographs are mostly recorded at a bias voltage of 400 mV and a tunneling current of 2 pA, allowing a tunneling impedance of $2 \cdot 10^{12}$ Ω. The high tunneling impedance is a requirement for a perturbation-free imaging of the molecular layer by the STM tip. Pt/Ir (80/20) tips are used as a probe.

The molecular structure is determined by DFT calculations performed with the program Dmol3.[20] The molecular structure is obtained using a BLYP gradient corrected density functional.[21] Periodic DFT calculations to model the monolayers are performed at the local density approximation (LDA) level using the Vosko-Wilk-Nusair (VWN) functional (Supporting information). As a basis set, double numerical atomic orbitals augmented by polarization functions are employed. Simulations with the COMPASS force field[22] are done using the Discover program suite (Accelrys).

Results and Discussion

Dithioacetamide monolayers. Photoelectron spectroscopy was used to determine binding chemistry, packing density and purity of the prepared SAMs.[23] Generally, for DMAAB and DMAAcH monolayers, we find a good agreement between molecular stoichiometry and the elemental areas from XPS core level spectra. In particular, the N *1s*/S *2p* ratio is close to the expected value of 1 (1 ± 0.05). Deviation from stoichiometry is found in case of oxygen, where an excess of 25-30% is detected. This is mainly attributed to the presence of water in the dithioacetamide monolayers. The average monolayer coverage is determined in reference to hexagonally close packed dodecanethiol SAMs,[12] i.e. by comparison of the respective S *2p*/Au *4f* intensity ratios (Fig. 2, b and c).

After 20h assembly time, the S *2p*/Au *4f* intensity ratio for a dithioacetamide monolayer is 1.9 times higher than for a dodecanethiol monolayer. After consideration of the photoelectron attenuation within the monolayer[24,25] (for atoms located deeper in the organic layer), this indicates that the packing density of a full-coverage dithioacetamide SAM is only 20% lower than that of a close packed alkanethiol SAM (note that each dithioacetamide molecule includes 2 sulfur atoms). DFT calculations of dithioacetamides on a Au(111) slab in a periodic surface model show that close to the experimental coverage the molecules assume a standing up orientation on Au (Fig. 3, a and b; Supporting information). However, STM images indicate the formation of disordered dithioacetamide monolayers (Fig. 5, right image and Fig. S5, supporting information). This is consistent with previous studies that revealed the tendency of amide groups to introduce disorder in the SAMs.[26]

The C *1s* spectrum of a DMAAB SAM (Fig. 2a), shown here as representative for both dithioacetamide compounds, consists of four energetically distinct components[27]. The components are related to the benzene ring[28] (BE of 284.4 eV), the two carbonyl groups (287.8 eV), and the methylene groups (286 eV). The relative peak areas of these three components are fixed to the stoichiometric ratio of 6:2:2 for peak fitting. An additional component (~25% of the total carbon content) arises from unspecific carbon contaminants (~ 285.2 eV).
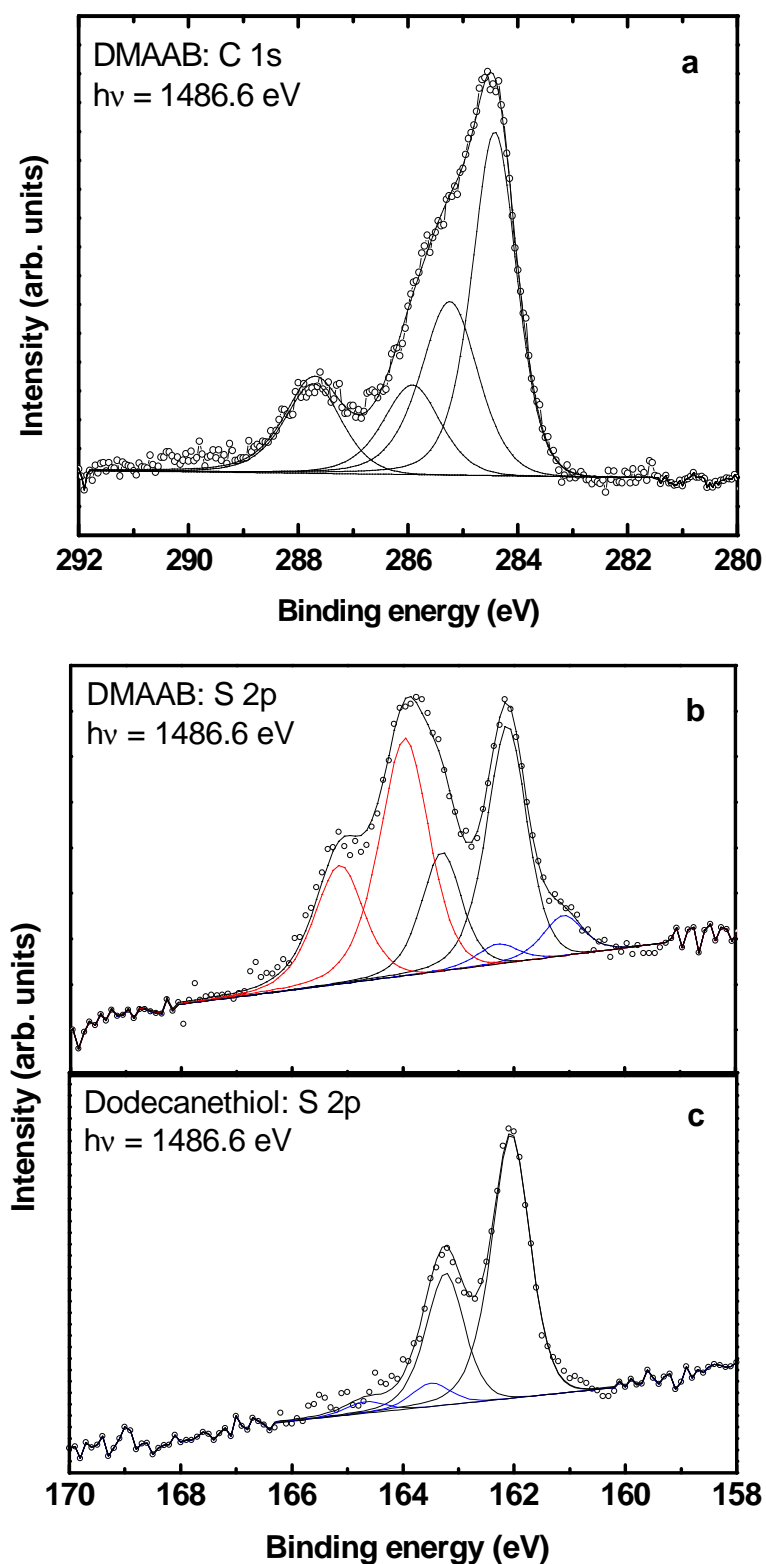
Figure 2: High resolution XPS spectra of a DMAAB and a dodecanethiol monolayer on Au(111). (a) DMAAB C *1s* core levels fitted with a fixed area of 6:2:2 for the components at 284.4 eV, 286 eV and 287.8 eV, respectively. The additional peak at 285.2 eV is assigned to hydrocarbon contaminants. (b) DMAAB S *2p* core levels with components at 161 eV, 162 eV and 163.5 eV (each component is a S *2p*$_{1/2}$/S *2p*$_{3/2}$ doublet). The intensity ratio between S2p(thiolate) and S2p(thiol) is ~1/1. (c) Dodecanethiol S *2p* core levels with one component at 162 eV. The small component at 163.5 eV (in blue) might be related to radiation damage.

In Fig. 2b and 2c, the sulfur *2p* XPS spectra of DMAAB and of dodecanethiol SAMs are compared. Each sulfur *2p* component consists of an S $2p_{1/2}$/S $2p_{3/2}$ doublet separated by 1.18 eV and with an intensity ratio of ½. The dodecanethiol monolayer shows a single component with the S $2p_{3/2}$ peak centered at a binding energy of 162 eV. This corresponds to the thiolate-Au bond formed upon deprotonation of the thiol group[29]. The spectrum of dithioacetamide monolayers (Fig. 2b), in contrast, shows three doublets with the S $2p_{3/2}$ peaks centered at 161 eV, 162 eV and 163.5 eV. While the components at 161 eV and at 162 eV are both associated to thiolate bound to Au (vide infra), the peak at 163.5 eV originates either from thiol sulfur or from disulfide.[30,31] These last two species cannot be distinguished by XPS within the experimental accuracy (Fig. S4, supporting information). However, when adding n-butylphosphine to the assembly solution, which is reported to suppress the formation of multilayers in oligophenyl-dithiol monolayers[32], no changes in the absolute and relative intensities of the S *2p* components are found. Furthermore, the ratio between the sulfur species related to the bound thiolate (161 eV and 162 eV) and the species at 163.5 eV remains 1/1, even for longer self-assembly times (Fig. 2b). These observations are seen as evidence that the formation of disulfide bonds between dithioacetamide molecules does not occur during monolayer growth. Thus, dithioacetamides form an oriented SAM, where the molecules are linked to the substrate through a single thiolate anchor group, while the component at 163.5 eV corresponds to the free thiol group exposed to the surface.

Several studies[33] have hypothesized a different XPS S *2p* core level binding energy for the two possible hybridization states of sulfur on Au, sp and sp^3. In these studies, the components at 162 eV and at 161 eV have been attributed to sp^3 and sp hybridized sulfur, respectively. The two hybridization states were associated with two different tilt angles of the molecular backbone towards the surface, corresponding to a Au-S-C bond angle of 109° (sp^3) and 180° (sp).[34] In DMAAB SAMs, depending on preparation conditions, we find a significant variation in the ratio of the two sulfur components at 161 eV and at 162 eV. This is interpreted as a variation in the fraction of DMAAB molecules oriented along each of these possible tilt angles. Indeed, the strong intermolecular forces between dithioacetamides caused by hydrogen bond formation could lead to a stacking of molecules in different directions towards the surface normal and thus force the thiolate headgroup to bind at angles predetermined by the orientation of the dithioacetamide aggregate. To verify this hypothesis, we

computed the interaction energy between DMAAB molecules by means of molecular mechanics calculations. The calculations are performed with the COMPASS force-field model, which has been proven to be reliable in the calculation of H-bond interactions.[22] The calculations show that two interacting DMAAB molecules, upon relaxation, form hydrogen bonds between the NH group and the carbonyl group (Fig. 3c), resulting in an energy gain of 2 eV. Agglomerates consisting of 6 DMAAB molecules give an interaction energy of 1.8 eV/molecule (Fig. 3d).
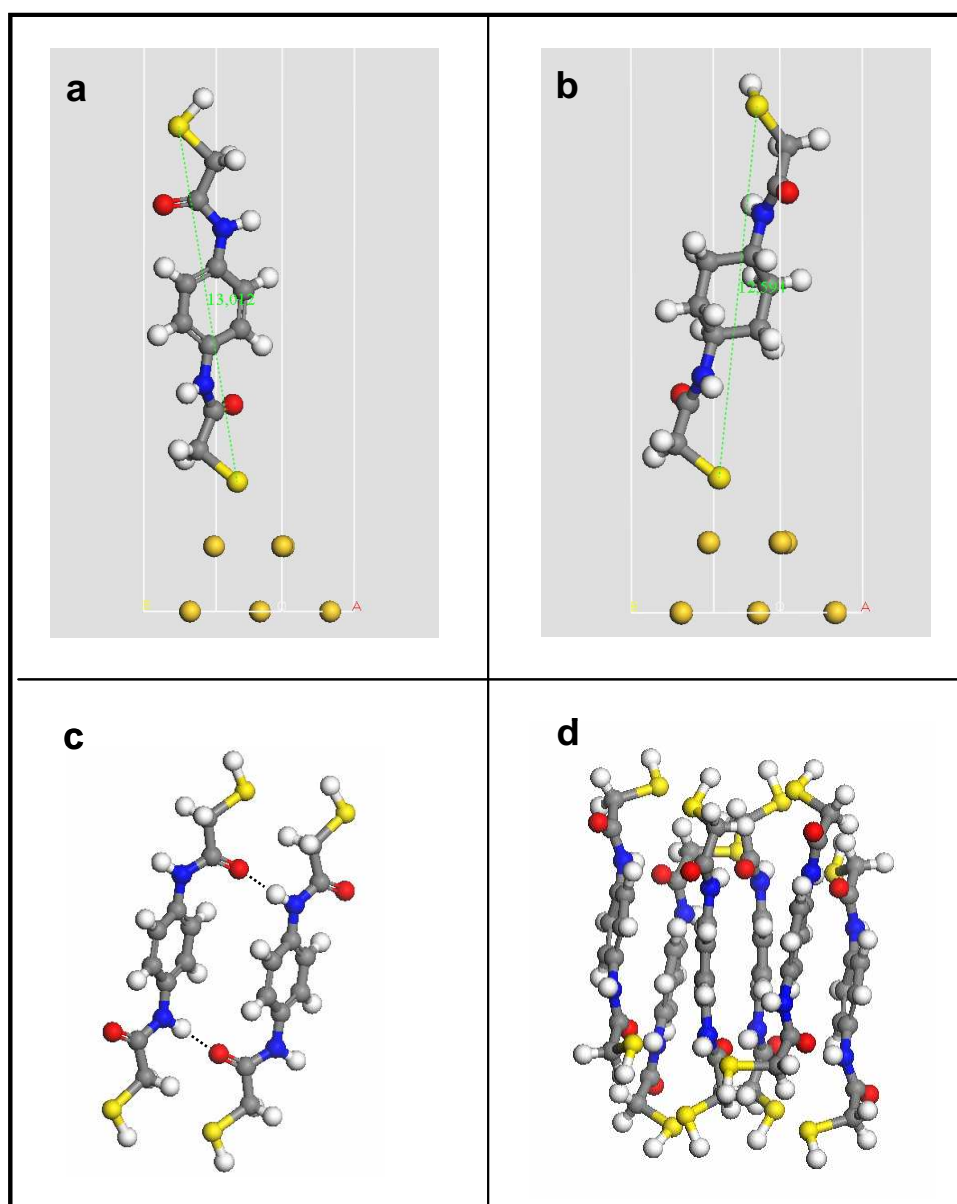
Figure 3: Relaxed structure of DMAAB (a) and DMAAcH (b) on a Au(111) slab from a periodic DFT calculation. Only a single cell is shown. (c and d) DMAAB aggregate structures obtained from a COMPASS forcefield calculation. (c) Relaxed geometry for 2 DMAAB molecules with the formation of hydrogen bonds (dashed lines). (d) Relaxed structure of an aggregate consisting of 6 DMAAB molecules, clearly showing π-stacking due to the presence of the benzene rings.

This is roughly twice the energy of the thiolate-Au bond and 4 times the interaction energy of alkane chains in close packed decanethiol SAMs, clearly showing that for dithioacetamides the intermolecular interaction is determining the monolayer structure. The high intermolecular forces between DMAAB molecules are manifest in the high melting temperatures found for DMAAB bulk material and in its limited solubility in common solvents (only DMF and DMSO dissolve DMAAB). It is pertinent to note that the repeat unit in aromatic polyamide (Kevlar), a very strong synthetic polymer, is identical to the monomer structure of DMAAB except for the two thiol end-groups.

To conclude, even though strong intermolecular forces lead to aggregation and disorder in dithioacetamide monolayers, as evidenced by different sulfur *2p* XPS species found for bound thiolate as well as by the lack of order in STM images, the body of the data show the formation of dense monolayers in which the dithioacetamide molecules are linked to Au by a single thiolate binding group.

More details on the growth behavior of DMAAB SAMs can be found in the Supporting Information (Fig. S3).

Mixed SAMs by co-assembly. In the co-assembly approach, dodecanethiol and DMAAB are grown on Au simultaneously. The relative coverages and the miscibility of the compounds within the SAM are determined by the Langmuir adsorption constant for each component and solution growth thermodynamics. Phase separation requires thermal annealing of the mixed monolayer[15] due to the large interaction forces between DMAAB molecules and the resulting low mobility of DMAAB aggregates at surface. An annealing temperature of at least 80°C is needed to initiate the growth of DMAAB islands, as observed in STM micrographs. However, XPS characterization shows that this annealing step does not significantly change the molecular composition of the monolayer.
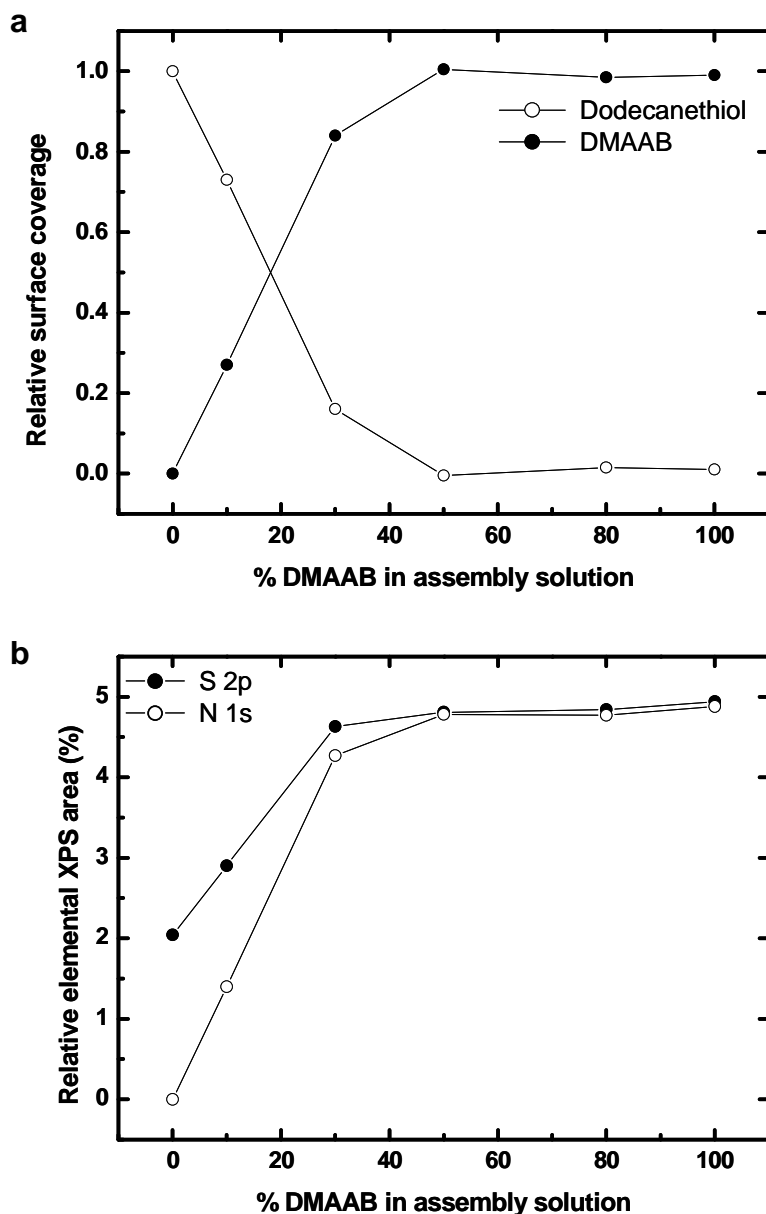
Figure 4. (a) Dependence of DMAAB and dodecanethiol coverage on concentration in solution. (b) Intensity of the N *1s* and S *2p* peaks, from which the coverages are determined by means of molecular stoichiometry.

Since a small fraction of dodecanethiol molecules desorb from surface at 80°C,[35] upon thermal annealing the substrates are immersed into a dodecanethiol solution to refill the vacancies and to form an equilibrated, close packed monolayer. XPS analysis confirmed that DMAAB is chemically stable under annealing conditions and also towards replacement by alkanethiols (Supporting information).[13]

Figure 4a shows the relative DMAAB coverage on Au for different DMAAB/dodecanethiol concentration ratios (in %) in the assembly solution. The coverage is determined from the XPS S *2p* and N *1s* signal intensities (Fig. 4b) and by

consideration of the stoichiometry of both compounds.[36] Figure 5 shows a sequence of STM images of mixed SAMs corresponding to each of the concentration ratios shown in Fig. 4a, along with a schematic drawing illustrating the monolayer structure.

100% SC12 0% DMAAB	90% SC12 10% DMAAB	70% SC12 30% DMAAB	50% SC12 50% DMAAB	0% SC12 100% DMAAB
65 x 65 nm	100 x 100 nm	100 x 100 nm	100 x 100 nm	100 x 100 nm
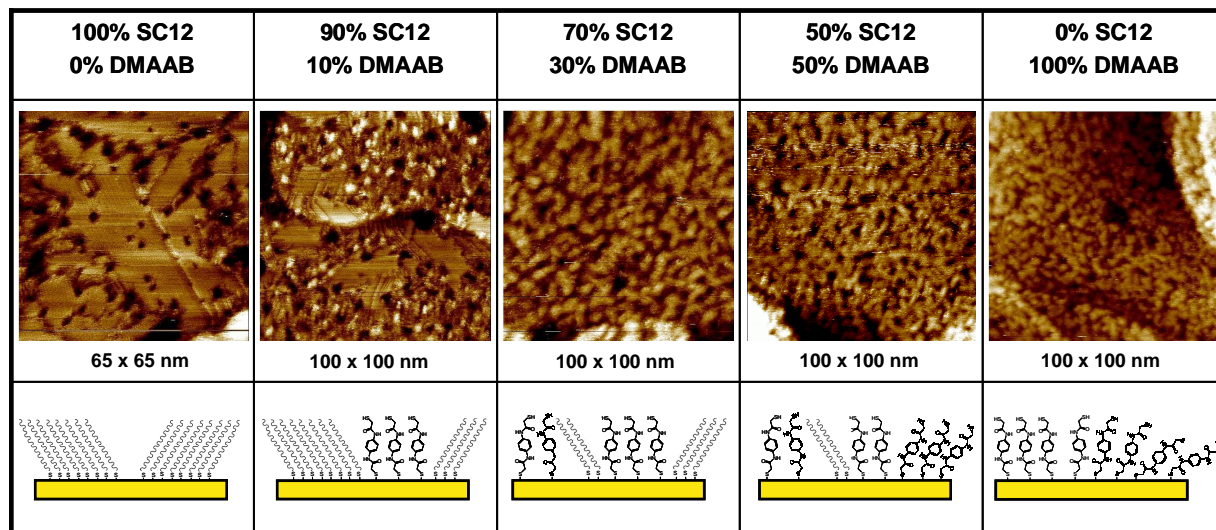
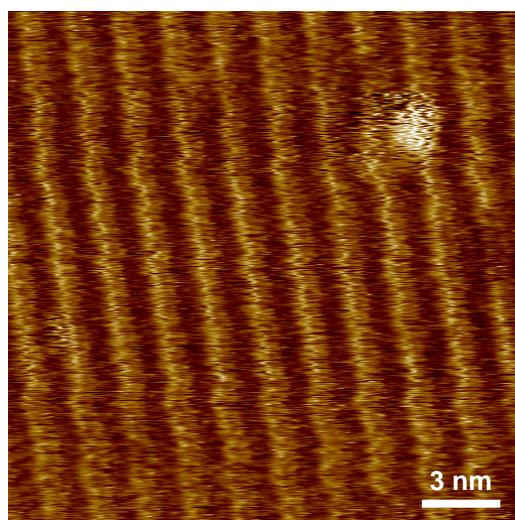**Figure 5.** STM scans of mixed DMAAB/dodecanethiol monolayers using different DMAAB/dodecanethiol concentration ratios in the assembly solution, as indicated in each of the figures. The monolayers are obtained upon assembly at RT and subsequent thermal annealing of the samples in the gas phase of a mixed DMAAB/dodectanethiol solution at 80°C. The structures at the bottom are schematic representations of the corresponding monolayer structure. The scans are recorded at a bias voltage of $U_{Gap} = 400$ mV and a tunneling current of $I_{tunn} = 2$ pA.

The island density, i.e. the density of bright spots in the second scan in Fig. 5, is consistent with the relative DMAAB coverage as determined from XPS (Fig. 4a) and from contact angle goniometry (Fig. S6, supporting information). The XPS, STM and contact angle results show that the DMAAB coverage is dominant if its ratio in solution is higher than 20%. The high DMAAB coverage at low DMAAB ratios in solution is interpreted as a consequence of the higher sticking coefficient to Au of dithioacetamides compared to alkanethiols, caused by the presence of two thiol end groups and by the attractive polar interactions between dithioacetamide molecules.[37] At DMAAB ratios of 30% and 50%, rod-like domains are observed in the STM images. Similar structures, consisting of two rows of stacked molecules, are also found in mixed SAMs with the aliphatic dithioacetamide DMAAcH (Fig. S7, supporting information). Well-separated DMAAB islands, surrounded by hexagonally close packed alkanethiol domains, are only observed at DMAAB ratios lower than 10%. In this case, areas with a high density of DMAAB islands often show local

disorder in the dodecanethiol phase, indicative of structural perturbations induced by the presence of strongly polar DMAAB molecules within the host layer.

Figure 6. Single DMAAB molecule inserted into a striped dodecanethiol low coverage phase. The striped phase is obtained upon thermal annealing of a mixed DMAAB/dodectanethiol SAM in solution (at ca. 98°C for 2h). Tunneling parameters: U_{Gap} = 500 mV, I_{tunn} = 200 pA.

At low DMAAB ratios (1% DMAAB) and high annealing temperatures ($T_{solution}$ ~ 98°C) isolated DMAAB molecules embedded in a low coverage dodecanethiol SAM were observed (Fig. 6). The low coverage phase is a consequence of thermal desorption of dodecanethiol from Au resulting from the annealing procedure. Unfortunately, isolated molecules diluted in a low density alkanethiol matrix are not suited for electrical characterization by STM, since such molecules are not supported by a dense alkanethiol matrix and the molecular orientation is ill defined in this case.

Mixed SAMs by insertion. Small, oriented domains of aromatic and aliphatic dithioacetamides are realized by insertion into defect sites of a fully grown, hexagonally close-packed alkanethiol monolayer.[8] Since close packed alkanethiols are not easily replaced, only small defects and domain boundaries within the alkanethiol SAM are available for the dithioacetamides to chemically bind to the Au surface. Around these small defects, the alkanethiol molecules are tilted away from the surface normal by an angle of 32°,[12] supporting the inserted molecules in an upright position. The insertion of the aromatic dithioacetamide DMAAB and its aliphatic conjugate DMAAcH proved to be easier in octanethiol than in dodecanethiol monolayers, probably due to the stronger blocking properties of long-chain alkanethiols at defect

sites (dodecanethiol monolayers are reported to be solid, whereas octanethiol monolayers are much softer[38]). In addition, on octanethiol monolayers the available tunneling impedances are sufficient for a perturbation-free imaging (vacuum gap between tip and SAM), allowing the extraction of the tunneling decay constant both on dithioacetamide and on alkanethiol domains.

Figure 7 shows an STM image of an octanethiol SAM before (Fig. 7a) and after (Fig. 7b) insertion of DMAAB molecules into monolayer defects. In the bottom left domain of the scan in Fig. 7a the c(4 x 2) reconstruction of the ($\sqrt{3}$ x $\sqrt{3}$)R30° octanethiol overlayer is visible.[39] The depressions are mono-atomic vacancy islands in the Au(111) substrate. The STM image in Figure 7b shows that the adsorption sites for DMAAB are represented by step edges, vacancy islands and octanethiol domain boundaries. Molecular resolution within the domains could not be achieved (even if this was possible in the octanethiol matrix), probably as a result of structural disorder induced by the polar intermolecular forces in the dithioacetamide phase. Although the bright DMAAB islands are limited in size (3 nm diameter in average), it is assumed that during DMAAB insertion some of the octanethiol molecules are desorbed from the surface and replaced by DMAAB, allowing the islands to grow beyond the original size of the defect in the octanethiol monolayer.

a) Octanethiol SAM	b) Octanethiol/DMAAB SAM
50 nm x 50 nm	200 nm x 200 nm
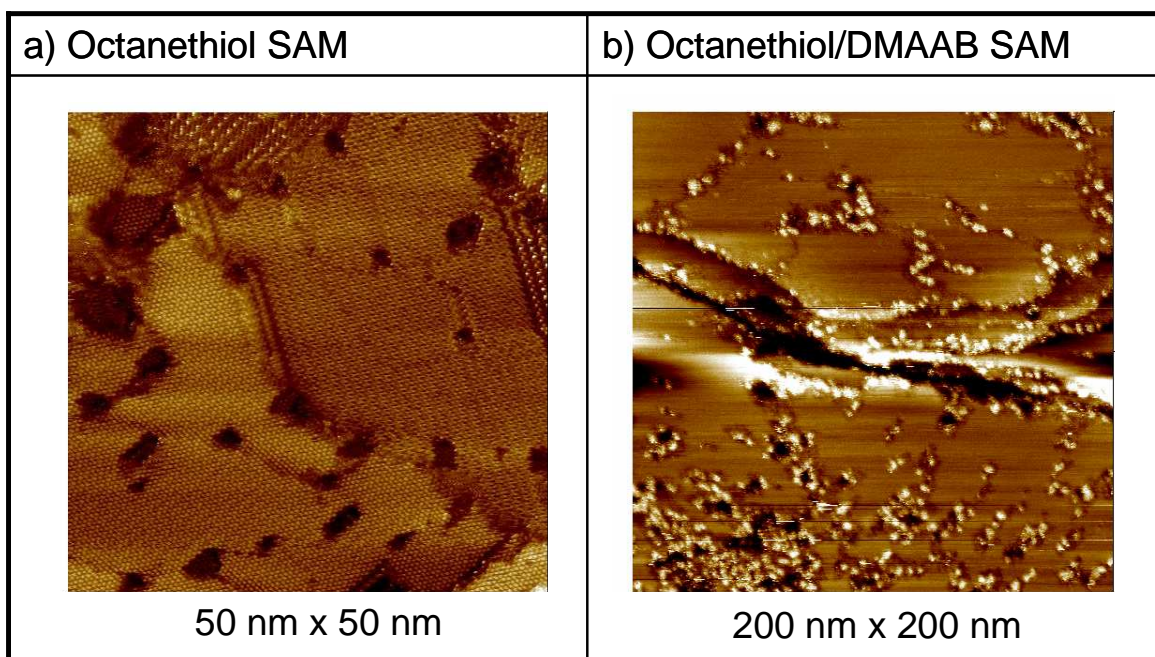
Figure 7. (a) STM image of a hexagonally close packed octanethiol monolayer before insertion of DMAAB (50 nm x 50 nm). The depressions are mono-atomic vacancy islands in the Au(111) substrate. These are created during SAM growth and are also covered by a ($\sqrt{3}$ x $\sqrt{3}$)R30° overlayer. (b) DMAAB molecules inserted into defect sites and domain boundaries of an octanethiol monolayer (200 nm x 200 nm). The scans are recorded at a bias voltage of U_{Gap} = 400 mV and a tunneling current of I_{tunn} = 2 pA.

An analysis of STM height profiles reveals a lower threshold of 1.5 nm for the apparent diameter of DMAAB islands. Taking into account the shape-broadening due to the STM imaging mechanism (0.7-1 nm for alkanethiols),[40] this shows that even smallest defects in the host are accessible for DMAAB insertion. The limited size of alkanethiol defects available for insertion and the good reproducibility of STM height differences for islands having different diameters indicate that domains consisting of only a few, upright dithioacetamide molecules are obtained with the insertion method (Fig. S2, supporting information). This overcomes some of the concerns on molecular orientation discussed in the previous sections. It is worth to note that most of the DMAAB islands in Fig. 7b are surrounded by a small depression within the octanethiol SAM (see also Fig. 8a). This effect could be due to the limited solubility of DMAAB in alkanes, leading to a reduced packing density of octanethiol molecules in the immediate vicinity of DMAAB domains.

The analysis of the molecular conductance in STM relies on the apparent topographic height difference Δh_{STM} between distinct domains.[17] In constant current mode, the height of the tip is a convolution of the sample topography and of the electronic properties of the SAM. Thus, the conductance across the molecular layer

can be obtained by combining the information on the monolayer thickness with the measured value of Δh_{STM}. The electron tunneling process between a STM tip and a conductive substrate is described by the following exponential model

$$G = G_0 \cdot \exp(-\beta h) \tag{1}$$

where G_0 is the contact conductance, β the tunneling decay constant, and h the tunneling distance. If the STM tip is above the molecular layer, the conductance G is the product of the two exponential terms characterizing the conductance through the monolayer and through the vacuum gap between the monolayer and the tip

$$G = A_M \cdot \exp(-\beta_M h_M) \cdot B \cdot \exp(-\beta_v h_G) \tag{2}$$

where A_M is the contact conductance between the metal substrate and the molecule, B is the contact conductance between the molecular layer and the vacuum gap, β_M and β_v the two tunneling decay constants of the molecule and of the vacuum respectively, h_M the thickness of the molecular layer and h_G the distance between the tip and the SAM. Since the STM is operated in constant current mode, the total conductance G does not depend on the imaged domain

$$G(alkanethiols) = G(dithioacetamides) \tag{3}$$

This equation can be solved for $\beta_{dithioacetamides}$ if the layer thickness h_{alk} and $h_{dithioacetamides}$ for alkanethiol and dithioacetamide domains is given and Δh_{STM} is measured. Assuming that the decay constant β_v above dithioacetamide and octanethiol domains is equal[41] and that the electrical coupling of the two molecules to the substrate (both thiols) is comparable ($A_{Alkanethiol} \approx A_{Dithioacetamide}$),[42] the decay constant of dithioacetamides is

$$\beta_{dithioacetamides} = \frac{\beta_v(\Delta h_{Top} - \Delta h_{STM}) + \beta_{alk} h_{alk}}{h_{dithioacetamides}} \tag{4}$$

where $\Delta h_{Top} = h_{dithioacetamides} - h_{alk}$ is the topographic height difference between the alkanethiol and the dithioacetamide domain and β_{alk} and h_{alk} denote the decay constant and the topographic height of alkanethiol SAMs.

For the calculation of $\beta_{dithioacetamides}$, a value of $\beta_v = 2.2/\text{Å}$ for vacuum and $\beta_{alk} = 1/\text{Å}$ for alkanes is used, based on previous STM measurements,[43,17] conductance measurements on networks of NP films[18] and Hg-drop experiments.[44] The monolayer thickness is estimated based on a molecular orientation of 32° away from the surface normal for octanethiols and dithioacetamides. This simplified assumption is based on

the fact that the dithioacetamides inserted into small defects are supported by the octanethiol matrix. But we are aware that also a perpendicular orientation of dithioacetamides is possible, which introduces a certain uncertainty in the relative topographic height difference Δh_{Top}. According to DFT calculations in the gas phase, the relaxed structures of octanethiol, DMAAB and DMAAcH have a length of d_{S-C8} = 1.05 nm, d_{S-S} = 1.33 nm and d_{S-S} = 1.33 nm respectively, with the cyclohexyl ring of DMAAcH in chair conformation. Since the molecular length within monolayers can differ from that in the gas phase, these results were compared with periodic DFT calculations of molecules assembled on a gold slab (Fig. 3), yielding a length of d_{S-C8} = 1.05 nm, d_{S-S} = 1.3 nm, d_{S-S} = 1.26 nm for octanethiol, DMAAB and DMAAcH, respectively. The shorter length determined for DMAAcH in a monolayer environment results from the higher flexibility of the cyclohexane ring compared to the aromatic ring in DMAAB.

Figure 8 shows the STM height profiles for DMAAB (a) and DMAAcH (b) domains in close-packed octanethiol monolayers. While DMAAcH domains form flat plateaus, DMAAB domains tend to form slightly hill-shaped islands, whose height becomes gradually lower at the edges. This effect might be due to the aromatic character of the DMAAB compound, leading to a partial transversal conductance across the island caused by the better electronic coupling between the π-stacked benzene rings.[45] The average of 30 sections across DMAAB domains and 20 sections across DMAAcH domains lead to Δh_{STM} = 0.25 ± 0.2 nm for DMAAB and Δh_{STM} = 0.175 ± 0.1 nm for DMAAcH. Assuming a tilt angle of α ~ 32° for dithioacetamides on Au, the monolayer thickness can be obtained from the molecular length with $h = (sin\,\alpha)\,d$. With Eq. (4), we obtain a tunneling decay constant of β_{DMAAB} = 0.76/Å and β_{DMAAcH} = 0.91/Å when using molecular lengths from gas phase calculations and β_{DMAAB} = 0.74/Å and β_{DMAAcH} = 0.84/Å when using molecular lengths from periodic DFT calculations (molecules on a Au slab).
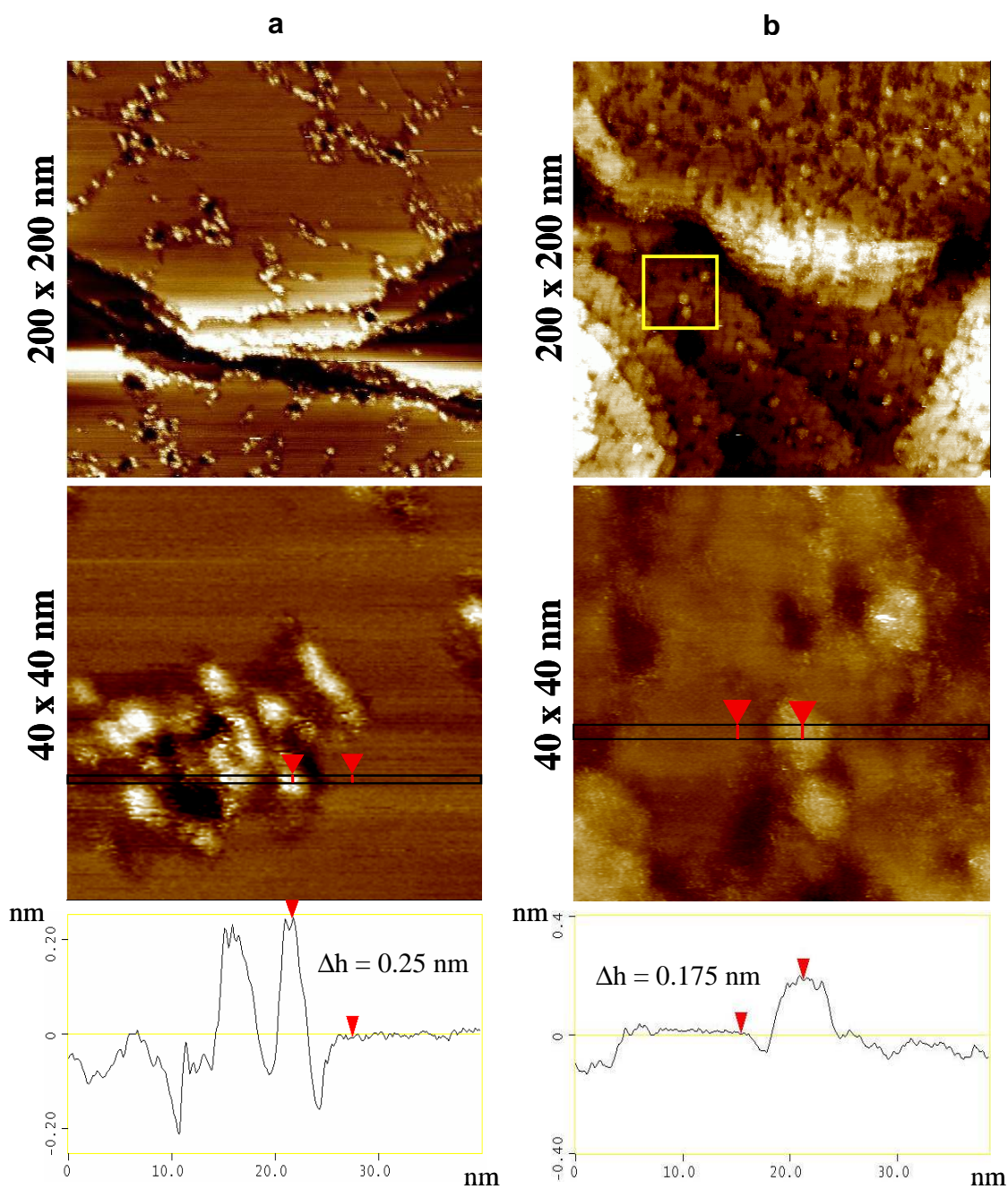
Figure 8. STM images of DMAAB (a) and DMAAcH (b) domains created by insertion of molecules into octanethiol monolayers. The cross sections show STM height profiles of DMAAB (a) and DMAAcH (b) domains along the scan direction. The sections are obtained by averaging over the set of scan-lines contained in the black rectangles. Tunneling parameters: $U_{Gap} = 400$ mV, $I_{tunn} = 2$ pA.

The difference in the β values for DMAAB and DMAAcH reflects the effect of conjugation within the cyclic core on the electrical transconductance. The conductance through DMAAB, as obtained by inserting the values for β into Eq. (1), is significantly higher than through the aliphatic compound DMAAcH, whose cyclohexyl ring electrically behaves like an insulating alkyl chain. If we split the

dithioacetamides into electronically independent sections, i.e. the central ring and the two acetamido groups, and if we further assume the same β value (0.91/Å) for the cyclohexane ring and the two saturated acetamido units, we find a decay constant of β = 0.52/Å for the phenyl ring in DMAAB. This value is very close to those reported for oligophenylenes[46,47] and shows that the difference in the tunneling decay constant found for DMAAB and DMAAcH is in reasonable agreement with their molecular structure. However, it should be considered that the decay constant critically depends on the length and thus on the conformation of a molecule within the monolayer. This introduces a larger uncertainty in the β values determined for the aliphatic dithioacetamide DMAAcH compared to those of the stiffer aromatic dithioacetamide DMAAB, as we have shown by molecular modeling.

Conclusions

In this study two assembly methods, co-assembly and insertion, are compared for the growth of mixed monolayers consisting of dithioacetamides and alkanethiols. The results show that the strong intermolecular hydrogen bond interactions prevent the formation of ordered dithioacetamide monolayers. Phase segregation of dithioacetamides and alkanethiols requires thermal annealing in the co-assembly process. In contrast, by sequential assembly, dithioacetamides are inserted into small defects within the alkanethiol monolayer, yielding well-defined, oriented dithioacetamide domains. These allow the determination of the tunneling decay constant of aromatic and cyclic dithioacetamides, based on a careful analysis of height profiles from STM images, surface densities from XPS data and molecular lengths from DFT calculations. The tunneling decay constant enables a direct comparison of the conductance of the aromatic and the aliphatic derivative, showing that it differs by roughly one order of magnitude. However, it is concluded that the general reliability of conductance measurements based on STM height profiles strongly depends on the molecular orientation and on the structural stability of the investigated compounds within the monolayer.

Supporting Information

DFT calculations. The relaxed structures of DMAAB (a) and DMAAcH (b) monolayers on a periodic Au(111) slab are shown in Fig. S1. The average packing density of the dithioacetamide molecules on Au, as determined from XPS data, is only 20% lower than in the ($\sqrt{3}$ x $\sqrt{3}$)R30° overlayer structure known from alkanethiols on Au(111). Thus, as an approximation, a ($\sqrt{3}$ x $\sqrt{3}$)R30° overlayer structure was assumed for the calculation. In the relaxed structure (equilibration of the dithioacetamide adsorbates but not of the Au slab), the dithioacetamides are chemisorbed to Au(111) with the sulfur atom located in between a "bridge site" and a "on top site". The next-neighbor S-Au bond distance is 2.5 Å and the tilt angle of the molecular backbone towards the surface normal is less than 20°. The molecular lengths are d_{S-S} = 1.3 nm for DMAAB and d_{S-S} = 1.26 nm for DMAAcH. Nevertheless, due to the various possible orientations of the molecule within the unit cell, other equilibrium structures of dithioacetamides on Au cannot be ruled out. Note that, in contrast to polar interactions (H-bonds), intermolecular dispersion forces (van der Waals forces) are not fully accounted for within the DFT model. This drawback of the model is probably of minor relevance due to the dominant character of H-bond interactions between the dithioacetamides in the monolayer.

A two layer Au(111) slab in a periodic ($\sqrt{3}$ x $\sqrt{3}$)R30° unit cell is employed to model the surface. Perpendicularly to the surface, the size of the unit cell is 28 Å. Thus, the vacuum gap thickness between adlayer and the Au layer of the adjacent cell is about 10 Å. DFT calculations are performed in the local density approximation using the VWN LDA functional[1] with a double numerical basis set with polarization functions (DND), as provided by Dmol3.

---

[1] Vosko, S. J.; Wilk, L.; Nusair, M. "Accurate spin-dependent electron liquid correlation energies for local spin density calculations: A critical analysis", *Can. J. Phys.*, **58**, 1200-1211 (1980).
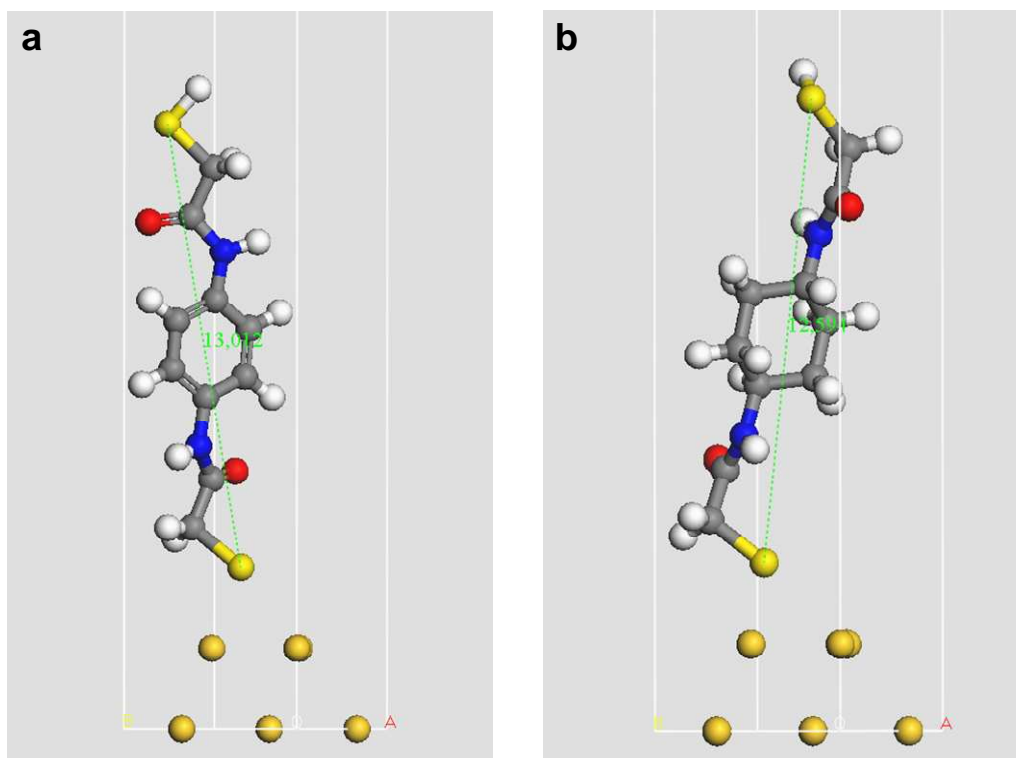
Figure S8. Relaxed structures of DMAAB (a) and DMAAcH (b) on a periodic Au(111) slab. The coordination of the thiolate to Au is similar in both cases, corresponding to a slightly off-axis bridge site. In the periodic case, the length of the two compounds differs due to the higher flexibility of the DMAAcH compound and due to the effect of intermolecular interactions. In both cases, the orientation of the molecule is almost perpendicular to the surface. The molecular lengths are d_{S-S} = 1.3 nm for DMAAB and d_{S-S} = 1.26 nm for DMAAcH.

Model of a DMAAB domain structure: In Fig. S2, the structure of a hypothetical DMAAB domain inserted in a ($\sqrt{3}$ x $\sqrt{3}$)R30° octanethiol monolayer on Au(111) is presented. It shows a section along the [11-2] direction of the Au(111) surface. The octanethiol layer was relaxed within a periodic DFT calculation in a ($2\sqrt{3}$ x $2\sqrt{3}$) unit cell, using the VWN LDA functional. Subsequently some of the octanethiol molecules were removed, creating a defect with the lateral size corresponding to two adjacent DMAAB molecules. Finally, the DMAAB molecules were relaxed within a COMPASS force-field calculation, while the host layer and the Au slab were kept frozen. As shown in Fig. S2, the physical size of the defect is 13.2 Å. Considering that the shape-broadening due to the STM imaging mechanism (i.e. completely neglecting further broadening due to tip convolution) is about 0.7-1 nm, an effective domain size of at least 20-23 Å is expected from STM images of this structure. Experimental STM profiles showed the presence of bright spots with diameters down to 1.5 nm (see

Article), thus allowing the conclusion that these small features might correspond to single DMAAB molecules isolated in the host matrix.
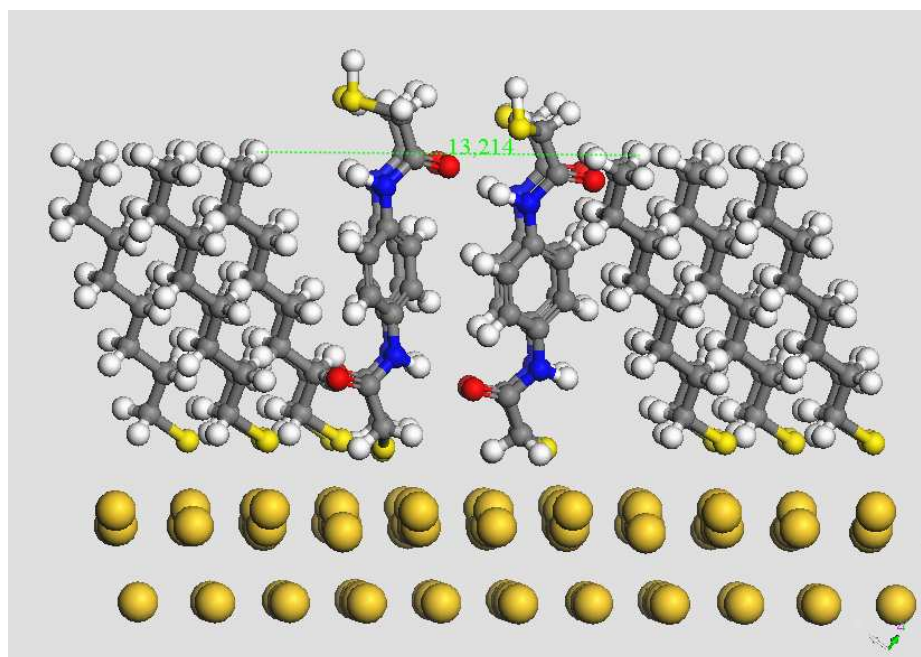
Figure S2. Structure of a hypothetical DMAAB domain inserted in a ($\sqrt{3}$ x $\sqrt{3}$)R30° octanethiol monolayer on Au(111). A section along the [11-2] direction of the Au(111) surface is shown. The octanethiol layer was relaxed within a periodic DFT calculation, while the inserted DMAAB molecules were placed into defects and relaxed with the COMPASS force field method. The octanethiol vacancy is selected in such a way that 2 DMAAB molecules fit into the defect site. The physical size of the gap bridging the defect is ~13.2 Å.

Growth kinetics of a dithioacetamide SAM. The SAM growth process is studied by monitoring adsorption chemistry and SAM coverage as a function of assembly time in a 1 mM DMAAB solution. Figure S3 shows the evolution of DMAAB coverage with assembly time. The XPS results suggest that the film growth is governed by two processes. In the initial phase, the growth is determined by the interaction of the thiol headgroup with the Au substrate, leading to the formation of a lying down phase. Indeed, the high S $2p$(thiolate)/S $2p$(total) ratio suggests that part of the molecules bind with both thiolate groups to the substrate. Within the first 10 minutes of SAM growth, the S $2p$(thiolate)/Au $4f$ ratio increases by 15% as a result of the higher density of molecules covalently linked to Au. During the same time, the DMAAB coverage increases by 20%, indicating that part of the molecules bound with both thiolate groups are forced into an upright position by polar interaction forces. Beyond an assembly time of 10 minutes, a long term growth process, associated with a further

96

increase of the S *2p* component at 163.5 eV BE takes place. In particular, while the S *2p*(thiolate)/Au *4f* ratio remains stable, an increase by 27% in the S *2p*(total)/Au *4f* ratio is observed, joined by an increase of the component related to the presence of thiol sulfur in the SAM (S *2p* at 163.5 eV BE).
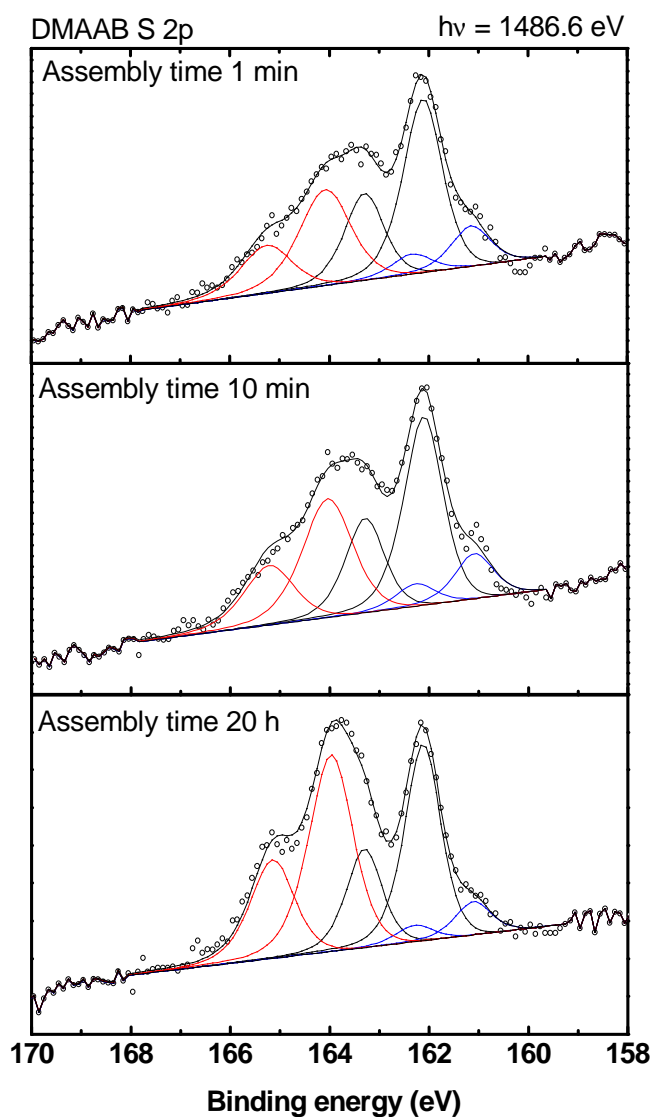
Figure S3. High resolution XPS S *2p* core level spectra of a DMAAB SAM at different stages of SAM growth. The contribution from thiolate sulfur (162 eV and 161 eV BE) increases within the first 10 minutes of SAM growth. (b) Between 10 min and 20 h assembly time, only the component associated to free thiol (163.5 eV BE) increases.

Thiol and disulfide S *2p* components in a dithioacetamide monolayer. Further experiments were performed to separate the contribution from the thiol and the disulfide species in dithioacetamide layers. First, the BE of the thiol sulfur in DMAAB was found by XPS measurements on DMAAB multilayers. The multilayers

are obtained by drop casting a saturated DMAAB solution on a Au substrate and evaporation of the solvent. The S *2p* signal for S-H sulfur is found at 163.5 ± 0.1 eV (Figure S4a). Second, the BE of the disulfide sulfur in DMAAB oligomers is determined by adding iodine (I_2) to solution before assembly. Iodine is an oxidation agent that is known to trigger the formation of oligomers via disulfide bridges. Here, the S *2p* signal for S-S sulfur (there might be also a minor contribution from S-H sulfur in this peak) is found at 163.5 ± 0.15 eV (Figure S4b). Since in the two experiments both the S-S and the S-H sulfur S *2p* signals are found at the same BE, a distinction of disulfides and thiols is not possible within the experimental accuracy.
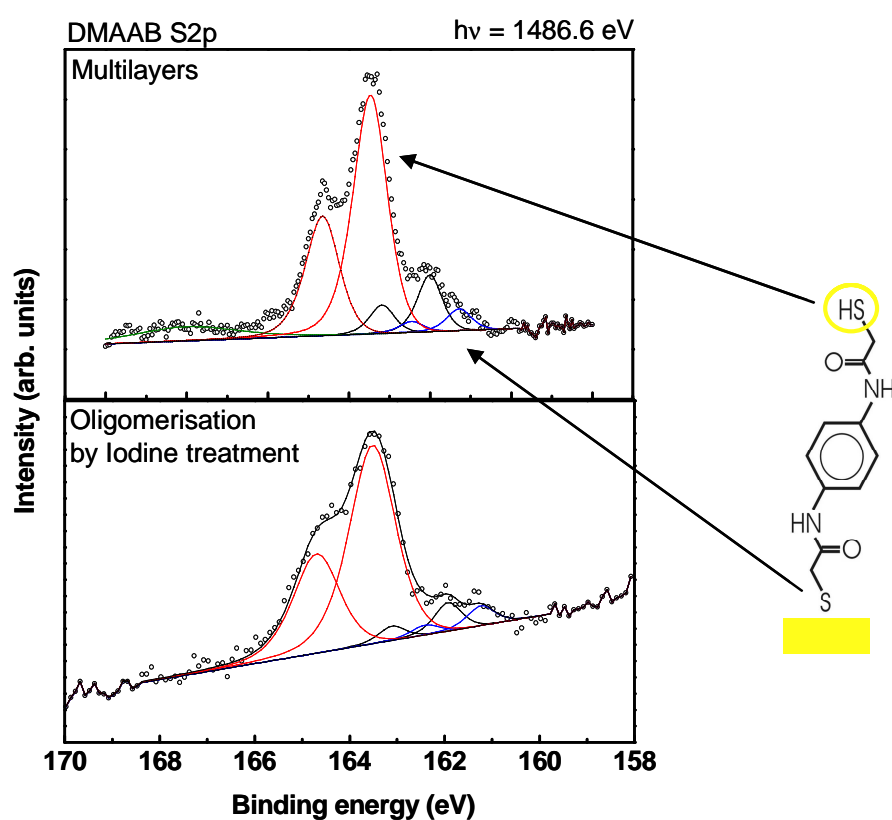
Figure S4: High resolution XPS S *2p* spectra of DMAAB multilayers (a) and of DMAAB SAMs treated with an iodine (I_2) solution (b). In DMAAB multilayers (a), the peak corresponding to thiol sulfur at 163.5 eV is dominant. In DMAAB SAMs prepared from iodine solution, the peak corresponding to disulfide sulfur is found at the same binding energy, i.e. at 163.5 eV.

Processes during thermal annealing and temperature stability of DMAAB. We found that an annealing temperature of 80°C is required to observe a ripening of DMAAB domains. Thus, it is assumed that a high activation energy is needed to initiate diffusion of DMAAB molecules or aggregates, since a single DMAAB

molecule is hardly removed from a DMAAB island (hydrogen bonds) and probably the DMAAB aggregates have to diffuse along the surface "en bloc". In turn, alkanethiols diffuse and partially desorb from surface at 80°C, reason for which the substrates are immersed in alkanethiol solution upon thermal annealing, such that alkanethiol molecules are allowed to refill the vacancies and to form an equilibrated, close packed SAM. XPS analysis is performed after each of the mentioned processing steps, and no significant change in the composition of the SAM is observed, showing that DMAAB is stable under annealing conditions and also towards replacement by alkanethiols. Furthermore, NMR experiments prove that no DMAAB decomposition occurs if the substance is heated for 1 h at 90°C in DMF.

STM topography of a DMAAB SAM. A characteristic overlayer structure is observed in STM images of a DMAAB monolayer, consisting of 3-4 nm sized bumps separated by depressions. The measured height profile is presented in Figure S5, showing an average modulation of 0.25 nm in the topography of the monolayer. It is attributed to differences in the molecular orientation of the DMAAB molecules as a result of an inhomogeneous growth of DMAAB aggregates on Au(111). A possible reconstruction of the Au(111) surface due to DMAAB adsorption is unlikely, since terrace edges are clearly visible and not much affected by the monolayer growth (not shown here).
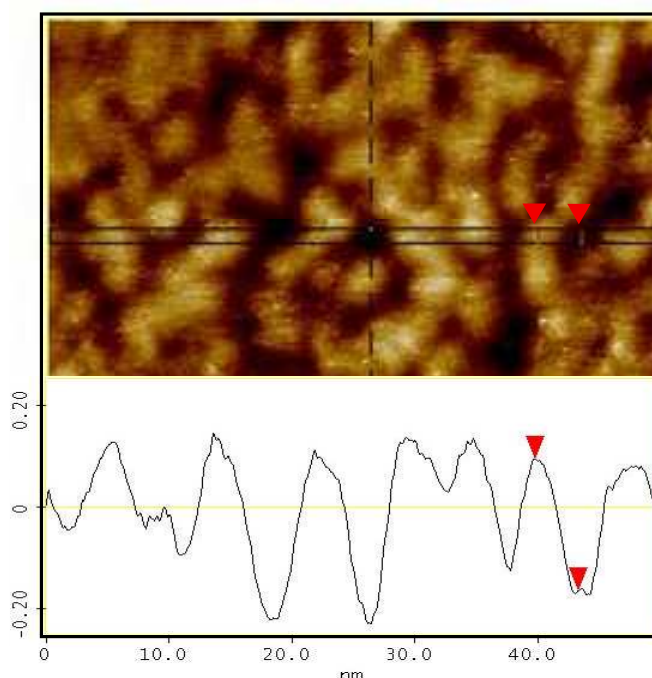
Figure S5: STM image (50nm x 30 nm) of a DMAAB monolayer on Au(111). A section along the scan direction, averaged over 15 scan lines, is shown at the bottom. The average STM height difference

between the islands and the depressed areas is ~ 0.25 nm. The STM height is measured at the position of the two red arrows.

Determination of dithioacetamide coverage by contact angle goniometry. A series of co-assembled, DMAAB/dodecanethiol monolayers with different DMAAB/dodecanethiol concentration ratios in solution is measured by STM, XPS and contact angle goniometry in parallel (See "Mixed SAMs by co-assembly" in the results section). Contact angle measurements with a water droplet are performed with a KSV CAM 100. From the contact angles on DMAAB and dodecanethiol SAMs, the two separate contributions are determined. Then the contact angle θ_{eff} for the mixed, two component SAM is measured. Coverages for the mixed SAMs are obtained using the Cassie equation

$$\cos\theta_{eff} = \varphi_A \cos\theta_A + \varphi_B \cos\theta_B$$

that relates the contact angle θ_{eff} of a multi-component surface to the contact angles θ_A and θ_B of surfaces covered with the single components A and B. From this equation, we obtain the relative coverages φ_A and φ_B using the relationship

$$\varphi_A = 1 - \varphi_B$$

Figure S6 shows a plot for the DMAAB coverage determined via the Cassie-equation. Comparison to the XPS data presented in Figure 4 shows a good agreement and demonstrates that this method is a valid alternative for a qualitative coverage determination. The mismatch at a DMAAB concentration higher than 30% (compared to XPS data) could be related to differences in the SAM structure.
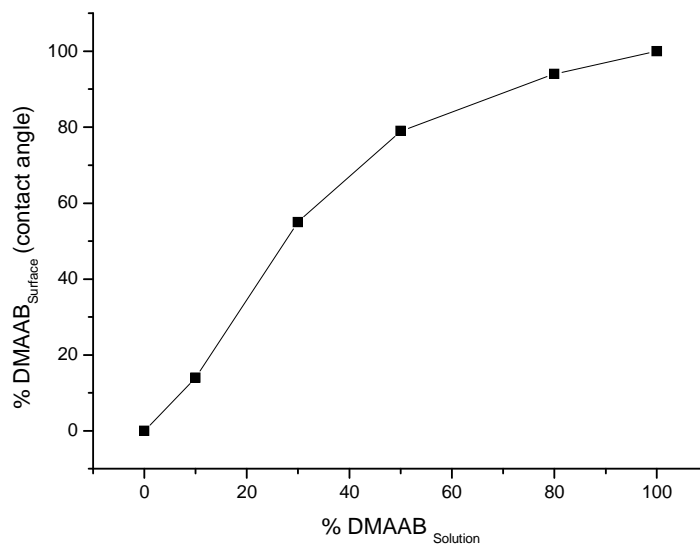
Figure S6. DMAAB coverage as determined from contact angle goniometry.

**Formation of DMAAcH rod-like domains**. Structures that are attributed to DMAAcH rod-like domains are observed in mixed DMAAcH/octanethiol monolayers (Figure S7). The monolayers are prepared by immersing the crystalline Au(111) substrates in a equimolar DMAAcH/octanethiol mixed solution (1 mM) for 24 h at RT. Finally, the monolayers are thermally annealed in the assembly solution at 95°C for 1 h. This allows phase segregation of DMAAcH and dodecanethiol. The rods have a length of ~ 6 nm and a width of ~ 2 nm. The molecular structure of a few of these rods could be resolved as seen in the STM scan in Fig. S7 (right image), showing the formation of a double row of stacked aliphatic DMAAcH molecules.
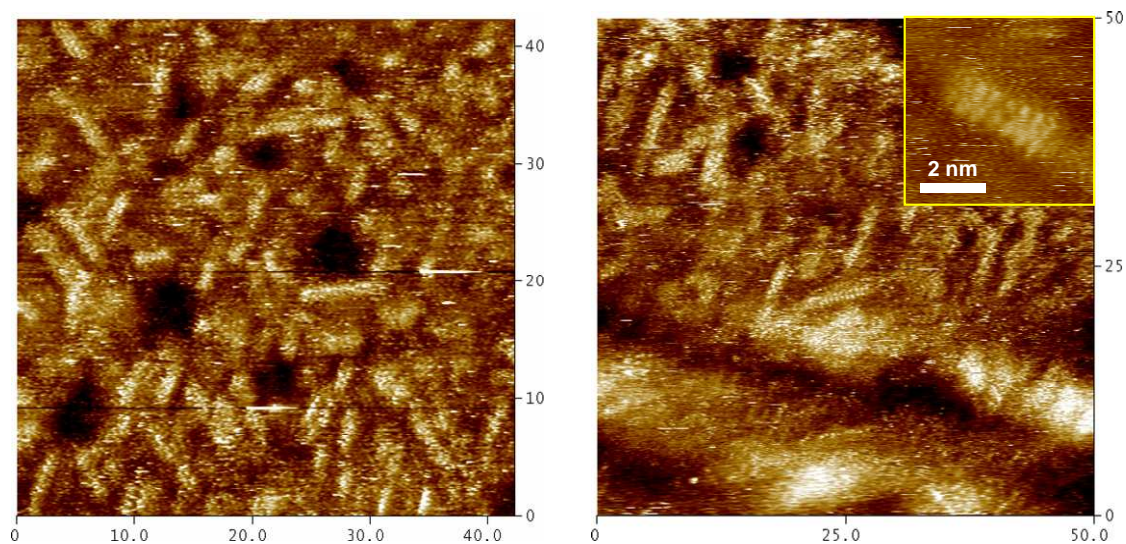
Figure S7. STM scans of mixed DMAAcH/octanethiol monolayers. The monolayers are obtained upon assembly at RT and subsequent thermal annealing of the samples in a 1:1 DMAAB/dodectanethiol solution at ca. 95°C for 1h. (a) The orientation of the rods follows the surface lattice orientation of Au(111), i.e. the relative orientation of the rods correspond to multiples of 60°. (b) The inset shows a high resolution image of a rod, consisting of two rows of DMAAcH molecules. The scans are recorded at a bias voltage of $U_{Gap} = 400$ mV and a tunneling current of $I_{tunn} = 2$ pA.

References

(1) Emmons, H. *Trans. Am. Inst. Chem. Eng.* **1939**, *35*, 109.

(2) (a) Haussling, L.; Knoll, W.; Ringsdorf, H.; Schmitt, F.-J.; Yang, J. *Macromol. Chem, Macromol. Symp.* **1991**, *46*, 145. (b) Zamborini, F.P.; Leopold, M.C.; Hicks, J.F.; Kulesza, P.J., Mali, M.A.; Murray, R.W. *J. Am. Chem. Soc.* **2002**, *124*, 8958. (c) Vossmeyer, T.; Guse, B.; Besnard, I.; Bauer, R.E.; Muellen, K.; Yasuda, A. *Adv. Mater.* **2002**, *14*, 238.

(3) Wang, D. H.; Ni, Y. H.; Huo, Q.; Tallman, D. E. *Thin Solid Films* **2005**, *471*, 177.

(4) Aviram, A.; Ratner, M. A. *Chem. Phys. Lett.* **1974**, *29*, 277.

(5) Laibnis, P. E.; Whitesides, G. M. *J. Am. Chem. Soc.* **1992**, *114*, 1990.

(6) Chen, Y; Jung, G.-Y.; Ohlberg, D. A. A.; Li, X.; Stewart, D. R.; Jeppesen, J. O.; Nielsen, K. A.; Stoddart, J. F.; Williams, R. S. *Nanotechnology* **2003**, *14*, 462.

(7) Wold, D. J.; Frisbie, C. D. *J. Am. Chem. Soc.* **2001**, *123*, 5549.

(8) (a) Cygan, M. T.; Dunbar, T. D.; Arnold, J. J.; Bumm L. A.; Shedlock, N. F.; Burgin, T. P.; Jones, L, II; Allara, D. A.; Tour, J. M.; Weiss, P. S. *J. Am. Chem. Soc.* **1998**, *120*, 2721. (b) Seferos, D. S.; Blum, A. S.; Kushmerick, J. G.; Bazan, G. C. *J. Am. Chem. Soc.* **2006**, *128*, 11260. (c) Cui, X. D.; Primak, A.; Zarate, X.; Tomfohr, J.; Sankey, O. F.; Moore, A. L.; Moore, T. A.; Gust, D.; Harris, G.; Lindsay, S. M. *Science.* **2001**, *294*, 571. (d) Lüssem, B.; Müller-Meskamp, L.; Karthäuser, S.; Waser, R.; Homberger, M.; Simon, U. *Langmuir* **2006**, *22*, 3021.

(9) Schreiber, F. *Prog. Surf. Sci.* **2000**, *65*, 151.

(10) Leung, T. Y. B.; Schwartz, P. V.; Scoles, G.; Schreiber, F.; Ulman, A. *Surf. Sci.* **2000**, *458*, 34.

(11) Jaschke, M.; Schönherr, H.; Wolf, H.; Butt, H. -J.; Bamberg, E.; Besocke, M. K.; Ringsdorf, H. *J. Phys. Chem.* **1996**, *100*, 2290.

(12) Nuzzo, R. G.; Dubois, L. H.; Allara, D. L. *J. Am. Chem. Soc.* **1990**, *112*, 558.

(13) (a) Tam-Chang, S.-W.; Biebuyck, H.A.; Whitesides, G.M.; Jeon, N.; Nuzzo, R. *Langmuir* **1995**, *11*, 4371. (b) Lewis, P. A.; Smith, R. K.; Kelly, K. F.; Bumm, L. A.; Reed, S. M.; Clegg, R. S.; Gunderson, J. D.; Hutchison, J. E.; Weiss, P. S. *J. Phys. Chem. B.* **2001**; *105*; 10630.

(14) Dhirani, A.; Zehner, R. W.; Hsung, R. P.; Guyot-Sionnest, P.; Sita, L. R. *J. Am. Chem. Soc.* **1996**, *118*, 3319.

(15) Bumm, L. A.; Arnold, J. J.; Charles, L. F.; Dunbar, T. D.; Allara, D. L.; Weiss, P. S. *J. Am. Chem. Soc.* **1999**, *121*, 8017.

(16) Bumm, L. A.; Arnold, J. J.; Cygan, M. T.; Dunbar, T. D.; Burgin, T. P.; Jones, L., II; Allara, D. L.; Tour, J. M.; Weiss, P. S., *Science*, **1996**, *271(5256)*, 1705-07.

(17) Bumm, L. A.; Arnold, J. J.; Dunbar, T. D.; Allara, D. L.; Weiss, P. S. *J. Phys. Chem. B.* **1999**, *103*, 8122.

(18) Wessels, J. M.; Nothofer H.-G.; Ford W. E.; von Wrochem, F.; Scholz, F.; Vossmeyer, T.; Schroedter, A.; Weller, H.; Yasuda, A. *J. Am. Chem. Soc.* **2004**, *126*, 3349.

(19) The following sensitivity factors are used: $SF_{S\,2p} = 0.668$, $SF_{N\,1s} = 0.477$, $SF_{O\,1s} = 0.780$, $SF_{C\,1s} = 0.377$, $SF_{Au\,4f} = 6.250$.

(20) Delley, B. *J. Chem. Phys.* **1990**, *92*, 508.

(21) (a) Becke, A. D. *J. Chem. Phys.* **1988**, *88*, 2547. (b) Lee, C.; Yang, W.; Parr, R. G. *Phys. Rev. B* **1988**, *37*, 786.

(22)   Sun, H. *J. Phys. Chem. B.* **1998**, *102*, 7338.

(23)   Duvez A.-S. *J. Electron Spectrosc. Relat. Phenom.* **2004***, 134*, 97.

(24)   Hansen, H. S.; Tougaard, S.; Biebuyck, H. *J. Electron Spectrosc. Relat. Phenom.* **1992**, *58*, 159.

(25)   The S *2p* signal intensity from dodecanethiol and dithioacetamide monolayers is corrected to compensate for the electron attenuation caused by the monolayer material. Hereby, an electron attenuation length (EAL) of $\lambda = 3.7$ nm is assumed as a result of a calculation with the program "NIST standard reference database 82". This value is close to the experimental value obtained when comparing alkanethiol SAMs with different chain lengths, and is also used for DMAAB SAMs (similar packing densitiy as dodecanethiol SAMs). DMAAB has roughly the same length as dodecanethiol, but one sulfur is located at the Au-molecule interface and the other one is exposed to the surface (no attenuation). Thus, for the DMAAB S 2p signal, only 1/2 the attenuation factor obtained for dodecanethiol is assumed. For further details, see appendix A.

(26)   Klegg, R. S.; Reed, S. M.; Smith, R. K.; Barron, B. L.; Rear, J. A.; Hutchison, J. E. *Langmuir* **1999**, *15*, 8876.

(27)   Beamson, G.; Briggs, D. *High-Resolution XPS on Organic Polymers*; John Wiley & Sons Ltd.: Chichester, U.K., 1992.

(28)   Heister, K.; Zharnikov, M.; Grunze, M.; Johansson, L. S. O. *J. Phys. Chem. B* **2001**, *105*, 4058-4061.

(29)   Laibinis, P. E.; Whitesides, G. M.; Allara, D. L.; Tao, Y.-T.; Parikh, A. N.; Nuzzo, R. G. *J. Am. Chem. Soc.* **1991**, 113, 7152.

(30)   Lindberg, B. J.; Hamrin, K.; Johansson, G.; Gelius, U.; Fahlman, A.; Nordling, C.; Siegbahn, C. *Physica Scripta* **1970**, *1*, 286.

(31)   Nuzzo, R. G.; Zegarski, B. R.; Dubois, L. H. *J. Am. Chem. Soc.* **1987**, *109*, 733.

(32)   Weckenmann, U; Mittler, S; Naumann, K; Fischer, R. A. *Langmuir* **2002**, *18*, 5479.

(33)   (a) Ishida, T.; Hara, M.; Kojima, I.; Tsuneda, S.; Nishida, N.; Sasabe, H.; Knoll, W. *Langmuir* **1994**, *10*, 4566. (b) Zhong, C.-J.; Porter, M. D. *J. Am. Chem. Soc.* **1994**, *116*, 11616. (c) Leavitt, A. J.; Beebe, T. P. *Jr. Surf. Sci.* **1994**, *314*, 23.

(34)   Sellers, H.; Ulman, A.; Shnidman, Y.; Eilers, J. E. *J. Am. Chem. Soc.* **1993**, *115*, 9389.

(35)   Camillone, N. et al. *J. Chem. Phys.* **1994**, *101*, 11031.

(36)   For the determination of relative DMAAB/dodecanethiol coverages, we exploited the circumstance that both compounds contain sulfur, but only DMAAB contains nitrogen. XPS intensities and some algebra then yield the desired coverage ratios.

(37)   Liao, S.; Shnidman, Y.; Ulman, A. *J. Am. Chem. Soc.* **2000**, *122*, 3688.

(38)   Porter, M.D.; Bright, T. B.; Allara, D. L.; Chidsey, C. E. D. *J. Am. Chem. Soc.* **1987**, *109*, 3559.

(39)   (a) Poirier, G. E.; Tarlov, M. J. *Langmuir* **1994**, *10*, 2853. (b) Delamarche, E.; Michel, B.; Gerber, C.; Anselmetti, D.; Güntherodt, H.-J.; Wolf, H.; Ringsdorf, H. *Langmuir* **1994**, *10*, 2869-2871. (c) Bucher, J. P.; Santesson, L.; Kern, K. *Appl. Phys. A* **1994**, *59*, 135.

(40)   Li, B.; Zeng, C.; Li, Q.; Wang, B.; Yuan, L.; Wang, H.; Yang, J.; Hou, J. G.; Zhu, Q. *J. Phys. Chem. B*. **2003**, *107*, 972.

(41)   Ishida, T.; Mizutani, W.; Choi, N.; Akiba, U.; Fujihira, M., Tokumoto, H. *J. Phys. Chem. B.* **2000**, *104*, 11680.

(42)   Wold, D. J.; Haag, R.; Rampi, M. A.; Frisbie, C. D. *J. Phys. Chem. B.* **2002**, *106*, 2813.

(43)   Yasutake, Y.; Shi, Z.; Okazaki, T.; Shinohara, H.; Majima, Y. *Nano Letters* **2005**, *5*, 1057.

(44)   Holmlin, R.; Haag, R.; Chabinyc, M. L.; Ismagilov, R. F.; Cohen, A. E.; Terfort, A.; Rampi, M. A.; Whitesides, G. M. *J. Am. Chem. Soc.* **2001**, *123,* 5075.

(45)   Ishida, T.; Mizutani, W.; Akiba, U.; Umemura, K.; Inoue, A., Choi, N., Fujihira, M., Tokumoto, H. *J. Phys. Chem. B.* **1999**, *103*, 1686.

(46)   Wakamatsu, S.; Fujii, S.; Akiba, U.; Fujihira, M. *Ultramicroscopy* **2002**, *97*, 19.

(47)   Moth-Poulsen, K.; Patrone, L.; Stuhr-Hansen, N.; Christensen, J. B.; Bourgoin, J.-P., Bjoernholm, T. *Nano Letters* **2005**, *5*, 783.

Appendix A

NIST standard reference database 82 settings for the calculation of the Electron Attenuation Length (EAL):

Attenuation of Au 4f and S 2p photoelectrons in hydrocarbons (decanethiol):

Binding energy (Au 4f) = 84 eV → E_{Kin}(Au 4f) = 1440 eV–84 eV = 1356 eV,

E_{Kin}(S 2p) = 1440 eV–162 eV= 1278 eV

Asymmetry factor for Au $_{4f\ 7/2}$: β = 1.04 (Al $_{K\alpha}$)

Number of valence electrons/element: 4 for carbon, 1 for H.

Bandgap for alkanes: $\Delta E_{HOMO\text{-}LUMO}$ ~ 5 eV.

Mass density of SAM: ρ ~ 0.94 g/cm^3.

X-ray incident angle: α = 45°

 - Resulting attenuation length for Au 4f electrons: EAL (Practical) = 3.82 nm for decanethiol monolayers.
 - Resulting attenuation length for C 1s electrons: EAL (Practical) = 3.73 nm for decanethiol monolayers.

Attenuation factors derived from the Lambert-Beer law:

The mean free path of electrons in a solid is 5-50 Å, depending on the kinetic energy of the emitted photoelectrons. The decay of the electron emission intensity due to scattering from a thin layer is described by an exponential decay law (Lambert-Beer law):

$$I = I_0 \exp(-x/\lambda)$$
$$x = d/\cos(\alpha)$$
$$\lambda \propto \sqrt{E}$$

where E is the kinetic energy of the photo-emitted electrons, d the thickness of the organic layer, α the takeoff angle of the emitted electrons and λ the EAL of the material (vide supra).

For dodecanethiol SAMs (d ~ 1.4 nm), the attenuation factor is thus determined by means of the layer thickness x and the EAL λ ($\alpha = 0°$ for our spectrometer):

$$\frac{I}{I_0}(S_{2p}) = \exp(-1.4nm/3.7nm) = 0.68$$

where λ = 3.7 nm results from the NIST standard reference database 82 as described above. For comparison, we determined λ experimentally obtaining an approximate value of ~ 4.4 nm. As a consequence, to correct for the attenuation of S 2p photoelectrons that are emitted from the sulphur headgroup, the S 2p signal intensity has is multiplied by a factor 1.37.

Appendix B

Procedure for the calculation of the chemisorption energy by thermal desorption of thiols from Au(111):

- Sample is mounted on appropriate copper stub using thermal conductive Ag-paint.

- Introduce sample into XPS measurement chamber.

- Acquisition program: 5 sweeps S 2p, 2 sweeps C1s, Pass energy 40 eV, step size 0.1eV.

- Acquire XPS spectra at 60, 80, 90, 100, 110, 120 and 140 °C sample temperature (Sample holder equipped with a thermocouple) trying to keep the average heat rate constant.

- From the sulfur 2p peak area determine the molecular coverage as a function of the temperature.

- Plot the coverage as a function of temperature in a graph.

- Estimate the temperature at maximum desorption rate from the graph.

- With this, calculate the chemisorption energy using the Redhead equation (*Phys. Rev. B* ***69***,*155406*)

Curriculum vitae

Florian von Wrochem

24.12.1969:	Born in Starnberg (Germany).
1976-1989:	School education in Milano (Italy).
1990-1993:	Studied music and physics at the University of Tübingen.
1994-1999:	Master in physics at the University of Tübingen.
1999:	Two month internship in the Department of Quantum Optics (Prof. Zimmermann) at the University of Tübingen.
1999-2001:	Master Thesis at the University of Tübingen (Prof. Wagner) and at TRIUMF, Vancouver (Canada). Title: „Untersuchung Differentieller Wikungsquerschnitte in the πp-Streuung mit dem CHAOS-Spektrometer".
Since 2002:	R&D Scientist at the Material Science Laboratory, Sony Deutschland GmbH, Stuttgart.
From 2003:	Ph.D. Thesis at the University of Basel (Prof. Schönenberger). Title: „Electron Structure and Charge Transport Properties of Thiols and Dithiocarbamates in Self-Assembled-Monolayers".

The following academic supervisors and colleagues contributed to my scientific education:

Werner Nakel, Gerhard J. Wagner, Herbert Müther, Rüdiger Staubert, Rudolf Meier, Jurina M. Wessels, William E. Ford, Thomas A. Jung, Christian Schönenberger.

Danksagung

Mein besonderer Dank gilt Prof. Christian Schönenberger, ohne den diese Doktorarbeit nicht möglich gewesen wäre. Für die Betreuung und die langjährige Unterstützung bin ich Dr. Jurina Wessels dankbar, die durch ihr Engagement eine wesentliche Voraussetzung für das Gelingen meiner Bemühungen war. Prof. Baratoff danke ich für seine hilfreichen Kommentare zur den quantenchemischen Berechnungen. Außerdem sind viele der Arbeiten mit der tatkräftigen Unterstützung meiner Kollegen beim Material Science Laboratory (Sony Deutschland GmbH) durchgeführt worden. Hier danke ich insbesondere Frank Scholz für die zuverlässige Probenpräparation und Akos Schreiber für die vielen Messungen am Rastertunnelmikroskop. Dr. Heinz-Georg Nothofer hat einige der Moleküle, die in dieser Arbeit vorgestellt werden, synthetisiert. Für die wertvollen Diskussionen und Ratschläge bin ich unter anderem Dr. William E. Ford, Dr. Yvonne Joseph und Dr. Björn Lüssem dankbar. Auch bin ich unseren Kollaborationspartnern Dr. Peter Morf und Dr. Thomas Jung vom Paul Scherrer Institut für die hilfreiche Zusammenarbeit erkenntlich.

Meinen Eltern möchte ich danken für die Unterstützung und das Vertrauen, das sie mir im Laufe meiner ganzen Ausbildung geschenkt haben. Nicht zuletzt haben mir jedoch meine Kinder Henrik, Frederik und Karl durch deren Freude und Vitalität immer wieder zu neuer Motivation verholfen.